SAPIENZA
UNIVERSITÀ DI ROMA

FACOLTÀ DI SCIENZE MATEMATICHE FISICHE E NATURALI
Dottorato in Matematica Applicata XXVII ciclo

Energy, enstrophy and symmetry preserving schemes for the numerical integration of non-linear advective problems

Advisor:
Prof. Bernardo Favini

Candidate:
Chiara Sorgentone

Anno Accademico 2014-2015
Dipartimento di Matematica 'Guido Castelnuovo'

Everyone is wrong about the future. Man can only be certain about the present moment. But is that quite true either? Can he really know the present? Is he in a position to make any judgment about it? Certainly not. For how can a person with no knowledge of the future understand the meaning of the present? If we do not know what future the present is leading us toward, how can we say whether this present is good or bad, whether it deserves our concurrence, or our suspicion, or our hatred?

Milan Kundera - Ignorance

Acknowledgments

Parte di questo lavoro di dottorato é stato svolto in collaborazione con i laboratori dell'ENEA - UTMEA di Anguillara, per cui un grazie va a tutte le persone che lo hanno reso possibile, primo tra tutti Sandro Calmanti. Grazie anche a Irene Milillo per il suo contributo relativo allo studio degli spettri del modello quasi-geostrofico.
Essenziale anche la collaborazione con l'Universitá di Linköping, che, oltre a permettermi di estendere il lavoro di tesi, mi ha dato la possibilitá di confrontarmi con un mondo universitario molto lontano da quello italiano; grazie all'intero gruppo di matematica computazionale, in particolare al Prof. Jan Nordström e a Cristina La Cognata, studentessa di dottorato con cui ho svolto parte del lavoro.
Grazie al Prof. Falcone per essere stato un punto di riferimento costante, oltre che un ottimo insegnante.
Grazie alla pallavolo perché se sono sopravvissuta ad anni di matematica e di matematici é anche merito suo; grazie alle mie compagne di squadra passate e presenti per il legame unico e per avermi ricordato che la palla continua a cadere anche se la mia equazione non ammette soluzione unica.
Grazie a Ilaria perché ha condiviso con me l'intero percorso, dalla maturitá al dottorato, step by step, e per aver fatto a metá di tutte le difficoltá.
Grazie ai miei genitori per avermi incoraggiato anche senza capirmi, e ai miei fratelli per avermi dato la competizione senza la quale non avrei avuto il coraggio di scegliere nessuna delle strade in salita che mi hanno portato fin qui.
Grazie a Enrico per essermi stato accanto dal giorno della prova di ammissione al dottorato e avermi reso, in questi anni, una persona migliore.
Al mio Professore, Bernardo Favini, vanno i ringraziamenti di certo piú sentiti ma allo stesso tempo piú difficili. Perché le parole sono importanti.

Contents

1. Introduction

1.1. Context

The dashing progress of technology and scientific computation in the last decades made the numerical modeling a discipline of growing and growing success. The huge potential of modeling in describing a very wide variety of processes through Partial Differential Equations (PDEs) is been applied to many different sciences: physics, engineering, biology, chemistry, medicine, but also to social sciences such as economics, sociology, political science and so on. Numerical methods allow to the translation of a mathematical model (which can be explicitly solved only occasionally) into algorithms that can be solved by computers under mathematical manipulation. Computational Fluid Dynamics (CFD) plays an important role in this scenario, providing a prediction of fluid flows solving mathematical modeling with numerical methods. Physical applications are various: numerical weather predictions, aerospace engineering, computational hemodynamics (study of blood flow/circulation) and so on.
This PhD thesis fosuses on the study, development and applications of numerical methods for non-linear differential problems in the CFD context. In particular I applied the theoretical study to a specific geophysical application, the quasi-geostrophic model, so I dealt with the vorticity equation and the Jacobian differential operator. In this chapter an introduction to this context with particular attention to atmospheric modeling is provided, trying to give to the reader a state of the art of the main results achieved during last decades.

1.1.1. Mimetic schemes

Once an appropriate mathematical model is chosen, we need to design a numerical method which obtains the solution with sufficient efficiency and accuracy for the problem considered. The main techniques used to convert the partial differential equations which form our mathematical model into a set of algebraic equations that can be solved on a computer are finite difference (our choice), finite volume, and finite element. Each of these methods involve dividing or discretizing space and time in some manner.
A significant class of numerical methods are the so-called mimetic schemes [1]; these schemes mimics fundamental properties of mathematical and physical systems such as conservation laws, symmetry and positivity of solutions, duality of differential operators, as well as exact mathematical identities of the vector and tensor calculus. The preservation of conservation laws in a discrete model is necessary for modeling flows with strong shocks or, as in our case, for non-linear problems, when the energy transfer

between different scales occurs and need to be correctly discretized to avoid numerical instabilities. Most of PDE's are formulated in terms of divergence, gradient and curl, and conservation of integral properties (e.g. mean kinetic energy or mean square vorticity) depends on analytical properties of such operators and resulting theorems of vector analysis. The need of conserving energy (as well as other physical quantities) is one of the most important example in fluid dynamics of the applications of mimetic schemes. A typical problem comes from the finite size of the mesh cells: while the PDEs can resolve all the scales of motion, its numerical simulation may be more restricted. For example, the energy dissipation due to the molecular viscosity could result to be important but at the same time cannot be resolved numerically. We need, then, to avoid unphysical energy growth with the correct numerical scheme.
The idea of constructing mimetic schemes, firstly appear in the late mid-fifties (even if the world *mimetic* appeared many years later), when easy strategies to construct discrete analogs of analytical differential operators orthogonal meshes are used [2], [3].
Based on rectangular meshes, Arakawa [4] proposed the construction of a finite difference scheme for the vorticity equation. In this paper Arakawa underlines the importance of integral constraints on quadratic quantities and he shows that these quantities would not be maintained using a general finite difference scheme unless the finite difference Jacobian expression for the advection term is restricted to a form which properly represents the interaction between grid points. It is shown that the derived form of the finite difference Jacobian prevents nonlinear computational instability and then allows to long-term numerical integrations, as we will see in details in Chapter I. In [5], Arakawa shows with numerical examples the necessity and the superiority of such conservative schemes. Together with Lamb, Arakawa proposed a potential enstrophy and energy conserving scheme for the shallow water equations [6]; the idea of this work has been then extended for mimetic finite elements by McRae and Cotter [7], who presented a family of conservative spatial discretizations of the nonlinear rotating shallow-water equations. These are based on two-dimensional mixed finite element methods and then do not require an orthogonal grid as some finite difference methods do. Another approach for a potential enstrophy and energy conserving scheme is given by Salmon [8] who used Nambu brackets: in this way one need only discretize the Nambu bracket in such a way that the antisymmetry property is maintained. Using this strategy, Salmon derives explicit finite-difference approximations for the shallow-water equations that conserve mass, circulation, energy, and potential enstrophy on a regular square grid and on an unstructured triangular mesh.
Almost twenty years earlier, Salmon and Talley proposed a generalization of Arakawa's Jacobian [9], where a simple method yields discrete Jacobians that obey analogues of the differential properties needed to conserve energy and enstrophy for a two-dimensional flow. This is a generalization in the sense that this method is independent of the type of discretization and thus applies to an arbitrary representation in grid points, finite elements, or spectral modes, or to any mixture of the three. In particular the method is illustrated by deriving simple energy and enstrophy conserving Jacobians for an irregular triangular mesh in a closed domain, and for a mixed grid point and mode representation in a semi-infinite channel.

Starting by Arakawa's works, other authors presented different kind of generalizations of Arakawa's conservative scheme, see [10], [11], [12], [13] for details; in Section 2.2.3 I explain the difference between mine and existing generalizations.
Mimetic methods with similar properties have been more recently proposed in [14] and [15] on triangular meshes and in 2008, Abba and Bonaventura also proposed a mimetic finite difference discretization for the incompressible Navier-Stokes equations [16]. The results obtained in different papers demonstrate the advantages and the superiority of mimetic methods especially for a long-term numerical integration of incompressible fluid motion.
In [17] discrete numerical approximations with conserved quantities are developed for barotropic geophysical flows using Poisson brackets. Mathematical, numerical, and also statistical properties of these approximations are studied.
In this class of works it's worth quoting also a paper of Bas van't Hof and Arthur E.P. Veldman [18], "Mass, momentum and energy conserving (MaMEC) discretizations on general grids for the compressible Euler and shallow water equations".
Different works, involving domain with complex shapes and Lagrangian approach appeared approximately in the mid-seventies. In this period the derivation of compatible discrete operators are not carried out independently for each operator as before and, in most papers, the stability and convergence are proved in the energy norms induced by the mimetic inner product. The energy estimate together with the mimetic ideas can also be found in the more recent works of Olsson [19], [20], Mattsson, Nordström and Svärd, [21], [22] (see Chapter IV for more references), where finite difference approximations of differential operators on rectangular grids and weighted inner products are composed in order to make the discrete analogous of summation by parts formula consistent with the continuous case. It's precisely the analogy between the discrete and the continuum calculus the basic idea, as a matter of fact the stability estimates for these finite difference schemes are obtained following the argument used for continuum initial and boundary value problems; this method has been mainly applied to hyperbolic, parabolic, and mixed hyperbolic-parabolic systems and will be further discussed and applied in Chapter IV.
A third class of mimetic schemes born with the beginning of a systematic devolopment of Discrete Vector and Tensor Calculus (DVTC) and the extension to more general meshes. In [23], natural discrete analogs of grad, curl and div are constructed and discrete analogs of several important theorems of the continuum calculus are then proved, as, for example, that $div(A) = 0$ if and only if $A = curl(B)$. In this paper, the world *mimetic* refered to a numerical discretization is adopted for the first time even if the word mimetic had already been used in another unpublished report of Hyman and Scovel (1988). In [24], the construction of the derived operators is based on the duality principle, e.g.

$$[u_h, G\tilde{R}ADp_h]_F = -[DIVu_h, p_h]_C, \ \forall u_h \in F_h, \ p_h \in C_h,$$

where F_h and $C_h$are discrete spaces for face and cell grid functions, respectively. The inner products in discrete spaces are introduced and corresponding matrices are developed. The set of primary and derived discrete operators allows to construct discrete analogs of other operators, like second-order operators as *div grad*, *grad div*, *curl curl*, and so

on, which are needed to discretize various PDEs.
Nowadays, when we refer to mimetic schemes, we think of research activity carried out by the collaboration between the Los Alamos National Laboratory, USA, and a research group of Pavia, Italy, see works of Brezzi, Cangiani, Lipnikov, Shashkov, Manzini etc. The application of new technology to a wide range of PDEs is developed for arbitrary-order discretizations concerning primarily elliptic problems, the stability analysis and discrete maximum principles. This work is not placed in this category, but for completeness the interested reader is referred to [25], [26], [27] and related bibliography.
Much more references about mimetic schemes can be found in [1].

1.1.2. Atmospheric modeling

It is considered that Wilhelm Bjerknes (1904) was the first to point out that the future state of the atmosphere can in principle be obtained by an integration of differential equations governing the atmosphere and a first practical attempt at a numerical weather prediction was made by Richardson. After very long computations, Richardson obtained a totally unacceptable result; his work is described in the famous book *Weather prediction by Numerical Process* [28]. Richardson estimated that 64000 men are necessary to advance the calculations as fast as the weather itself is advancing; this, together with the total wrong result, left some doubt if the method would be of practical use. Later, a number of developments that followed improved the situation: Courant, Friedrichs and Lewy (1928) figured out that space and time increments in integrations of this type have to meet a certain stability criterion (CFL condition), Rossby's works in the late 1930's on easiest model for describing large-scale motions of the atmosphere and finally, in 1945, the first electronic computer ENIAC (Electronic Numerical Integrator and Computer) was constructed. In late 1940's, the vorticity conservation equation, and this first electronic computer, were used by Charney, Fjørtoft and von Neumann [29] for the first successful numerical forecast. This, together with the improvement of faster and faster computers, has been the starting point for the development of increasingly sophisticated numerical simulations.
Most models in atmospheric science are formulated by starting from conservation laws: conservation of mass, conservation of momentum, conservation of thermodynamic energy, and the radiative transfer equation. A priori, these equations can describe the evolution of the atmosphere in extreme detail, but practically, of course, we cannot use too high spatial and temporal resolution, and so we must represent some important processes parametrically [30], [31]. Parameterization in a climate model within numerical weather prediction refers to the method of replacing processes that are too small-scale, e.g. cloud microphysics, radiative parameterizations, etc. Obviously, mathematical methods are needed to solve the equations of a model, and in practice the methods are almost always approximate, which means that they entail errors. Many different errors arise in the numerical solution of a geophysical model: the model is sensitive to the initial and boundary conditions, the approximation of the model itself, the numerical method used to discretize the equation will also introduce errors and so on. There are various types of numerical models designed for atmospheric purposes, a good introductory course is

given by Randall [32]; he also made a collection of significant papers in [33]. A brief history of atmospheric general circulation modeling (GCM) is given by Edwards: starting from the early 20th century, with Bjerknes, going through the Richardson forecasts, the war, the Swedish Institute of Meteorology (the first in the world to begin routine real-time numerical weather forecasting, meaning broadcast of forecasting in advance of weather) and the Joint Numerical Weather Prediction Unit (built by Von Neumann, Charney and others around 1952), he traced the history of atmospheric modeling until late '80s. The first laboratory to develop a continuing program in general circulation modeling opened in 1955: the General Circulation Research Section, under the direction of Joseph Smagorinsky. In 1955-1956, Smagorinsky collaborated with Von Neumann, Charney and Phillips to develop a two-level model using a subset of the primitive equations; in 1959 he continued with a nine-level primitive equation model and he studied the need to couple ocean models to atmospheric GCMs. Jacob Bjerknes, already presented, founded the UCLA Department of Meteorology in 1940 and his interest in the problem of atmospheric circulation continued with Yale Mintz, a graduate student of him. Mintz recruited a Japanese meteorologist, Akio Arakawa, to help him in building GCMs. The first generation UCLA-GCM was completed in 1963; then Arakawa went back to Japan, but Mintz persuaded him to return to UCLA permanently in 1965, where he is now an Emeritus Professor (1.1). There exist a very interesting interview to Arakawa made by Edwards at University of California, Los Angeles in 1997, where his scientific history (and not only) is narrated.

Figure 1.1.: Akio Arakawa

As already underlined in the previous paragraph, Arakawa's work was innovative for his different way in approach numerical modeling, his attention was focused on the realism of the physical properties in the discrete system (in this sense mimetic). Historically, the incentive for this approach came by Norman Phillips who discovered the mechanism of non linear instability due to the systematic distorsion of the energy spectrum studied on a two-dimensional incompressible flow [34]. A straightforward remedy adopted by Phillips was a Fourier filtering aimed to prevent the fatal accumulation of energy at the smallest scales. Arakawa's mimetic solution [4], instead, was able to prevent nonlinear instability maintaining the discrete analogs of domain-averaged kinetic energy and en-

strophy, ensuring no change in the average wave number, [5], [35] (and see chapter 2 for details). Other relevant papers to underline how mimetic methods can result essential for climate modeling are: [36], where Mesinger and Arakawa proposed a publication reviewing methods for numerical simulation of the atmosphere and [6] and [37] where Arakawa and Lamb proposed also a new parametrization of the sub-grid scale processes. It's worth noting that, in 1960s, another important research center was established: the National Center for Atmospheric Research -NCAR-, with scientists such as Kasahara and Washington who started developing a two-layer global model.
After this brief historical presentation, some more practical considerations about numerical techniques: a general introduction to numerical analysis for computational fluid mechanics is given in [38], where the author shows and analyze the main numerical techniques to integrate PDEs with particular attention to the Navier-Stokes equations. By far, this (N-S equationss) is the most commonly used model for fluid dynamics; the Navier-Stokes equations can accurately predict the dynamics of most common fluids under a wide range of conditions (the most notable exceptions are non-Newtonian fluids, rarefied gases, and flows with very strong shock waves). In addition to the direct numerical simulation (DNS), where the Navier-Stokes equations are numerically solved without any turbulence model, meaning that the whole range of spatial and temporal scales of the turbulence must be resolved, we can treat N-S equations at different levels:

1. Averaging (or more generally filtering) is one of the primary means of simplifying our mathematical model. For example, as long as the process that we wish to simulate is approximately two-dimensional we can average the Navier-Stokes equations in one space dimension, or apply a scale analysis in order to select the magnitude of each dimension (e.g. Quasi-Geostrophic Model).

2. We can otherwise use a low-pass filter in space to obtain the so-called Large Eddy Simulation (LES) equations. This model can be useful for turbulent flows which generally have a wide range of spatial length scales. By using a low-pass filter we only include the large scales, or eddies, in our computation while the small-scale eddies are modeled using empirical relationships. This is convenient because the large eddies contain most of the energy, while the small eddies are nearly isotropic and therefore easier to model.

3. At the next level, we can average the Navier-Stokes equations also in time, where the equations obtained are called the Reynolds Averaged Navier-Stokes (RANS) equations. The idea behind the equations is Reynolds decomposition, whereby an instantaneous quantity is decomposed into its time-averaged and fluctuating quantities, an idea first proposed by Osborne Reynolds.

This list is clearly just a simplification of mathematical models for CFD; it is possible, under certain circumstances, to make further approximations that take into account special physical characteristics of the flow under consideration.
Another important issue in numerical discretization, lies in the *form* that we choose for our model; to be more precise let's consider the advection equation. This is based on

one of the following forms:

$$\frac{\partial q}{\partial t} + \mathbf{v} \cdot \nabla q = 0, \quad Eulerian\ advective\ form \tag{1.1}$$

$$\frac{\partial mq}{\partial t} + \nabla \cdot (m\mathbf{v}q) = 0, \quad Eulerian\ flux\ (divergence)\ form \tag{1.2}$$

$$\frac{Dq}{Dt} = 0, \quad Lagrangian\ form \tag{1.3}$$

Here q is a quantity per unit mass to be advected, $\mathbf{v}$ is the velocity field, m is the mass per unit and D/Dt is the material time derivative. Each of the previous forms, automatically satisfy a specific property: eq. 1.1 has the *constancy*, meaning that, if initially q is constant, it remains so in time; eq. 1.2 is conservative, in the sense that the area-averaged over a closed domain $\overline{mq}$ does not change in time (note that the conservation here refers just to the first moment, $\overline{mq}$ and not to higher moments such as $\overline{mq^2}$); finally, the automatic property of eq. 1.3 is to be stable in the sense of the boundedness of predicted q. Maybe the constancy is the minimum requirement for an advection scheme, anyway it is not always guaranteed for example in the case of the flux divergence form. Generally, Lagrangian schemes do satisfy constancy but not conservation and they have the advantage of no restriction in time step, in contrast to Eulerian schemes (our choice) that are restricted by the Courant-Friedrich-Levy (CFL) condition. Of course it is possible, and sometimes necessary, mix different forms to obtain one or more properties in the discrete space, as we will see in details for the Arakawa's Jacobian. The splitting technique and its relation with stability problems is also discussed by Nordström using SBP operators ([39] and related bibliography).

1.2. The Burgers equation

In order to clarify the meaning of non-linear energy transfer, we consider a simple 1D model, the Burgers equation:

$$\frac{\partial u}{\partial t} + u\frac{\partial u}{\partial x} = \nu\frac{\partial^2 u}{\partial x^2} \tag{1.4}$$

For simplicity, we consider the solution defined in the domain $D = [0, 2\pi)$ and to be periodic with zero mean value. We can expand the solution as:

$$u(x,t) = \sum_{k=1}^{\infty} A_k(t) sin(kx). \tag{1.5}$$

Using this expansion, we have:

$$\frac{\partial u}{\partial t} = \sum_{k=1}^{\infty} \dot{A}_k(t) sin(kx) \tag{1.6}$$

$$\frac{\partial u}{\partial x} = \sum_{k=1}^{\infty} k A_k(t) cos(kx) \tag{1.7}$$

$$\frac{\partial^2 u}{\partial x^2} = -\sum_{k=1}^{\infty} k^2 A_k(t) sin(kx) \tag{1.8}$$

$$\begin{aligned} u\frac{\partial u}{\partial x} &= \sum_{l=1}^{\infty}\sum_{m=1}^{\infty} A_l(t) A_m(t) m sin(lx) cos(mx) \\ &= \sum_{l=1}^{\infty}\sum_{m=1}^{\infty} \frac{A_l(t) A_m(t) m}{2} \{sin[(l+m)x] + sin[(l-m)x]\}. \end{aligned} \tag{1.9}$$

Putting all of this inside eq. 1.4, we obtain:

$$\begin{aligned} \sum_{k=1}^{\infty} \dot{A}_k(t) sin(kx) + \sum_{l=1}^{\infty}\sum_{m=1}^{\infty} \frac{A_l(t) A_m(t) m}{2} \{sin[(l+m)x] + sin[(l-m)x]\} \\ = -\nu \sum_{k=1}^{\infty} k^2 A_k(t) sin(kx). \end{aligned} \tag{1.10}$$

Now we recall the orthogonality of the function sin:

$$\int_0^{2\pi} sin(px) sin(qx) = \pi(\delta_{p,q} - \delta_{-p,q}), \tag{1.11}$$

and then, multiplying eq. 1.10 times $sin(kx)$ and integrating over D, we have:

$$\dot{A}_k(t)\pi + \sum_{l=1}^{\infty}\sum_{m=1}^{\infty} \frac{\pi A_l(t) A_m(t) m}{2} = -\pi\nu k^2 A_k(t), \quad k = 1, 2, \ldots, \infty \tag{1.12}$$

where the two summations consider only indices m and l such that

- $l + m = k$
- $l - m = k$
- $l - m = -k$
- $l + m = -k$ (this condition brings nothing because it means $l < 0$).

So eq. 1.12 becomes

$$\dot{A}_k + \sum_{m=1}^{\infty} m\left(\frac{A_m A_{k-m}}{2} + \frac{A_m A_{k+m}}{2} - \frac{A_m A_{m-k}}{2}\right) = -\nu k^2 A_k, \quad k = 1, 2, \ldots, \infty \tag{1.13}$$

This equation says that the change of A_k in time depend on two different causes: one linear and one non-linear.

- Linear terms:
  If we consider only linear terms, eq. 1.13 becomes

$$\dot{A}_k = -\nu k^2 A_k \Rightarrow A_k(t) = A_k(0)e^{-\nu k^2 t}, \quad k = 1, 2, \ldots, \infty \tag{1.14}$$

  meaning that each component A_k decreases as fast as the fluid is viscous and the structure is small (meaning that k is large). The important remark on the linear term is that the evolution of each A_k is independent from the others, so if initially $A_k(0)$ depends only on a finite number of k (for example $k = 1, 2, 3$), it means that the solution would decrease only on initial modes ($k = 1, 2, 3$) each one independently from the others.

- Non-linear terms:
  Differently, non-linear terms completely modify the structure of the solution, transferring the momentum of the k-component to components $k + m$, $k - m$, $m - k$. If we consider, for simplicity, only the first three terms in the general summation (instead of ∞), we have, by eq. 1.13:

$$\begin{aligned}
\dot{A}_1 + \frac{1}{2}(A_1A_0 + A_1A_2 - A_1A_0) + (A_2A_{-1} + A_2A_3 - A_2A_1) \\
+\frac{3}{2}(A_3A_{-2} + A_3A_4 - A_3A_2) = -\nu A_1 \\
\dot{A}_2 + \frac{1}{2}(A_1A_1 + A_1A_3 - A_1A_{-1}) + (A_2A_0 + A_2A_4 - A_2A_0) \\
+\frac{3}{2}(A_3A_{-1} + A_3A_5 - A_3A_1) = -\nu 4 A_2 \\
\dot{A}_3 + \frac{1}{2}(A_1A_2 + A_1A_4 - A_1A_{-2}) + (A_2A_1 + A_2A_5 - A_2A_{-1}) \\
+\frac{3}{2}(A_3A_0 + A_3A_6 - A_3A_0) = -\nu 9 A_3
\end{aligned} \tag{1.15}$$

  but considering $A_p = 0$ for $p < 0$ and $p > 3$,

$$\begin{aligned}
\dot{A}_1 - \frac{1}{2}A_1A_2 - \frac{1}{2}A_2A_3 = -\nu A_1 \\
\dot{A}_2 + \frac{1}{2}A_1A_1 - A_1A_3 = -\nu 4 A_2 \\
\dot{A}_3 + \frac{3}{2}A_1A_2 = -\nu 9 A_3
\end{aligned} \tag{1.16}$$

  Now, if we consider an initial condition containing only A_1, it's immediate to see it'll results $\dot{A}_2 \neq 0$, due to the term $\frac{A_1A_1}{2}$; similarly, when $A_2 \neq 0$, it'll results also $\dot{A}_3 \neq 0$, and so on: if we didn't limit k as we did but we consider the infinite summation, we would have an energy transfer towards smaller and smaller scales (bigger k).

This easy example shows the basic mechanism of turbulence, which will be discussed in Chapter V: the Reynolds number is defined as the ratio of inertial forces to viscous forces and it is often used to characterize different flow regimes such as laminar or turbulent flow. For what we have seen so far, when the Reynolds number is small, viscous forces will dominate over inertial forces and then the energy will decrease and the energy transfer will be restrained. Differently, when we consider a fluid with high Reynolds number, non-linear terms will dominate viscous effects, the energy transfer will be activated and the original structure will bring smaller fluid-dynamical structures.

1.3. Organization

This PhD thesis focuses on the study, development and application of numerical methods for nonlinear advective problems with additional conservative and symmetry properties. In particular, the work is of interest in climatology and meteorology with particular attention to the quasi-geostrophic model characterized by the dynamic of the vorticity equation.
The work is divided in three main parts:

Part 1

- In Chapter 2 I recall basic notions about the vorticity equation and a particular finite-difference scheme to discretize it: I start with the Navier-Stokes equation to derive the vorticity equation for a two-dimensional incompressible flow, I show analytical properties of the Jacobian operator involved, and then I give to the reader a review of Arakawa's work, a mimetic finite difference discretization for the vorticity equation.
- Chapter 3 is about the development of a systematic method to construct mimetic finite difference schemes. In particular the whole chapter is intended to a particular application of this method: the generalization of Arakawa's Jacobian. The general scheme found is then studied both in physical and Fourier space and many numerical examples are given.
  This work has been submitted to Journal of Computational Physics [40] and presented in [41].

Part 2 In Chapter 4 I deal with Summation-by-parts (SBP) operators: I will give an introduction to the argument to then show how it is possible to read the original Arakawa's Jacobian in an abstract form using SBP operators and then proving all the mimetic properties desired in this more general space [42].

Part 3 Chapter 5 is the geophysical application of this theorical study: I present the simulation of a quasi-geostrophic model discretized using mimetic finite-difference presented in the previous chapters. In particular I investigate about the energy spectra and on physical and numerical parameters of the Q.G. model [43].

In the last Chapter I summarize the conclusions and the possible further developments of this work.

2. Introduction to finite-difference schemes for incompressible flows

2.1. The Vorticity Equation

Consider the Euler equation for an incompressible inviscid fluid

$$\begin{aligned} \frac{\partial \mathbf{v}}{\partial t} + \mathbf{v} \cdot \nabla \mathbf{v} &= -\nabla p \\ \nabla \cdot \mathbf{v} &= 0 \end{aligned} \tag{2.1}$$

for $\mathbf{x} \in D$, where D is a bounded region in $\Re^3$. The vorticity vector ω is defined as the curl of the velocity field $\mathbf{v}$, i.e.,

$$\omega = \nabla \times \mathbf{v} \tag{2.2}$$

such that in a Cartesian frame with coordinate (x, y, z) and corresponding velocity component (u, v, w), we have

$$\omega = \left(\frac{\partial w}{\partial y} - \frac{\partial v}{\partial z}, \frac{\partial u}{\partial z} - \frac{\partial w}{\partial x}, \frac{\partial v}{\partial x} - \frac{\partial u}{\partial y} \right). \tag{2.3}$$

For deriving the vorticity equation we recall the following identity

$$\mathbf{v} \cdot \nabla \mathbf{v} = \omega \times \mathbf{v} + \nabla \frac{\left(|\mathbf{v}|^2\right)}{2},$$

(for details see [44],[45]) which transforms the Euler equation (2.1) to

$$\begin{aligned} \frac{\partial \mathbf{v}}{\partial t} + \omega \times \mathbf{v} &= -\nabla \left(p + \frac{|\mathbf{v}^2|}{2} \right) \\ \nabla \cdot \mathbf{v} &= 0 \end{aligned} \tag{2.4}$$

By taking the curl of the momentum equation in (2.4) and using the incompressible relation, we get

$$\frac{\partial \omega}{\partial t} + \mathbf{v} \cdot \nabla \omega - \omega \cdot \nabla \mathbf{v} = 0. \tag{2.5}$$

By considering a velocity field with a zero vertical component w we obtain the vorticity for a two-dimensional incompressible fluid. In this setting, (2.3) becomes $\omega = (0, 0, \zeta)$, where $\zeta = (\partial v/\partial x - \partial u/\partial y)$. From (2.5) the vorticity equation for an incompressible

flow on a general two-dimensional spatial domain is

$$\frac{\partial \zeta}{\partial t} + \mathbf{v} \cdot \nabla \zeta = 0. \tag{2.6}$$

with

$$\nabla \cdot \mathbf{v} = 0. \tag{2.7}$$

In this section we will work in a biperiodic domain D. Thanks to relation 2.7, we can write eq. 2.6 as

$$\frac{\partial \zeta}{\partial t} + \nabla \cdot (\mathbf{v}\zeta) = 0 \tag{2.8a}$$

and introduce the stream function ψ such that:

$$\mathbf{v} = \mathbf{k} \times \nabla \psi \tag{2.8b}$$

$$\zeta = \mathbf{k} \cdot \nabla \times \mathbf{v} = \nabla^2 \psi \tag{2.8c}$$

where $\mathbf{k}$ is the unit vector normal to the plane of motion. We can introduce the Jacobian operator

$$J(a,b) = \frac{\partial a}{\partial x}\frac{\partial b}{\partial y} - \frac{\partial a}{\partial y}\frac{\partial b}{\partial x} \tag{2.9}$$

with the following properties:

- Skew-symmetry:
$$J(a,b) = -J(b,a) \tag{2.10}$$
- Integral property:
$$\overline{aJ(b,c)} = \overline{cJ(a,b)} \tag{2.11}$$
where $\overline{f} = \frac{1}{|D|}\int_D f dxdy$.

The skew-symmetry property (2.10) follows by definition, while property (2.11) follows by integration by parts over a biperiodic domain:

$$\begin{aligned}
\overline{aJ(b,c)} &= \frac{1}{|D|}\int\int (a\frac{\partial b}{\partial x}\frac{\partial c}{\partial y} - \frac{\partial b}{\partial y}\frac{\partial c}{\partial x}dxdy) \\
&= \frac{1}{|D|}\int\int [-c\frac{\partial}{\partial y}(a\frac{\partial b}{\partial x}) + c\frac{\partial}{\partial x}(a\frac{\partial b}{\partial y})dxdy] \\
= \frac{1}{|D|}\int\int (-c\frac{\partial a}{\partial y}\frac{\partial b}{\partial x} - ca\frac{\partial^2 b}{\partial x \partial y} + c\frac{\partial a}{\partial x}\frac{\partial b}{\partial y} + ca\frac{\partial^2 b}{\partial y \partial x})dxdy \\
&= \frac{1}{|D|}\int\int (-c\frac{\partial a}{\partial y}\frac{\partial b}{\partial x} + c\frac{\partial a}{\partial x}\frac{\partial b}{\partial y})dxdy = \overline{cJ(a,b)}
\end{aligned} \tag{2.12}$$

We can rewrite equation (2.8a) as:

$$\frac{\partial \zeta}{\partial t} = J(\zeta, \psi). \tag{2.13}$$

Conserved quantities:
For any motion governed by equation (2.6) we have physical constraints such as conservation of mean kinetic energy,

$$\begin{aligned}(\frac{\partial K}{\partial t}) = \overline{\frac{1}{2}\frac{\partial(\nabla\psi)^2}{\partial t}} = \overline{(\nabla\psi)\cdot\frac{\partial(\nabla\psi)}{\partial t}} = -\overline{\psi\frac{\partial(\Delta\psi)}{\partial t}} \\ = \overline{-\psi\frac{\partial\zeta}{\partial t}} = \overline{-\psi J(\zeta,\psi)} = 0\end{aligned} \tag{2.14}$$

and conservation of enstrophy, defined as the mean square vorticity, which is a quantity directly related to the kinetic energy and it is particularly useful in the study of turbulent flows,

$$(\frac{\partial G}{\partial t}) = \overline{\frac{1}{2}\frac{\partial(\zeta^2)}{\partial t}} = \overline{\zeta\frac{\partial\zeta}{\partial t}} = \overline{\zeta J(\zeta,\psi)} = 0. \tag{2.15}$$

The RHS of both equations is zero thanks to the skew-symmetric (2.10) and the integral (2.11) properties with, respectively, $a = c = \psi$ and $a = b = \zeta$.
Expanding ψ into the series of orthogonal armonic functions, ψ_n, which satisfy

$$\nabla^2\psi_n + k_n^2\psi_n = 0, \tag{2.16}$$

we get that the average wave number k, defined as

$$k^2 = \frac{\sum_n k_n^2 K_n}{\sum_n K_n} \tag{2.17}$$

is conserved, thanks to the energy and enstrophy conservation:

$$\frac{d}{dt}\sum_n K_n = 0, \quad with\ K_n = \frac{1}{2}\overline{(\nabla\psi_n)^2} \tag{2.18}$$

$$\frac{d}{dt}\sum_n G_n = 0, \quad with\ G_n = \frac{1}{2}\overline{(\nabla^2\psi_n)^2} = k_n^2 K_n. \tag{2.19}$$

This means that no systematic one-way cascade of energy into smaller scales can occur. It is well known that non-linear problems as system (2.6) require the correct modeling of sub-grid terms (see, for example, J. Smagorinsky 1963 [30], J. W. Deardorff 1970 [31]). Moreover, a false transfer of energy between different scales can occour depending on different forms of truncation error, corresponding to different forms of discretization. In 1959 Phillips [34], treating non-linear numerical instability, proposed to add a smoothing term to equation (2.8a), but his solution resulted to be physically incorrect and to compromise the simulation. To overcome this problem, Arakawa [4] introduced the use of a mimetic scheme and, alternatively, higher order schemes have been devoloped ([46], [47], [48]). The latter choice is not necessarily preferable to a mimetic solution as pointed out in [49]; in this paper higher order schemes are compared with Arakawa's Jacobian which results to be the better candidate for under-resolved simulations.

Arakawa's solution is a mimetic scheme able to conserve integral quantities and then satisfying other important constraints on the spectral distribution of the energy. His scheme has been widely used (see, for example [49],[13],[50]) and studied: Dubinkina and Frank [51] examined the statistical properties of Arakawa's discretization, while Lilly [52] proposed a detailed paper based on a spectral analysis.
Also different generalization of the particular Arakawa's solution have been presented (see [10], [11],[9], [12]) but none of them is a general procedure to produce the overall set of solutions.
We will start introducing and analyzing Arakawa's solution, then we will present our general proceduce to create mimetic finite-difference schemes and we will finally compare the particular Jacobian of Arakawa with the general solution found with the new method.

2.2. Arakawa's Jacobian

In this section $\mathbf{i}$ will denote a generic grid point $\mathbf{i} = (i, j)$ and a generic discrete Jacobian is:

$$h^2 J_{\mathbf{i}}(\zeta, \psi) = \sum_{\mathbf{i}'} \sum_{\mathbf{i}''} c_{\mathbf{i}',\mathbf{i}''} \zeta_{\mathbf{i}+\mathbf{i}'} \psi_{\mathbf{i}+\mathbf{i}''} \tag{2.20}$$

where h is the spatial step size, supposed to be uniform in x and y direction. Arakawa looked for a mimetic Jacobian discretization, satisfying then the discrete analogous of (2.14)-(2.15), so he imposed:

$$\sum_{\mathbf{i}} h^2 \zeta_{\mathbf{i}} J_{\mathbf{i}}(\zeta, \psi) = 0 \tag{2.21}$$

$$\sum_{\mathbf{i}} h^2 \psi_{\mathbf{i}} J_{\mathbf{i}}(\zeta, \psi) = 0 \tag{2.22}$$

It is useful to write equation (2.20) as:

$$h^2 J_{\mathbf{i}}(\zeta, \psi) = \sum_{\mathbf{i}'} a_{\mathbf{i},\mathbf{i}+\mathbf{i}'} \zeta_{\mathbf{i}+\mathbf{i}'} \tag{2.23}$$

where

$$a_{\mathbf{i},\mathbf{i}+\mathbf{i}'} = \sum_{\mathbf{i}''} c_{\mathbf{i}',\mathbf{i}''} \psi_{\mathbf{i}+\mathbf{i}''} \tag{2.24}$$

Multiplying eq. (2.23) times ζ_i, we obtain:

$$h^2 \zeta_{\mathbf{i}} J_{\mathbf{i}}(\zeta, \psi) = \sum_{\mathbf{i}'} a_{\mathbf{i},\mathbf{i}+\mathbf{i}'} \zeta_{\mathbf{i}} \zeta_{\mathbf{i}+\mathbf{i}'} \tag{2.25}$$

If we sum over $\mathbf{i}$, the RHS must be zero in order to satisfy (2.21), and then the enstrophy conservation; this is true if we impose

$$a_{\mathbf{i}+\mathbf{i}',\mathbf{i}} = -a_{\mathbf{i},\mathbf{i}+\mathbf{i}'}, \quad \forall \mathbf{i}, \mathbf{i}'. \tag{2.26}$$

Similarly, Arakawa imposed the energy conservation, with a similar trick he wrote the discrete jacoabian as:

$$h^2 J_{\mathbf{i}}(\zeta,\psi) = \sum_{\mathbf{i}''} b_{\mathbf{i},\mathbf{i}+\mathbf{i}''}\psi_{\mathbf{i}+\mathbf{i}''} \tag{2.27}$$

where

$$b_{\mathbf{i},\mathbf{i}+\mathbf{i}''} = \sum_{\mathbf{i}'} c_{\mathbf{i}',\mathbf{i}''}\zeta_{\mathbf{i}+\mathbf{i}'}, \tag{2.28}$$

obtaining now

$$b_{\mathbf{i}+\mathbf{i}'',\mathbf{i}} = -b_{\mathbf{i},\mathbf{i}+\mathbf{i}''}, \quad \forall \mathbf{i},\mathbf{i}''. \tag{2.29}$$

The Laplacian operator can be easily discretized using central finite-difference:

$$\zeta_{i,j} = \frac{1}{h^2}(\psi_{i+1,j} + \psi_{i-1,j} + \psi_{i,j+1} + \psi_{i,j-1} - 4\psi_{i,j}) \tag{2.30}$$

which satisfies $\overline{\psi\nabla^2\psi} = -\overline{(\nabla\psi)}^2$.
Arakawa considered three analogous analytical forms for the Jacobian:

1. $J(\zeta,\psi) = \zeta_x\psi_y - \zeta_y\psi_x$
2. $J(\zeta,\psi) = -\frac{\partial}{\partial_x}(\zeta_y\psi) + \frac{\partial}{\partial y}(\zeta_x\psi)$
3. $J(\zeta,\psi) = \frac{\partial}{\partial_x}(\zeta\psi_y) - \frac{\partial}{\partial y}(\zeta\psi_x)$

corresponding to three different discretization:

$$(J_1)_{i,j} = \frac{1}{4h^2}[(\zeta_{i+1,j} - \zeta_{i-1,j})(\psi_{i,j+1} - \psi_{i,j-1}) - (\zeta_{i,j+1} - \zeta_{i,j-1})(\psi_{i+1,j} - \psi_{i-1,j})] \tag{2.31}$$

$$\begin{aligned}(J_2)_{i,j} = \frac{1}{4h^2}[&-(\zeta_{i+1,j+1} - \zeta_{i+1,j-1})\psi_{i+1,j} + (\zeta_{i-1,j+1} - \zeta_{i-1,j-1})\psi_{i-1,j} \\ &+(\zeta_{i+1,j+1} - \zeta_{i-1,j+1})\psi_{i,j+1} - (\zeta_{i+1,j-1} - \zeta_{i-1,j-1})\psi_{i,j-1}]\end{aligned} \tag{2.32}$$

$$\begin{aligned}(J_3)_{i,j} = \frac{1}{4h^2}[&(\psi_{i+1,j+1} - \psi_{i+1,j-1})\zeta_{i+1,j} - (\psi_{i-1,j+1} - \psi_{i-1,j-1})\zeta_{i-1,j} \\ &-(\psi_{i+1,j+1} - \psi_{i-1,j+1})\zeta_{i,j+1} + (\psi_{i+1,j-1} - \psi_{i-1,j-1})\zeta_{i,j-1}]\end{aligned} \tag{2.33}$$

Using the above mentioned discrete properties, Arakawa proved that:

- J_1 is only skew-symmetric
- J_2 is only enstrophy-conserving
- J_3 is only energy-conserving

Moreover, J_3 is written in divergence form, and we can read in the same form also J_1 and J_2 just rotating the axis:

$$\begin{aligned}(J_1)_{i,j} = -\frac{1}{\sqrt{2}h}[&\frac{\psi_{i+1,j}-\psi_{i,j+1}}{\sqrt{2}h}\frac{\zeta_{i+1,j}+\zeta_{i,j+1}}{2} - \frac{\psi_{i,j-1}-\psi_{i-1,j}}{\sqrt{2}h}\frac{\zeta_{i,j-1}+\zeta_{i-1,j}}{2} \\ &+\frac{\psi_{i,j+1}-\psi_{i-1,j}}{\sqrt{2}h}\frac{\zeta_{i,j+1}+\zeta_{i-1,j}}{2} - \frac{\psi_{i+1,j}-\psi_{i,j-1}}{\sqrt{2}h}\frac{\zeta_{i+1,j}+\zeta_{i,j-1}}{2}]\end{aligned} \tag{2.34}$$

$$\begin{aligned}(J_2)_{i,j} = -\frac{1}{\sqrt{2}h}[&\frac{\psi_{i+1,j}-\psi_{i,j+1}}{\sqrt{2}h}\frac{\zeta_{i+1,j+1}+\zeta_{i,j}}{2} - \frac{\psi_{i,j-1}-\psi_{i-1,j}}{\sqrt{2}h}\frac{\zeta_{i,j}+\zeta_{i-1,j-1}}{2} \\ &+\frac{\psi_{i,j+1}-\psi_{i-1,j}}{\sqrt{2}h}\frac{\zeta_{i-1,j+1}+\zeta_{i,j}}{2} - \frac{\psi_{i+1,j}-\psi_{i,j-1}}{\sqrt{2}h}\frac{\zeta_{i,j}+\zeta_{i+1,j-1}}{2}]\end{aligned} \tag{2.35}$$

In this form, expressions in brackets represent vorticity fluxes calculated on the diagonals of the grid (fig. 2.1).

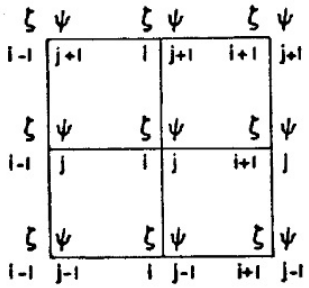

Figure 2.1.: A square grid used for the finite-difference vorticity equation

We observe that another possible skew-symmetric form, opposite to J_1, can be made writing the classical Jacobian $J(\zeta,\psi) = \zeta_x\psi_y - \zeta_y\psi_x$ but using again rotated axis:

$$\begin{aligned}J^{\times\times}_{i,j}(\zeta,\psi) = \frac{1}{8h^2}[&(\zeta_{i+1,j+1}-\zeta_{i-1,j-1})(\psi_{i-1,j+1}-\psi_{i+1,j-1}) \\ &-(\zeta_{i-1,j+1}-\zeta_{i+1,j-1})(\psi_{i+1,j+1}-\psi_{i-1,j-1})]\end{aligned} \tag{2.36}$$

Looking for a discrete Jacobian with all the above mentioned properties, Arakawa considered the linear combination of J_1, J_2, J_3 and $J^{\times\times}$:

$$J_A(\zeta,\psi)_{i,j} = \alpha(J_1)_{i,j} + \beta(J_2)_{i,j} + \gamma(J_3)_{i,j} + \delta(J^{\times\times})_{i,j} \tag{2.37}$$

with $\alpha+\beta+\gamma+\delta = 1$, and he proved that the choice $\alpha = \beta = \gamma = 1/3$ and $\delta = 0$, is the only possible linear combination of J_1, J_2, J_3 and $J^{\times\times}$ which is together skew-symmetric, energy and enstrophy preserving. From now on we will refer to this solution as Arakawa's Jacobian.

Other possible discretizations:
It is possible to construct more discretizations of the Jacobian different from $J_1, J_2, J_3, J^{\times\times}, J_A$

but always considering the linear combination of J_1, J_2, J_3, some examples follow. In figure (2.2) we emphasize verified properties for each jacobian and the grid points used.

- $J_4 = \frac{1}{2}(J_1 + J_2)$
- $J_5 = \frac{1}{2}(J_2 + J_3)$
- $J_6 = \frac{1}{2}(J_1 + J_3)$

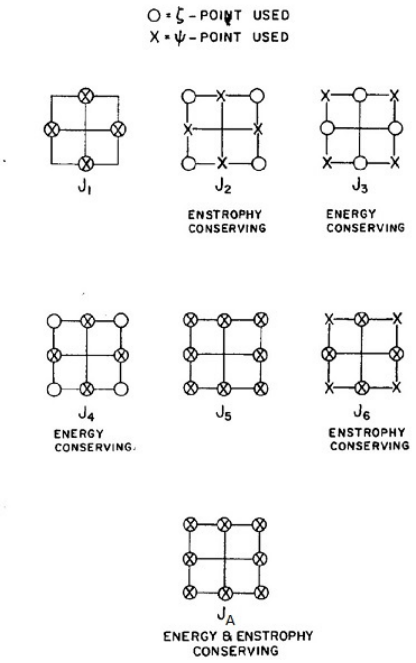

Figure 2.2.: Schematic representation of ζ and ψ points used in constructing the finite-difference Jacobians

Remark 2.1. *Due to the grid points used, as well as in 2.36, we can interchangeably refer to*

- J_1 *as* J^{++}
- J_2 *as* $J^{\times+}$
- J_3 *as* $J^{+\times}$

If we consider more grid points (figure 2.3), Arakawa showed how it is possible to construct a forth order scheme with all properties required. Considering also grid points

(i+2,j), (i-2,j), (i,j+2) e (i,j-2) we can define:

$$J_B(\zeta,\psi) = \frac{1}{3}[J^{\times\times}(\zeta,\psi) + J^{4\times+}(\zeta,\psi) + J^{4+\times}(\zeta,\psi)] \tag{2.38}$$

where $J^{\times\times}(\zeta,\psi)$ is defined in (2.36) and

$$\begin{aligned}(J^{4\times+})_{i,j} = \frac{1}{8h^2}[&(\psi_{i,j+2} - \psi_{i+2,j})\zeta_{i+1,j+1} - (\psi_{i-2,j} - \psi_{i,j-2})\zeta_{i-1,j-1} \\ &-(\psi_{i,j+2} - \psi_{i-2,j})\zeta_{i-1,j+1} + (\psi_{i+2,j} - \psi_{i,j-2})\zeta_{i+1,j-1}]\end{aligned} \tag{2.39}$$

$$\begin{aligned}(J^{4+\times})_{i,j} = \frac{1}{8h^2}[&(\psi_{i+1,j+1} - \psi_{i+1,j-1})\zeta_{i+2,j} - (\psi_{i-1,j+1} - \psi_{i-1,j-1})\zeta_{i-2,j} \\ &-(\psi_{i+1,j+1} - \psi_{i-1,j+1})\zeta_{i,j+2} + (\psi_{i+1,j-1} - \psi_{i-1,j-1})\zeta_{i,j-2}]\end{aligned} \tag{2.40}$$

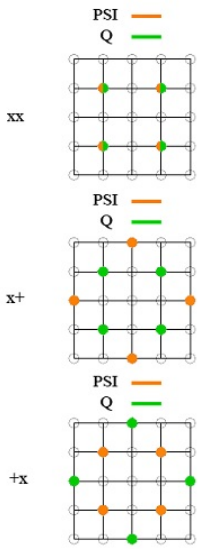

Figure 2.3.: Grids used for J_B

It's worth noting that J_B presents the same structure of truncation error of J_A as we will see in the next section.

2.2.1. Analysis of truncation error

Using Taylor expansion, we obtain:

$$J_1(\zeta,\psi) = J(\zeta,\psi) + \frac{h^2}{6}[\frac{\partial\zeta}{\partial x}\frac{\partial^3\psi}{\partial y^3} - \frac{\partial\zeta}{\partial y}\frac{\partial^3\psi}{\partial x^3} + \frac{\partial^3\zeta}{\partial x^3}\frac{\partial\psi}{\partial y} - \frac{\partial^3\zeta}{\partial y^3}\frac{\partial\psi}{\partial x}] + O(h^4) \tag{2.41}$$

$$\begin{aligned} J_2(\zeta,\psi) = J(\zeta,\psi) + \frac{h^2}{6}[&+\frac{\partial\zeta}{\partial x}\frac{\partial^3\psi}{\partial y^3} - \frac{\partial\zeta}{\partial y}\frac{\partial^3\psi}{\partial x^3} + \frac{\partial^3\zeta}{\partial x^3}\frac{\partial\psi}{\partial y} - \frac{\partial^3\zeta}{\partial y^3}\frac{\partial\psi}{\partial x} \\ &+3\frac{\partial^2\zeta}{\partial x\partial y}(\frac{\partial^2\psi}{\partial y^2} - \frac{\partial^2\psi}{\partial x^2}) + 3(\frac{\partial\psi}{\partial y}\frac{\partial^3\zeta}{\partial x\partial^2 y} - \frac{\partial\psi}{\partial x}\frac{\partial^3\zeta}{\partial y\partial^2 x}) + O(h^4)] \end{aligned} \tag{2.42}$$

$$\begin{aligned} J_3(\zeta,\psi) = J(\zeta,\psi) + \frac{h^2}{6}[&\frac{\partial\zeta}{\partial x}\frac{\partial^3\psi}{\partial y^3} - \frac{\partial\zeta}{\partial y}\frac{\partial^3\psi}{\partial x^3} + \frac{\partial^3\zeta}{\partial x^3}\frac{\partial\psi}{\partial y} - \frac{\partial^3\zeta}{\partial y^3}\frac{\partial\psi}{\partial x} \\ &+3(\frac{\partial\zeta}{\partial x}\frac{\partial^3\psi}{\partial x^2\partial y} - \frac{\partial\zeta}{\partial y}\frac{\partial^3\psi}{\partial x\partial y^2}) + 3(\frac{\partial^2\zeta}{\partial x^2} - \frac{\partial^2\zeta}{\partial y^2})\frac{\partial^2\psi}{\partial x\partial y}] + O(h^4) \end{aligned} \tag{2.43}$$

$$\begin{aligned} \rightarrow J_A(\zeta,\psi) = J(\zeta,\psi) + \frac{h^2}{6}[&\frac{\partial\zeta}{\partial x}\frac{\partial^3\psi}{\partial y^3} - \frac{\partial\zeta}{\partial y}\frac{\partial^3\psi}{\partial x^3} + \frac{\partial^3\zeta}{\partial x^3}\frac{\partial\psi}{\partial y} - \frac{\partial^3\zeta}{\partial y^3}\frac{\partial\psi}{\partial x} \\ &+(\frac{\partial\zeta}{\partial x}\frac{\partial^3\psi}{\partial x^2\partial y} - \frac{\partial\zeta}{\partial y}\frac{\partial^3\psi}{\partial x\partial y^2}) + (\frac{\partial^2\zeta}{\partial x^2} - \frac{\partial^2\zeta}{\partial y^2})\frac{\partial^2\psi}{\partial x\partial y} \\ &-(\frac{\partial\psi}{\partial x}\frac{\partial^3\zeta}{\partial x^2\partial y} - \frac{\partial\psi}{\partial y}\frac{\partial^3\zeta}{\partial x\partial y^2}) - (\frac{\partial^2\psi}{\partial x^2} - \frac{\partial^2\psi}{\partial y^2})\frac{\partial^2\zeta}{\partial x\partial y}] + O(h^4) \end{aligned} \tag{2.44}$$

In terms of velocity this means:

$$J_1(\zeta,\psi) = J(\zeta,\psi) + \frac{h^2}{6}[\frac{\partial\zeta}{\partial x}\frac{\partial^2 u}{\partial y^2} + \frac{\partial\zeta}{\partial y}\frac{\partial^2 v}{\partial x^2} + \frac{\partial^3\zeta}{\partial x^3}u + \frac{\partial^3\zeta}{\partial y^3}v] + O(h^4) \tag{2.45}$$

$$\begin{aligned} J_2(\zeta,\psi) = J(\zeta,\psi) + \frac{h^2}{6}[&\frac{\partial\zeta}{\partial x}\frac{\partial^2 u}{\partial y^2} + \frac{\partial\zeta}{\partial y}\frac{\partial^2 v}{\partial x^2} + \frac{\partial^3\zeta}{\partial x^3}u + \frac{\partial^3\zeta}{\partial y^3}v \\ &+3\frac{\partial^2\zeta}{\partial x\partial y}(\frac{\partial v}{\partial x} + \frac{\partial u}{\partial y}) + 3(u\frac{\partial^3\zeta}{\partial x\partial^2 y} + v\frac{\partial^3\zeta}{\partial y\partial^2 x})] + O(h^4) \end{aligned} \tag{2.46}$$

$$\begin{aligned} J_3(\zeta,\psi) = J(\zeta,\psi) + \frac{h^2}{6}[&\frac{\partial\zeta}{\partial x}\frac{\partial^2 u}{\partial y^2} + \frac{\partial\zeta}{\partial y}\frac{\partial^2 v}{\partial x^2} + \frac{\partial^3\zeta}{\partial x^3}u + \frac{\partial^3\zeta}{\partial y^3}v \\ &+3(\frac{\partial\zeta}{\partial x}\frac{\partial^2 u}{\partial x^2} + \frac{\partial\zeta}{\partial y}\frac{\partial^2 v}{\partial y^2}) + 3(\frac{\partial^2\zeta}{\partial x^2} - \frac{\partial^2\zeta}{\partial y^2})\frac{\partial u}{\partial x}] + O(h^4) \end{aligned} \tag{2.47}$$

$$\begin{aligned} \rightarrow J_A(\zeta,\psi) = J(\zeta,\psi) + \frac{h^2}{6}[&\frac{\partial\zeta}{\partial x}\frac{\partial^2 u}{\partial y^2} + \frac{\partial\zeta}{\partial y}\frac{\partial^2 v}{\partial x^2} + \frac{\partial^3\zeta}{\partial x^3}u + \frac{\partial^3\zeta}{\partial y^3}v \\ &+\frac{\partial^2\zeta}{\partial x\partial y}(\frac{\partial v}{\partial x} + \frac{\partial u}{\partial y}) + (u\frac{\partial^3\zeta}{\partial x\partial^2 y} + v\frac{\partial^3\zeta}{\partial y\partial^2 x}) \\ &+(\frac{\partial\zeta}{\partial x}\frac{\partial^2 u}{\partial x^2} + \frac{\partial\zeta}{\partial y}\frac{\partial^2 v}{\partial y^2}) + (\frac{\partial^2\zeta}{\partial x^2} - \frac{\partial^2\zeta}{\partial y^2})\frac{\partial u}{\partial x}] + O(h^4) \end{aligned} \tag{2.48}$$

And, for J_B:

$$\begin{aligned} J_B(\zeta,\psi) = J(\zeta,\psi) + \frac{h^2}{3}[&\frac{\partial\zeta}{\partial x}\frac{\partial^3\psi}{\partial y^3} - \frac{\partial\zeta}{\partial y}\frac{\partial^3\psi}{\partial x^3} + \frac{\partial^3\zeta}{\partial x^3}\frac{\partial\psi}{\partial y} - \frac{\partial^3\zeta}{\partial y^3}\frac{\partial\psi}{\partial x} \\ &+(\frac{\partial\zeta}{\partial x}\frac{\partial^3\psi}{\partial x^2\partial y} - \frac{\partial\zeta}{\partial y}\frac{\partial^3\psi}{\partial x\partial y^2}) + (\frac{\partial^2\zeta}{\partial x^2} - \frac{\partial^2\zeta}{\partial y^2})\frac{\partial^2\psi}{\partial x\partial y} \\ &-(\frac{\partial\psi}{\partial x}\frac{\partial^3\zeta}{\partial x^2\partial y} - \frac{\partial\psi}{\partial y}\frac{\partial^3\zeta}{\partial x\partial y^2}) - (\frac{\partial^2\psi}{\partial x^2} - \frac{\partial^2\psi}{\partial y^2})\frac{\partial^2\zeta}{\partial x\partial y}] + O(h^4) \end{aligned} \tag{2.49}$$

2.2.2. Spectral analysis

Here after I present the analysis made by Lilly [52], this is a spectral analysis to show different errors generated by Arakawa's Jacobian. Lilly showed there are three kinds of errors, two of them are related to the truncation error of first and second order derivatives (and then they can be minimized raising the order of accuracy), and the last type is the aliasing error, responsible of instability problems showed by Phillips in ([34]).
The starting point for Lilly's analysis is expressing the stream function and the vorticity as a series of complex exponential functions with vector wave number $M = (m, n)$, as follows:

$$\psi = \sum_M A_M e^{i(M\cdot R)} = \sum_M \psi_M \tag{2.50}$$

where $R = (x, y)$. The vorticity will be:

$$\zeta = -\sum_M |M|^2 A_M e^{i(M\cdot R)} = -\sum_M |M|^2 \psi_M \tag{2.51}$$

and the Jacobian:

$$J(\psi,\zeta) = \sum_{M',M''} (k\cdot M'\times M'')|M''|^2\psi_{M'}\psi_{M''} = \frac{1}{2}\sum_{M',M''} (k\cdot M'\times M'')(|M''|^2-|M'|^2)\psi_{M'}\psi_{M''} \tag{2.52}$$

An important fact is that the three different Jacobians of Arakawa's construction, correspond respectively to

1. $J_1(\psi,\zeta) = \delta_x\overline{\psi}^x\delta_y\overline{\zeta}^y - \delta_y\overline{\psi}^y\delta_x\overline{\zeta}^x$
2. $J_2(\psi,\zeta) = \delta_x\overline{(\psi\delta_y\overline{\zeta}^y)}^x - \delta_y\overline{(\psi\delta_x\overline{\zeta}^x)}^y$
3. $J_3(\psi,\zeta) = -\delta_x\overline{(\zeta\delta_y\overline{\psi}^y)}^x + \delta_y\overline{(\zeta\delta_x\overline{\psi}^x)}^y$

where (assuming uniform grid $h = \Delta x = \Delta y$)

$$\delta_x F(x) = \frac{1}{h}[F(x+\frac{h}{2}) - F(x-\frac{h}{2})],$$

$$\overline{F(x)}^x = \frac{1}{2}[F(x+\frac{h}{2}) + F(x-\frac{h}{2})],$$

$$\delta_x \overline{F(x)}^x = \delta_{2x} F(x) = \frac{1}{2h}[F(x+h) - F(x-h)],$$
$$\nabla F = (\delta_x \overline{F}^x, \delta_y \overline{F}^y).$$

Following this notation:

$$\nabla e^{i(M\cdot R)} = S(M) i e^{i(M\cdot R)} \tag{2.53}$$

where

$$S(M) = (\frac{sin(m\Delta x)}{h}, \frac{sin(nh)}{h}) \tag{2.54}$$

and:

$$\nabla^2 e^{i(M\cdot R)} = -4|S(M/2)|^2 e^{i(M\cdot R)}. \tag{2.55}$$

We don't have algebraic identities between analytical and numerical derivates because $S(M) \neq M$. Lilly analyzed then spectral forms of each Jacobian, obtaining:

$$J_1 = k \cdot \nabla\psi \times \nabla\zeta = 2 \sum_{M',M''} k \cdot [S(M') \times S(M'')]\{|S(\frac{M''}{2})|^2 - S(\frac{M'}{2})|^2\}\psi_{M'}\psi_{M''} \tag{2.56}$$

$$\begin{aligned} J_2 &= k \cdot \nabla \times (\psi\nabla\zeta) \\ &= 2\textstyle\sum_{M',M''} k \cdot S(M'+M'') \times \{S(M'')|S(\frac{M''}{2})|^2 + S(M')|S(\frac{M'}{2})|^2\}\psi_{M'}\psi_{M''} \end{aligned} \tag{2.57}$$

$$\begin{aligned} J_3 &= -k \cdot \nabla \times (\zeta\nabla\psi) \\ &= -2\textstyle\sum_{M',M''} k \cdot S(M'+M'') \times \{S(M'')|S(\frac{M'}{2})|^2 + S(M')|S(\frac{M''}{2})|^2\}\psi_{M'}\psi_{M''} \end{aligned} \tag{2.58}$$

$$\begin{aligned} J_A &= \tfrac{2}{3}\textstyle\sum_{M',M''} k \cdot \{S(M') \times S(M'') \\ &\quad +[S(M'+M'')] \times [S(M'') - S(M')]\} \cdot \{|S(\tfrac{M''}{2})|^2 - |S(\tfrac{M'}{2})|^2\}\psi_{M'}\psi_{M''} \end{aligned} \tag{2.59}$$

Comparing equations (2.56)-(2.59) with equation (2.52), Lilly focused on three kinds of error:

- *First derivative errors:*
  Errors due to first derivatives approximation arise because $S(M) \neq M$, that is the replacement of wave numbers by their sines, and this replacement is present in almost every interaction. sono presenti in quasi tutte le interazioni; these errors may be reduced by using a higher order difference scheme, for which S(M) is replaced by the Fourier sine series converging toward M in the range from $-\pi/h$ to π/h in each coordinate direction.

- *Second derivative errors:*
  Errors due to second derivative approximation arise because $4S(M/2)^2 \neq M \cdot M$ which comes from the calculation of the vorticity as the laplacian of the stream

function. Again these errors can be reduced by expanding the network of points to compute the Laplacian.

- *Aliasing error:*
  We cannot see aliasing error in the spectral equations, this kind of error arises because only limited wave numbers can be representabled in a discrete space; the highest representable wave number is $\tilde{m} = \frac{\pi}{h}$, higher wave numbers will be misinterpreted as wave numbers $-\frac{\pi}{h} + m$ causing spurious interactions involving reflections of one or both components.

It is clear that wrong interactions arise for all discrete Jacobians, but numerical instabilities arise only with the non-conservative ones, as shown in [5].

2.2.3. Generalizations

Different kinds of Arakawa's generalization have been presented in literature; hereafter I will give just a summary of the main ones in order to show differences and strengths of the systematic method I developed to discretize mimetic non-linear operator.

- in 1974-1975 Jespersen [10] and Fix [11] studied different classes of conservative finite-element Jacobians. In particular Jespersen reinterpreted Arakawa's solution as a finite-element method, showing how any nine-point second-order method obeying the conservation laws is a linear combination of two finite-element schemes, bilinear elements in rectangles and linear elements in triangles. He showed conservative finite-difference nine-points schemes is a one-parameter family solution;

- In 1989, Salmon and Talley [9] proposed a generalization of Arakawa's Jacobian in terms of indipendence of type of discretization. The method presented is an integral generalization of Arakawa's solution to apply to an arbitrary number of gridpoints for finite-difference schemes, or finite elements, or spectral modes, or to any mixture of the three. In particular they derived Arakawa's Jacobian as the particular solution for the 9 grid-points, an energy-enstrophy conserving Jacobian for an irregular triangular mesh in a closed domain and for a mixed gridpoint/mode representation in a semi-infinite channel;

- In 1998, McLachlan [12] using symmetry groups and skew-symmetric finite difference tensors, presented a systematic method for discretizing PDEs with a known list of integrals. The problem of this method is that the required symmetry properties make the the finite differences unavoidably complicated, except for special cases (as Arakawa's solution);

- In collaboration with Professor Nordström and PhD student Cristina La Cognata of Linköping University, I also found a generalization of Arakawa's Jacobian written in terms of Summation-by-parts operator [42]. This generalization will be presented in a succeeding chapter.

Also Hu and Fulton, in the technical report [13], tried to generalize Arakawa's idea for a general second order compact stencil conservative and skew-symmetric scheme. They found a whole set of solution depending on one parameter, exactly the same that I will find in the next sections, the problem of their work is that it is ill-posed. As a matter of fact, they impose the consistency of the general discrete scheme with the analytical Jacobian imposing the following three properties:

1. $J_{i,j}(1,\psi) = 0$
2. $J_{i,j}(\zeta,1) = 0$
3. $J_{i,j}(x,y) = 1$

for all suitably smooth functions ζ and ψ. It's easy to show that these conditions are necessary but not sufficient to guarantee consistency. To prove that, let's consider the following counterexample:

$$JJ(\zeta,\psi) = \frac{\partial^2\zeta}{\partial x\partial y}(\frac{\partial\psi}{\partial x}+\frac{\partial\psi}{\partial y}) - \frac{\partial^2\psi}{\partial x\partial y}(\frac{\partial\zeta}{\partial x}+\frac{\partial\zeta}{\partial y}) - \frac{\partial\psi}{\partial x}\frac{\partial\zeta}{\partial y} + \frac{\partial\psi}{\partial y}\frac{\partial\zeta}{\partial x} \tag{2.60}$$

Discretizing such operator (for example with central finite differences) we obtain a discrete operator which respects properties 1.-2.-3. (and which is also skew-symmetric) but this is anyway not consistent with an analytical Jacobian.
The solution obtained by Hu and Fulton is correct only because they consider the class of solution which obey concurrently to 1.-2.-3., skew-symmetry, energy and enstrophy preserving requirements. It is only the intersection of these properties which guarantees consistency, but if we would consider only subsets of solutions, the method results to be incorrect.
The systematic method to construct mimetic finite-difference schemes for incompressible flows presented below is the correct generalization of this method to a generic nonlinear operator which uses arbitrary grid-points and with arbitrary order of accuracy and properties. Moreover, this is the only generalization able to guarantee the overall set of solutions for each specific class of schemes we are looking for.

3. A systematic method to construct mimetic finite-difference schemes for incompressible flows

3.1. The General Method

We start by considering a general finite differences discretization of a general non-linear operator L in N variables:

$$L_{\mathbf{i}}(\phi^1, ..., \phi^N) = \sum_{\mathbf{i}_1} \sum_{\mathbf{i}_2} \cdots \sum_{\mathbf{i}_N} \widetilde{\phi}_{\mathbf{i}_1,\mathbf{i}_2,...,\mathbf{i}_N} \prod_{k=1}^{N} \phi^k_{\mathbf{i}+\mathbf{i}_k} \tag{3.1}$$

where $\mathbf{i}$ is a generic index which has as many components as the dimension of the problem (one for a scalar problem, two for a bi-dimensional problem and so on) and $\mathbf{i}_j$ has the same size of $\mathbf{i}$ but it is defined depending on the stencil we are using. This is a special form in writing a non-linear operator: the non-linearity is hidden in the products of sequences which contains every variables, while the coefficients are out of the product but depend on each variable. In such a way it's natural to construct a linear system for the coefficients $\widetilde{\phi}_{\mathbf{i}_1,...,\mathbf{i}_N}$. As a matter of fact, once we specify domain and stencil, we will translate numerical and physical requests on the general operator in terms of linear equations for coefficients $\widetilde{\phi}_{\mathbf{i}_1,...,\mathbf{i}_N}$.
To be more precise, the N-summations indexes depend on the stencil we are using: if we consider a compact stencil, the summation will include only the nearest grid-point, and will then include only $0, +1, -1$; if we consider a larger stencil with one more point it will be on $-2, -1, 0, 1, 2$, and so on. The general coefficient $\widetilde{\phi}_{\mathbf{i}_1,\mathbf{i}_2,...,\mathbf{i}_N}$ should generally take care and correlate each variable, this is the reason of all the indexes. Of course we could a priori also consider a different stencil and a different correlation for each variable, and the general expression 3.1 include them all.
In this way we just need to impose any property that we need to the coefficients $\widetilde{\phi}_{\mathbf{i}_1,\mathbf{i}_2,...,\mathbf{i}_N}$, we could ask for example the skew-symmetric property alone or all three Arakawa's requests together and so on. Every different choice leads to different linear systems and then to different solutions; in next section we will consider a special case in order to show how to apply the general procedure concretely.

3.2. An application: Non uniqueness of Arakawa's Jacobian

Let us consider a specific case: we fix the set of solutions as the set of all non-linear discrete operators with a compact stencil, constant spatial step size h, with the following properties:

a) skew symmetry (eq. 2.10);

b) enstrophy conserving (eq. 2.15);

c) energy conserving (eq. 2.14);

d) second order consistency with the analytical Jacobian (eq. 2.9).

In order to impose such constraints, we started from Arakawa's work [4] to generalize his idea. We re-write equation (3.1) as

$$J_{\mathbf{i}}(\zeta,\psi) = \sum_{\mathbf{i'}} \sum_{\mathbf{i''}} c_{\mathbf{i'},\mathbf{i''}} \zeta_{\mathbf{i}+\mathbf{i'}} \psi_{\mathbf{i}+\mathbf{i''}} \tag{3.2}$$

where now it is clear that the generic $\mathbf{i}$ index is defined as $\mathbf{i} = (i,j)$, $\mathbf{i'}, \mathbf{i''}$ can assume values in the set $A \times A$ with $A = \{0, 1, -1\}$, and of course $J_{\mathbf{i}}(\zeta,\psi) \equiv J(\zeta(x_i, y_j), \psi(x_i, y_j))$. In this explicit example it is easy to see the trick in writing linear equations: $c_{\mathbf{i'},\mathbf{i''}}$ are coefficients of the non-linear variable $\zeta\psi$, for this reason we don't have 9+9 non-linear unknowns but a linear system in the 81 unknows $c_{\mathbf{i'},\mathbf{i''}}$ (which correspond to the general coefficients $\widetilde{\phi}_{\mathbf{i}_1,\ldots,\mathbf{i}_N}$ of the original operator (3.1)).
It is useful to read again the Jacobian as Arakawa did:

$$J_{\mathbf{i}}(\zeta,\psi) = \sum_{\mathbf{i'}} a_{\mathbf{i},\mathbf{i}+\mathbf{i'}} \zeta_{\mathbf{i}+\mathbf{i'}}, \quad where \quad a_{\mathbf{i},\mathbf{i}+\mathbf{i'}} = \sum_{i''} c_{\mathbf{i'},\mathbf{i''}} \psi_{\mathbf{i}+\mathbf{i''}} \tag{3.3}$$

or

$$J_{\mathbf{i}}(\zeta,\psi) = \sum_{\mathbf{i''}} b_{\mathbf{i},\mathbf{i}+\mathbf{i''}} \psi_{\mathbf{i}+\mathbf{i''}} \quad where \quad b_{\mathbf{i},\mathbf{i}+\mathbf{i''}} = \sum_{\mathbf{i'}} c_{\mathbf{i'},\mathbf{i''}} \zeta_{\mathbf{i}+\mathbf{i'}} \tag{3.4}$$

in order to translate properties $a) - b) - c) - d)$ in terms of coefficients $a_{\mathbf{i'},\mathbf{i''}}$, $b_{\mathbf{i'},\mathbf{i''}}$, , $c_{\mathbf{i'},\mathbf{i''}}$. Indeed, discrete analogues of requirements $a) - b) - c) - d)$ are:

a) $J_{\mathbf{i}}(\zeta,\psi) = -J_{\mathbf{i}}(\psi,\zeta), \ \forall \mathbf{i}$:

$$\begin{aligned} \sum_{\mathbf{i'}} \sum_{\mathbf{i''}} c_{\mathbf{i'},\mathbf{i''}} \zeta_{\mathbf{i}+\mathbf{i'}} \psi_{\mathbf{i}+\mathbf{i''}} &= -\sum_{\mathbf{i'}} \sum_{\mathbf{i''}} c_{\mathbf{i'},\mathbf{i''}} \zeta_{\mathbf{i}+\mathbf{i''}} \psi_{\mathbf{i}+\mathbf{i'}} \\ &\Rightarrow c_{\mathbf{i'},\mathbf{i''}} = -c_{\mathbf{i''},\mathbf{i'}} \end{aligned} \tag{3.5}$$

b) $\sum_{\mathbf{i}} \zeta_{\mathbf{i}} J_{\mathbf{i}}(\zeta,\psi) = 0$:

$$\begin{aligned} \sum_{\mathbf{i}} \zeta_{\mathbf{i}} J_{\mathbf{i}}(\zeta,\psi) = \sum_{\mathbf{i}} \sum_{\mathbf{i'}} a_{\mathbf{i},\mathbf{i}+\mathbf{i'}} \zeta_{\mathbf{i}} \zeta_{\mathbf{i}+\mathbf{i'}} &= 0 \\ \Rightarrow a_{\mathbf{i}+\mathbf{i'},\mathbf{i}} &= -a_{\mathbf{i},\mathbf{i}+\mathbf{i'}} \end{aligned} \tag{3.6}$$

c) $\sum_{\mathbf{i}} \psi_{\mathbf{i}} J_{\mathbf{i}}(\zeta, \psi) = 0$:

$$\sum_{\mathbf{i}} \psi_{\mathbf{i}} J_{\mathbf{i}}(\zeta, \psi) = \sum_{\mathbf{i}} \sum_{\mathbf{i''}} b_{\mathbf{i},\mathbf{i+i''}} \psi_{\mathbf{i}} \psi_{\mathbf{i+i''}} = 0 \\ \Rightarrow b_{\mathbf{i+i'},\mathbf{i}} = -b_{\mathbf{i},\mathbf{i+i'}} \tag{3.7}$$

d) to obtain consistency we use Taylor expansion of equation (3.2) in each grid point (x_i, y_j):

$$J^T(\zeta, \psi) = \sum_{i',j'} \sum_{i'',j''} c_{i',j',i'',j''} [(\sum_{l=0}^{n-1} \sum_{m=0}^{n-1} \frac{(i'h)^l (j'h)^m}{l!m!} \frac{\partial^{l+m} \zeta(x_i, y_j)}{\partial x^l \partial y^m}) \\ (\sum_{l=0}^{n-1} \sum_{m=0}^{n-1} \frac{(i''h)^l (j''h)^m}{l!m!} \frac{\partial^{l+m} \psi(x_i, y_j)}{\partial x^l \partial y^m})] \tag{3.8}$$

With the help of a symbolic manipulator, we obtain linear equations for coefficients $c_{\mathbf{i'},\mathbf{i''}}$ nullifying any equation proportional to h^0, h^1, h^3, and we save only the contribution proportional to h^2 of the Jacobian, meaning $(\frac{\partial \zeta}{\partial x} \frac{\partial \psi}{\partial y})$ and $(\frac{\partial \zeta}{\partial y} \frac{\partial \psi}{\partial x})$.

Equations (3.5) and (3.8) are clearly written in terms of coefficients $c_{\mathbf{i'},\mathbf{i''}}$ while equations (3.6) and (3.7) are, respectively, in terms of $a_{\mathbf{i},\mathbf{i+i'}}$ and $b_{\mathbf{i},\mathbf{i+i''}}$. By definition (3.3)-(3.4) coefficients $a_{\mathbf{i},\mathbf{i+i'}}$ and $b_{\mathbf{i},\mathbf{i+i''}}$ are linear combinations of ψ and ζ, so that we can read equations (3.6) and (3.7) as system of equations in the unknowns $c_{\mathbf{i'},\mathbf{i''}}$.
It's worth noting that analytical identities from LHS to RHS of equations (2.14)-(2.15) are not exactly verified in the discrete space; as a matter of fact, with regards to enstrophy conservation, the identity is verified except for time derivative approximations, while for energy conservation we go through integration by parts:

$$\overline{(\nabla \psi) \cdot \frac{\partial (\nabla \psi)}{\partial t}} = -\overline{\psi \frac{\partial (\Delta \psi)}{\partial t}} \tag{3.9}$$

and then what we are actually imposing is the integral constraint

$$\overline{\psi J(\zeta, \psi)} = 0 \tag{3.10}$$

for energy conservation and

$$\overline{\zeta J(\zeta, \psi)} = 0 \tag{3.11}$$

for enstrophy conservation. We want to underline that this is just a possible choice, as well as the choice of imposing all requirements $a) - b) - c) - d)$; we could impose less properties to look for wider sets of solutions.
By imposing conditions $a) - b) - c) - d)$ we obtain a huge number of equations, but, using a symbolic manipulator, we can see that only 80 of them are linearly independent, meaning that the system exhibits ∞^1 solutions. We proved the following theorem:

Theorem 3.2.1. ***Non-uniqueness of Arakawa's Jacobian***

There exists a whole set of solutions for the discrete 2^{nd} order Jacobian which satisfies conservation of energy and enstrophy and skew-symmetric property; this set depends on one parameter, when the parameter is zero, we recover Arakawa's solution.

This discrete set of solutions can be written in each grid point $\mathbf{i} = (i, j)$ as:

$$J^s_{\mathbf{i}}(\zeta, \psi) = \vec{\psi_{\mathbf{i}}}^T S \vec{\zeta_{\mathbf{i}}} \tag{3.12}$$

where:

$$\vec{\psi_{\mathbf{i}}} = (\psi_{i+1,j+1}, \psi_{i+1,j}, \psi_{i+1,j-1}, \psi_{i,j+1}, \psi_{i,j}, \psi_{i,j-1}, \psi_{i-1,j+1}, \psi_{i-1,j}, \psi_{i-1,j-1})^T;$$
$$\vec{\zeta_{\mathbf{i}}} = (\zeta_{i+1,j+1}, \zeta_{i+1,j}, \zeta_{i+1,j-1}, \zeta_{i,j+1}, \zeta_{i,j}, \zeta_{i,j-1}, \zeta_{i-1,j+1}, \zeta_{i-1,j}, \zeta_{i-1,j-1})^T;$$

and

$$S = \frac{1}{12h^2} \begin{pmatrix} 0 & -s^- & 0 & s^- & 0 & 0 & 0 & 0 & 0 \\ s^- & 0 & s^+ & -s^+ & 0 & -s^- & 0 & 0 & 0 \\ 0 & -s^+ & 0 & 0 & 0 & s^+ & 0 & 0 & 0 \\ -s^- & s^+ & 0 & 0 & 0 & 0 & -s^+ & s^- & 0 \\ 0 & 0 & 0 & 0 & 0 & 0 & 0 & 0 & 0 \\ 0 & s^- & -s^+ & 0 & 0 & 0 & 0 & s^+ & -s^- \\ 0 & 0 & 0 & s^+ & 0 & 0 & 0 & -s^+ & 0 \\ 0 & 0 & 0 & -s^- & 0 & -s^+ & s^+ & 0 & s^- \\ 0 & 0 & 0 & 0 & 0 & s^- & 0 & -s^- & 0 \end{pmatrix}$$

with $s^- = s - 1$ and $s^+ = s + 1$.

3.2.1. Special cases: $s = \pm 1$

Let's start by analyzing the special case $s = 1$; the general scheme becomes:

$$\begin{aligned} J_{s=1}(\zeta, \psi) = \frac{1}{6h^2}\{&\zeta_{i+1,j}(\psi_{i,j+1} - \psi_{i+1,j-1}) - \zeta_{i-1,j}(\psi_{i,j-1} - \psi_{i-1,j+1}) \\ &+\zeta_{i,j+1}(\psi_{i-1,j+1} - \psi_{i+1,j}) - \zeta_{i,j-1}(\psi_{i+1,j-1} - \psi_{i-1,j}) \\ &+\zeta_{i+1,j-1}(\psi_{i+1,j} - \psi_{i,j-1}) - \zeta_{i-1,j+1}(\psi_{i-1,j} - \psi_{i,j+1})\} \end{aligned} \tag{3.13}$$

If we want to give a geometric reading of the special scheme (3.13), we can see that it uses grid points in figures (3.1)-(3.2) that we can read, respectively, as:

$$\zeta_x(\psi_y - \frac{\psi_x}{2}) - \zeta_y(\psi_x + \frac{\psi_y}{2}) \quad (figure\ 3.1)$$

$$(\zeta_x + \zeta_y)(\frac{\psi_x + \psi_y}{2}) \quad (figure\ 3.2)$$

which, combined, give rise to the Jacobian. With a better analysis, we can decompose such discretization as in figures (3.3-3.4-3.5 and (3.6):

Now it is clear the new reading of the scheme, adding and subtracting the ghost-node

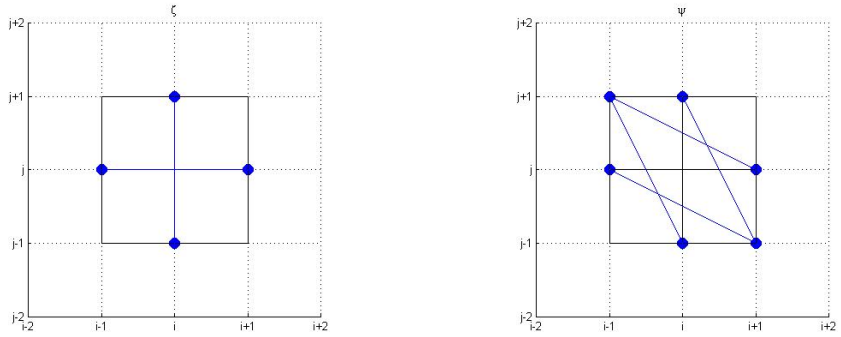

Figure 3.1.: $\zeta_x(\psi_y - \frac{\psi_x}{2}) - \zeta_y(\psi_x + \frac{\psi_y}{2})$

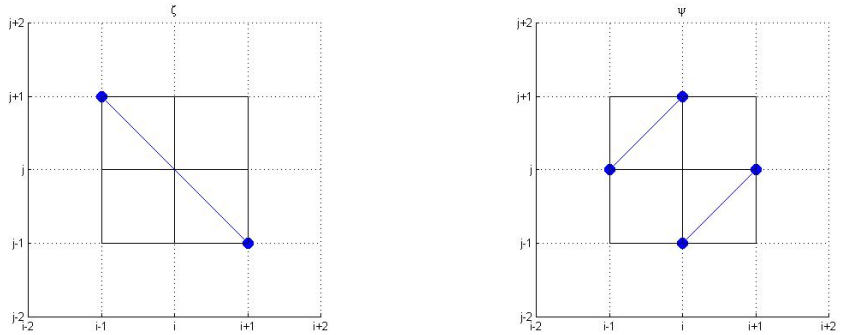

Figure 3.2.: $(\zeta_x + \zeta_y)(\frac{\psi_x+\psi_y}{2})$

(i, j):

$$
\begin{aligned}
J_{s=1}(\zeta,\psi) = \frac{1}{6h^2}\{&[(\zeta_{i+1,j}-\zeta_{i,j})(\psi_{i,j+1}-\psi_{i,j}+\psi_{i,j}-\psi_{i+1,j-1}) \\
&+(\zeta_{i,j}-\zeta_{i-1,j})(\psi_{i-1,j+1}-\psi_{i,j}+\psi_{i,j}-\psi_{i,j-1})] \quad (figure 3.7) \\
&-[(\zeta_{i,j+1}-\zeta_{i,j})(\psi_{i+1,j}-\psi_{i,j}+\psi_{i,j}-\psi_{i-1,j+1}) \\
&+(\zeta_{i,j}-\zeta_{i,j-1})(\psi_{i+1,j-1}-\psi_{i,j}+\psi_{i,j}-\psi_{i-1,j})] \quad (figure 3.8) \\
&-[(\psi_{i+1,j}-\psi_{i,j})(\zeta_{i,j}-\zeta_{i+1,j-1}) \\
&+(\psi_{i,j}-\psi_{i-1,j})(\zeta_{i-1,j+1}-\zeta_{i,j})] \quad (figure 3.9) \\
&+[(\psi_{i,j+1}-\psi_{i,j})(\zeta_{i,j}-\zeta_{i-1,j+1}) \\
&+(\psi_{i,j}-\psi_{i,j-1})(\zeta_{i+1,j-1}-\zeta_{i,j})]\} \quad (figure 3.10)\}
\end{aligned}
\tag{3.14}
$$

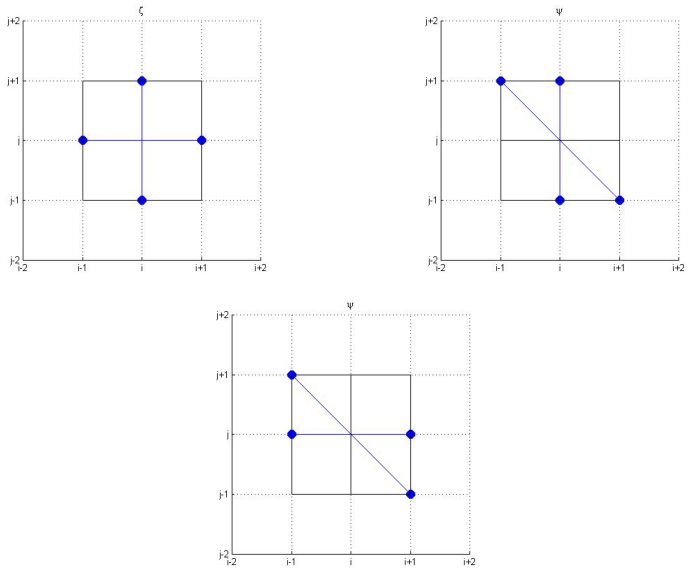

Figure 3.3.: $\zeta_x(\psi_y - \frac{\psi_x}{2}) - \zeta_y(\psi_x + \frac{\psi_y}{2})$

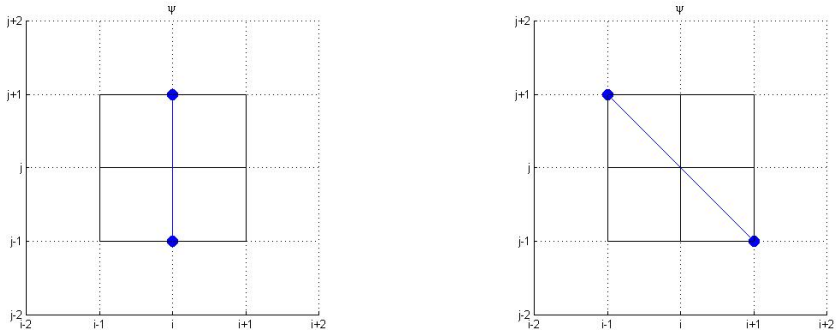

Figure 3.4.: Scomposizione di ψ_y

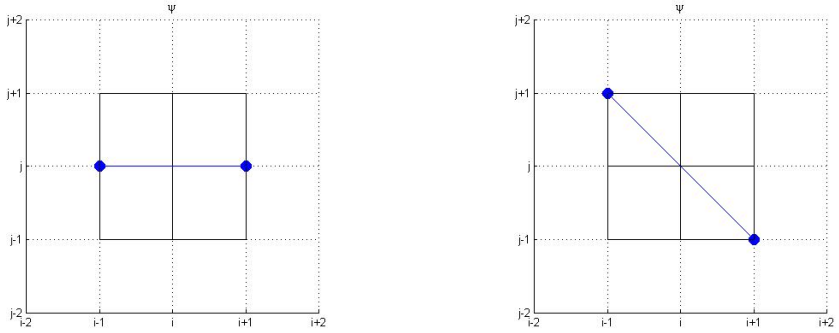

Figure 3.5.: Scomposizione di ψ_x

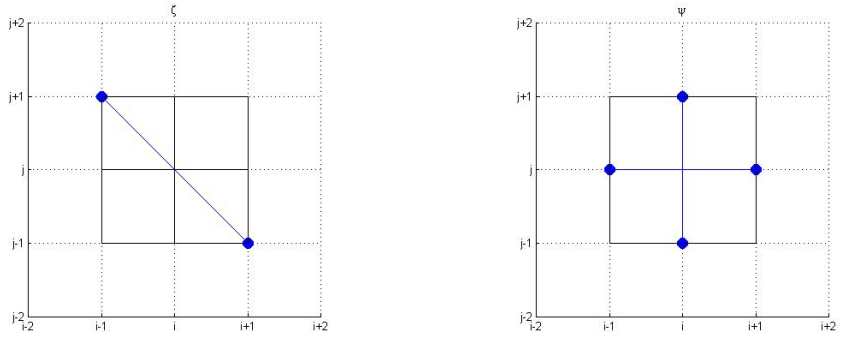

Figure 3.6.: $(\zeta_x + \zeta_y)(\frac{\psi_x+\psi_y}{2})$

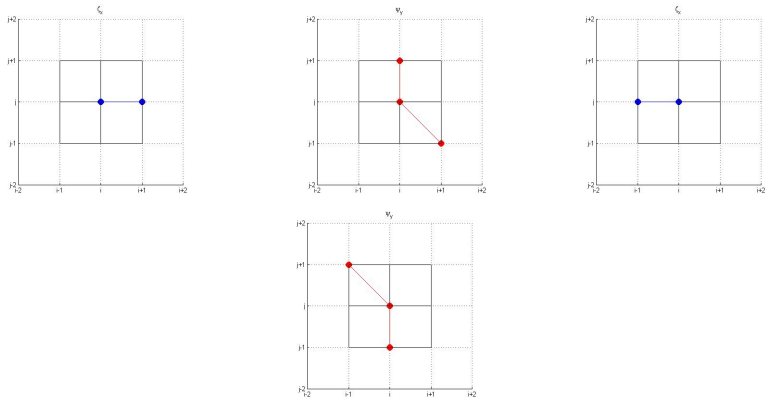

Figure 3.7.: $\zeta_x\psi_y$

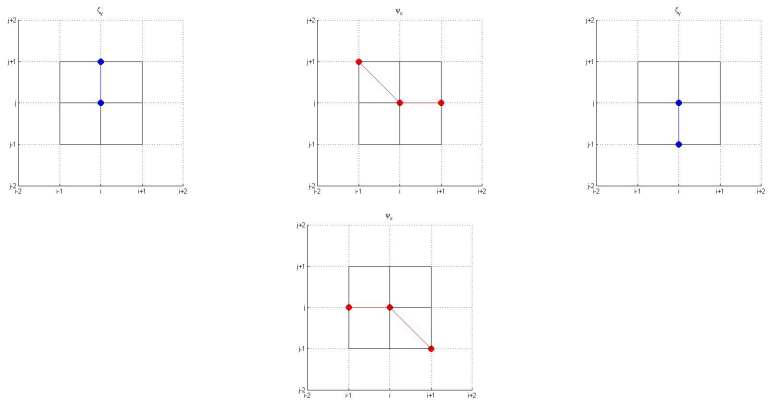

Figure 3.8.: $\zeta_y\psi_x$

The special case $s = -1$ is symmetric respect to $s = 1$ using the opposite diagonals:

$$\begin{aligned} J_{s=-1}(\zeta,\psi) = \frac{1}{6h^2}\{&\zeta_{i+1,j+1}(\psi_{i,j+1} - \psi_{i+1}) - \zeta_{i-1,j-1}(\psi_{i,j-1} - \psi_{i-1,j}) \\ &+\zeta_{i,j+1}(\psi_{i-1,j} - \psi_{i+1,j+1}) - \zeta_{i,j-1}(\psi_{i+1,j} - \psi_{i-1,j-1}) \\ &+\zeta_{i+1,j}(\psi_{i+1,j+1} - \psi_{i,j-1}) - \zeta_{i-1,j}(\psi_{i-1,j-1} - \psi_{i,j+1})\} \end{aligned} \tag{3.15}$$

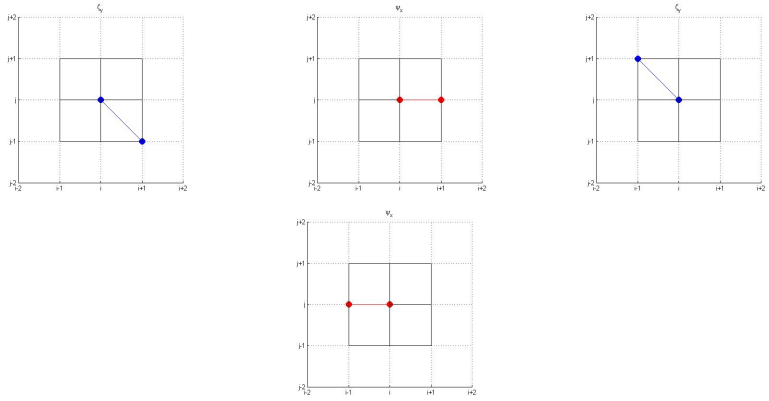

Figure 3.9.: $\zeta_y \psi_x$

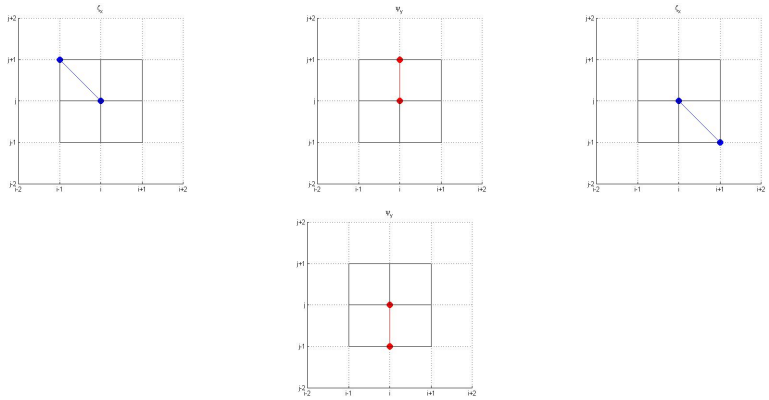

Figure 3.10.: $\zeta_x \psi_y$

and the grid points used are those in figures (3.11-3.12).

Remark 3.1. *As already noted, Arakawa's Jacobian is the linear combination of three different readings of the analytical Jacobian:*

- $\zeta_x \psi_y - \zeta_y \psi_x$
- $-\frac{\partial}{\partial x}(\zeta_y \psi) + \frac{\partial}{\partial y}(\zeta_x \psi)$
- $\frac{\partial}{\partial x}(\zeta \psi_y) - \frac{\partial}{\partial y}(\zeta \psi_x)$.

We can easily note that also the special cases $J_{s=1}$ and $J_{s=-1}$ are linear combination of such three readings, what changes is the way of discretization, the grid points used.

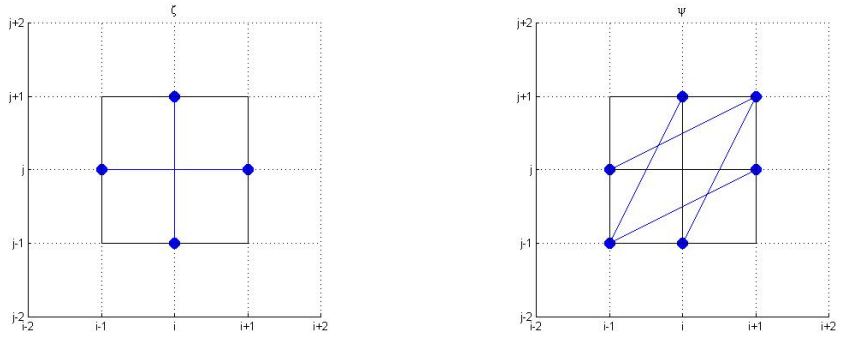

Figure 3.11.: $s = -1$

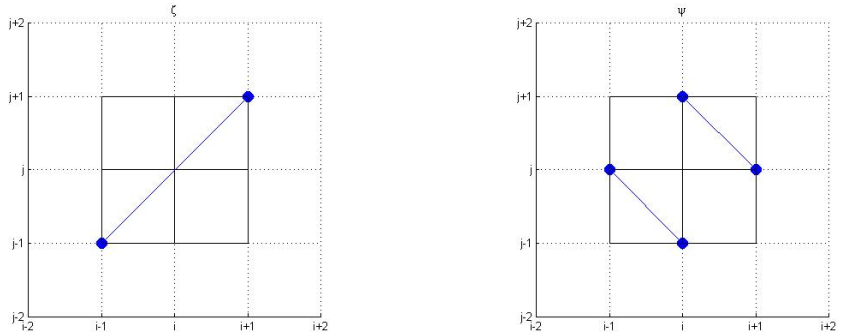

Figure 3.12.: $s = -1$

3.2.2. J_s and sub-solutions

The previous observation, leads to write the general Jacobian as

$$J_s = \frac{J_s^{(1)} + J_s^{(2)} + J_s^{(3)}}{3},$$

where:

$$\begin{aligned} J_s^{(1)}(\zeta,\psi) = \frac{1}{4h^2}\{&(\zeta_{i+1,j} - \zeta_{i-1,j})(\psi_{i,j+1} - \psi_{i,j-1}) \\ &+s(\zeta_{i+1,j} - 2\zeta_{i,j} + \zeta_{i,j-1})(\psi_{i+1,j} - 2\psi_{i,j} + \psi_{i,j-1}) \\ &-(\psi_{i+1,j} - \psi_{i-1,j})(\zeta_{i,j+1} - \zeta_{i,j-1}) \\ &-s(\psi_{i+1,j} - 2\psi_{ij} + \psi_{i,j-1})(\zeta_{i+1,j} - 2\zeta_{i,j} + \zeta_{i,j-1})\} \end{aligned} \tag{3.16}$$

$$\begin{aligned} J_s^{(2)}(\zeta,\psi) = \frac{1}{4h^2}\{&-(\psi_{i+1,j}[(\zeta_{i+1,j+1}-\zeta_{i+1,j-1}) - s(\zeta_{i+1,j+1}-2\zeta_{i,j}+\zeta_{i+1,j-1})] \\ &-\psi_{i-1,j}[(\zeta_{i-1,j+1}-\zeta_{i-1,j-1}) + s(\zeta_{i-1,j+1}-2\zeta_{i,j}+\zeta_{i-1,j-1})]) \\ &+\psi_{i,j+1}[(\zeta_{i+1,j+1}-\zeta_{i-1,j+1}) - s(\zeta_{i+1,j+1}-2\zeta_{i,j}+\zeta_{i-1,j+1})] \\ &-\psi_{i,j-1}[(\zeta_{i+1,j-1}-\zeta_{i-1,j-1}) + s(\zeta_{i+1,j-1}-2\zeta_{i,j}+\zeta_{i-1,j-1})]\} \end{aligned} \tag{3.17}$$

$$\begin{aligned} J_s^{(3)}(\zeta,\psi) = \frac{1}{4h^2}\{&\zeta_{i+1,j}[(\psi_{i+1,j+1}-\psi_{i+1,j-1}) - b(\psi_{i+1,j+1}-2\psi_{i,j}+\psi_{i+1,j-1})] \\ &-\zeta_{i-1,j}[(\psi_{i-1,j+1}-\psi_{i-1,j-1}) + s(\psi_{i-1,j+1}-2\psi_{i,j}+\psi_{i-1,j-1})] \\ &-(\zeta_{i,j+1}[(\psi_{i+1,j+1}-\psi_{i-1,j+1}) - s(\psi_{i+1,j+1}-2\psi_{i,j}+\psi_{i-1,j+1})] \\ &-\zeta_{i,j-1}[(\psi_{i+1,j-1}-\psi_{i-1,j-1}) + s(\psi_{i+1,j-1}-2\psi_{i,j}+\psi_{i-1,j-1})])\} \end{aligned} \tag{3.18}$$

The truncation error shows that only in the special case $s = 0$, each of the three Jacobian is consistent, while, in general only $J_s^{(1)}$ and $(J_s^{(2)} + J_s^{(3)})/2$ mantain consistency:

$$\begin{aligned} J_s^{T(1)} = &(\psi_y\zeta_x - \psi_x\zeta_y) \\ &+h^2(\frac{1}{6}(\psi_y\zeta_{xxx} - \psi_{xxx}\zeta_y - \psi_x\zeta_{yyy} + \psi_{yyy}\zeta_x) - \frac{s}{4}(\psi_{xx}\zeta_{yy} + \psi_{yy}\zeta_{xx})) \\ &+h^4(\frac{1}{36}(\psi_{yyy}\zeta_{xxx} - \psi_{xxx}\zeta_{yyy}) + \frac{s}{48}(\psi_{yy}\zeta_{xxxx} - \psi_{xxxx}\zeta_{yy} - \psi_{xx}\zeta_{yyyy} + \psi_{yyyy}\zeta_{xx})) \\ &+h^6\frac{s}{576}(\psi_{yyyy}\zeta_{xxxx} - \psi_{xxxx}\zeta_{yyyy}) \end{aligned} \tag{3.19}$$

$$
\begin{aligned}
J_s^{T(2)} = (\psi_y\zeta_x - \psi_x\zeta_y) + s(\psi_x\zeta_x - \psi_y\zeta_y) \\
+h^2(\frac{1}{6}(\psi_y\zeta_{xxx} - 3\psi_x\zeta_{xxy} - 3\psi_{xx}\zeta_{xy} - \psi_{xxx}\zeta_y - \psi_x\zeta_{yyy} + 3\psi_y\zeta_{yyx} + 3\psi_{yy}\zeta_{xy} + \psi_{yyy}\zeta_x) \\
+\frac{s}{12}(3\psi_{xx}\zeta_{yy} - 3\psi_{yy}\zeta_{xx} + 2\psi_x\zeta_{xxx} + 3\psi_{xx}\zeta_{xx} + 2\psi_{xxx}\zeta_x \\
+6\psi_x\zeta_{yyx} - 6\psi_y\zeta_{xxy} - 2\psi_y\zeta_{yyy} - 3\psi_{yy}\zeta_{yy} - 2\psi_{yyy}\zeta_y)) \\
+h^4(\frac{1}{72}(6\psi_{yy}\zeta_{xxxy} - 6\psi_{xxx}\zeta_{xxy} - 3\psi_{xxxx}\zeta_{xy} - 6\psi_{xx}\zeta_{yyyx} - 6\psi_{xx}\zeta_{xxxy} \\
-2\psi_{xxx}\zeta_{yyy} + 2\psi_{yyy}\zeta_{xxx} + 6\psi_{yy}\zeta_{yyyx} + 6\psi_{yyy}\zeta_{yyx} + 3\psi_{yyyy}\zeta_{xy}) \\
+\frac{s}{144}(3\psi_{xx}\zeta_{xxxx} + 4\psi_{xxx}\zeta_{xxx} + 3\psi_{xxxx}\zeta_{xx} + 18\psi_x x\zeta_{xxyy} \\
-3\psi_{yy}\zeta_{xxxx} + 12\psi_{xxx}\zeta_{yyx} + 3\psi_{xxxx}\zeta_{yy} + 3\psi_{xx}\zeta_{yyyy} - 18\psi_{yy}\zeta_{xxyy} \\
-12\psi_{yyy}\zeta_{xxy} - 3\psi_{yyyy}\zeta_{xx} - 3\psi_{yy}\zeta_{yyyy} - 4\psi_{yyy}\zeta_{yyy} - 3\psi_{yyyy}\zeta_{yy})) \\
+\frac{h^6}{576}(4\psi_{yyyy}\zeta_{xxxy} - 4\psi_{xxxx}\zeta_{yyyx} - 4\psi_{xxxx}\zeta_{xxxy} + 4\psi_{yyyy}\zeta_{yyyx} \\
+s(\psi_{xxxx}\zeta_{xxxx} + 6\psi_{xxxx}\zeta_{xxyy} + \psi_{xxxx}\zeta_{yyyy} - \psi_{yyyy}\zeta_{xxxx} - 6\psi_{yyyy}\zeta_{xxyy} - \psi_{yyyy}\zeta_{yyyy}))
\end{aligned}
\tag{3.20}
$$

$$
\begin{aligned}
J_s^{T(3)} = (-\zeta_y\psi_x + \zeta_x\psi_y) - s(\zeta_x\psi_x - \zeta_y\psi_y) \\
-h^2(\frac{1}{6}(\zeta_y\psi_{xxx} - 3\zeta_x\psi_{xxy} - 3\zeta_{xx}\psi_{xy} - \zeta_{xxx}\psi_y - \zeta_x\psi_{yyy} + 3\zeta_y\psi_{yyx} + 3\zeta_{yy}\psi_{xy} + \zeta_{yyy}\psi_x) \\
+\frac{s}{12}(3\zeta_{xx}\psi_{yy} - 3\zeta_{yy}\psi_{xx} + 2\zeta_x\psi_{xxx} + 3\zeta_{xx}\psi_{xx} + 2\zeta_{xxx}\psi_x \\
+6\zeta_x\psi_{yyx} - 6\zeta_y\psi_{xxy} - 2\zeta_y\psi_{yyy} - 3\zeta_{yy}\psi_{yy} - 2\zeta_{yyy}\psi_y)) \\
-h^4(\frac{1}{72}(6\zeta_{yy}\psi_{xxxy} - 6\zeta_{xxx}\psi_{xxy} - 3\zeta_{xxxx}\psi_{xy} - 6\zeta_{xx}\psi_{yyyx} - 6\zeta_{xx}\psi_{xxxy} \\
-2\zeta_{xxx}\psi_{yyy} + 2\zeta_{yyy}\psi_{xxx} + 6\zeta_{yy}\psi_{yyyx} + 6\zeta_{yyy}\psi_{yyx} + 3\zeta_{yyyy}\psi_{xy}) \\
+\frac{s}{144}(3\zeta_{xx}\psi_{xxxx} + 4\zeta_{xxx}\psi_{xxx} + 3\zeta_{xxxx}\psi_{xx} + 18\zeta_{xx}\psi_{xxyy} \\
-3\zeta_{yy}\psi_{xxxx} + 12\zeta_{xxx}\psi_{yyx} + 3\zeta_{xxxx}\psi_{yy} + 3\zeta_{xx}\psi_{yyyy} - 18\zeta_{yy}\psi_{xxyy} \\
-12\zeta_{yyy}\psi_{xxy} - 3\zeta_{yyyy}\psi_{xx} - 3\zeta_{yy}\psi_{yyyy} - 4\zeta_{yyy}\psi_{yyy} - 3\zeta_{yyyy}\psi_{yy})) \\
-\frac{h^6}{576}(4\zeta_{yyyy}\psi_{xxxy} - 4\zeta_{xxxx}\psi_{yyyx} - 4\zeta_{xxxx}\psi_{xxxy} + 4\zeta_{yyyy}\psi_{yyyx} \\
+s(\zeta_{xxxx}\psi_{xxxx} + 6\zeta_{xxxx}\psi_{xxyy} + \zeta_{xxxx}\psi_{yyyy} - \zeta_{yyyy}\psi_{xxxx} - 6\zeta_{yyyy}\psi_{xxyy} - \zeta_{yyyy}\psi_{yyyy}))
\end{aligned}
\tag{3.21}
$$

The global truncation error is then:

$$\begin{aligned} J^s(\zeta,\psi) &= \psi_y\zeta_x - \psi_x\zeta_y \\ &+\frac{h^2}{6}[\psi_y\zeta_{xxx} - \psi_x\zeta_{xxy} - \psi_{xx}\zeta_{xy} + \psi_{xy}\zeta_{xx} - \psi_{xxx}\zeta_y + \psi_{xxy}\zeta_x \\ &-\psi_x\zeta_{yyy} + \psi_y\zeta_{yyx} - \psi_{xy}\zeta_{yy} + \psi_{yy}\zeta_{xy} - \psi_{yyx}\zeta_y + \psi_{yyy}\zeta_x \\ &+\frac{s}{2}(2\psi_x\zeta_{yyx} - 2\psi_y\zeta_{xxy} + \psi_{xx}\zeta_{yy} - \psi_{yy}\zeta_{xx} + 2\psi_{xxy}\zeta_y - 2\psi_{yyx}\zeta_x)] \\ &+O(h^4). \end{aligned} \tag{3.22}$$

In a more compact form, we can read the general scheme as Arakawa's Jacobian plus a term depending on the parameter:

$$J_s = J_A + s\tilde{J} \tag{3.23}$$

where

$$\begin{aligned} \tilde{J} = &\zeta_{i,j+1}(\psi_{i+1,j+1} + \psi_{i-1,j+1} - \psi_{i+1,j} - \psi_{i-1,j}) \\ &+\zeta_{i,j-1}(\psi_{i+1,j-1} + \psi_{i-1,j-1} - \psi_{i+1,j} - \psi_{i-1,j}) \\ &-\zeta_{i+1,j}(\psi_{i+1,j+1} + \psi_{i+1,j-1} - \psi_{i,j+1} - \psi_{i,j-1}) \\ &-\zeta_{i-1,j}(\psi_{i-1,j+1} + \psi_{i-1,j-1} - \psi_{i,j+1} - \psi_{i,j-1}) \\ &+\zeta_{i+1,j+1}(\psi_{i+1,j} - \psi_{i,j+1}) \\ &+\zeta_{i+1,j-1}(\psi_{i+1,j} - \psi_{i,j-1}) \\ &+\zeta_{i-1,j+1}(\psi_{i-1,j} - \psi_{i,j+1}) \\ &+\zeta_{i-1,j-1}(\psi_{i-1,j} - \psi_{i,j-1}) \end{aligned} \tag{3.24}$$

3.2.2.1. Different sets of solutions

As outlined before, many classes of possible solutions arise: one possible choice is the family of skew-symmetric 2nd-order Jacobians. To obtain this special set of schemes we should impose only conditions a) and d), obtaining a wider family of solutions depending on many parameters. Here we observe that the special cases presented in the previous section $J_s^{(1)}$ and $(J_s^{(2)} + J_s^{(3)})/2$ belong to this subset. For semplicity, we will rename them as:

$$J^{s+}(\zeta,\psi) = J_s^{(1)} \tag{3.25}$$

and

$$\begin{aligned} J^{s*}(\zeta,\psi) = (J_s^{(2)} + J_s^{(3)})/2 = \frac{1}{8h^2} \\ \{-(\psi_{i+1,j}[(\zeta_{i+1,j+1} - \zeta_{i+1,j-1}) - s(\zeta_{i+1,j+1} + \zeta_{i+1,j-1})] \\ -\psi_{i-1,j}[(\zeta_{i-1,j+1} - \zeta_{i-1,j-1}) + s(\zeta_{i-1,j+1} + \zeta_{i-1,j-1})]) \\ +\psi_{i,j+1}[(\zeta_{i+1,j+1} - \zeta_{i-1,j+1}) - s(\zeta_{i+1,j+1} + \zeta_{i-1,j+1})] \\ -\psi_{i,j-1}[(\zeta_{i+1,j-1} - \zeta_{i-1,j-1}) + s(\zeta_{i+1,j-1} + \zeta_{i-1,j-1})] \\ +\zeta_{i+1,j}[(\psi_{i+1,j+1} - \psi_{i+1,j-1}) - s(\psi_{i+1,j+1} + \psi_{i+1,j-1})] \\ -\zeta_{i-1,j}[(\psi_{i-1,j+1} - \psi_{i-1,j-1}) + s(\psi_{i-1,j+1} + \psi_{i-1,j-1})] \\ -(\zeta_{i,j+1}[(\psi_{i+1,j+1} - \psi_{i-1,j+1}) - s(\psi_{i+1,j+1} + \psi_{i-1,j+1})] \\ -\zeta_{i,j-1}[(\psi_{i+1,j-1} - \psi_{i-1,j-1}) + s(\psi_{i+1,j-1} + \psi_{i-1,j-1})])\} \end{aligned} \tag{3.26}$$

refering to the grid points that they use.
We summarize some examples of different subsets of solutions in table (3.12) and, in the next section, we will show their different behaviors.

Table 3.12.: Examples of 2nd order Jacobians with different properties

Skew-symmetric	Enstrophy Conserving	Energy Conserving
J^s	J^s	J^s
J^{s*}	$(J^{+\times} + J^{++})/2$	$(J^{\times+} + J^{++})/2$
J^{s+}	$J^{\times+}$	$J^{+\times}$

3.2.3. Analysis of the general scheme

3.2.3.1. Error analysis in the physical space

Let's consider now the special case where the velocity field is assumed to be constant, $(k_1, k_2) = (u, v)$, meaning $\psi(x, y) = -uy + vx$. In terms of truncation error, this corresponds to:

$$\begin{aligned} R_s &= \frac{h^2}{6}[-(u\zeta_{xxx} + u\zeta_{yyx} + v\zeta_{xxy} + v\zeta_{yyy}) + s(v\zeta_{yyx} + u\zeta_{xxy})] \\ &= \frac{h^2}{6}[-u\zeta_{xxx} - v\zeta_{yyy} + \zeta_{yyx}(sv - u) + \zeta_{xxy}(su - v)]. \end{aligned} \tag{3.27}$$

Remark 3.2. *For the special case $s = 0$ some terms nullify. If we consider a general s, we observe that some choice will make disappear mixed terms, in particular:*

- $(u, v) = (k, k)$

In this case the best choice is $s = 1$, the resulting truncation error is:

$$R_s = \frac{h^2}{6}[k(-\zeta_{xxx} - \zeta_{yyy})]. \tag{3.28}$$

- $(u, v) = (k, -k)$
  In this case the best choice is $s = -1$, the resulting truncation error is:

$$R_s = \frac{h^2}{6}[k(\zeta_{yyy} - \zeta_{xxx})]. \tag{3.29}$$

To eliminate one or another mixed derivative, I should check $s = \frac{u}{v}$ or $s = \frac{v}{u}$.

3.2.3.2. Error analysis in the Fourier space

In this section we focus on the modified wave number (MWN); we will consider the special case (advection equation) where the velocity field is constant but the stream function and the vorticity function are not correlated and they can be expressed as:

$$\begin{aligned} \psi(x, y) &= -uy + vx \\ \zeta(x, y) &= \overline{\zeta} e^{i(mx+ny)}. \end{aligned} \tag{3.30}$$

For this particular choice, the analytical Jacobian results to be:

$$J(\zeta, \psi) = -i(mu + nv)\zeta(x, y) \tag{3.31}$$

while the discrete Jacobian, J_s (with $mx \to mjh = j\alpha$, $ny \to nlh = l\beta$):

$$\begin{aligned} J_s(\zeta, \psi) = i\frac{\zeta(x, y)}{3h}[&-v(2sin(\beta) + sin(\beta)cos(\alpha)) - u(2sin(\alpha) + sin(\alpha)cos(\beta)) \\ &+s(v(-sin(\alpha) + sin(\alpha)cos(\beta)) - u(sin(\beta) - sin(\beta)cos(\alpha)))] \end{aligned} \tag{3.32}$$

Similar to the physical space, also for the modified wave number we observe that there are special choices where some terms nullify. We have, again:

- $(u, v) = (\tilde{u}, \tilde{u})$
  In this case the best choice to nullify mixed terms is $s = 1$, the resulting MWN is:

$$J_s(\zeta, \psi) = \frac{-\tilde{u}\zeta(x, y)}{h}[sin(\beta) + sin(\alpha)] \tag{3.33}$$

- $(u, v) = (\tilde{u}, -\tilde{u})$
  In this case the best choice to nullify mixed terms is $s = -1$, the resulting MWN is:

$$J_s(\zeta, \psi) = \frac{\tilde{u}\zeta(x, y)}{h}[sin(\beta) - sin(\alpha)] \tag{3.34}$$

Clearly, these choices are not meant to be the best, because we imposed only that mixed terms nullify which does not necessarily mean a minimization of the error, as we will see in the following analysis.
I will now present some plots: firsts represent the 2D projection of the difference between real and modified wave numbers, while in the 3D plot I will show separately real and MWN. In both case I will show the dependence from the parameter.

2D plots comparing analytical and modified wave numbers

a) Case (u,v)=(0,1)

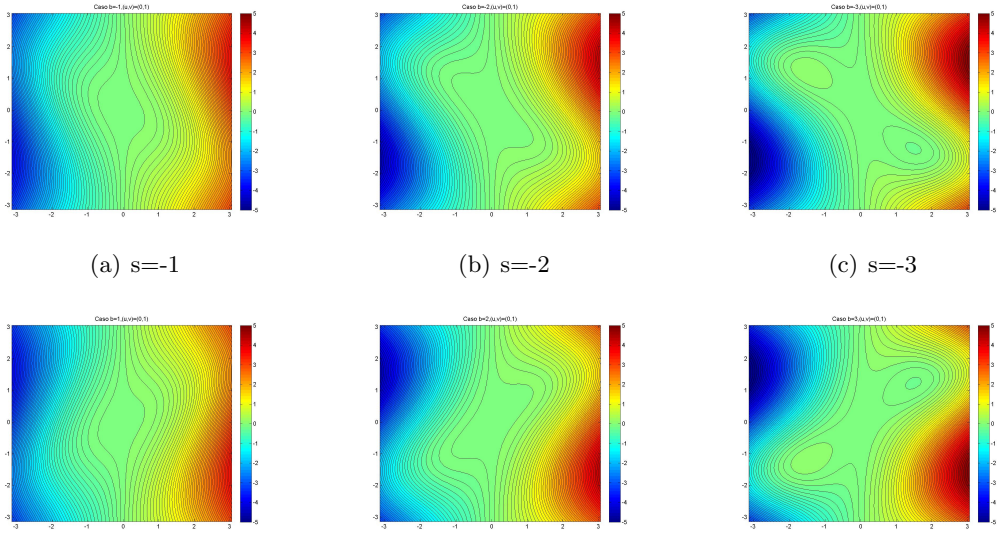

(a) s=-1 (b) s=-2 (c) s=-3

(d) s=1 (e) s=2 (f) s=3

Figure 3.13.: MWN - ((u,v)=(0,1))

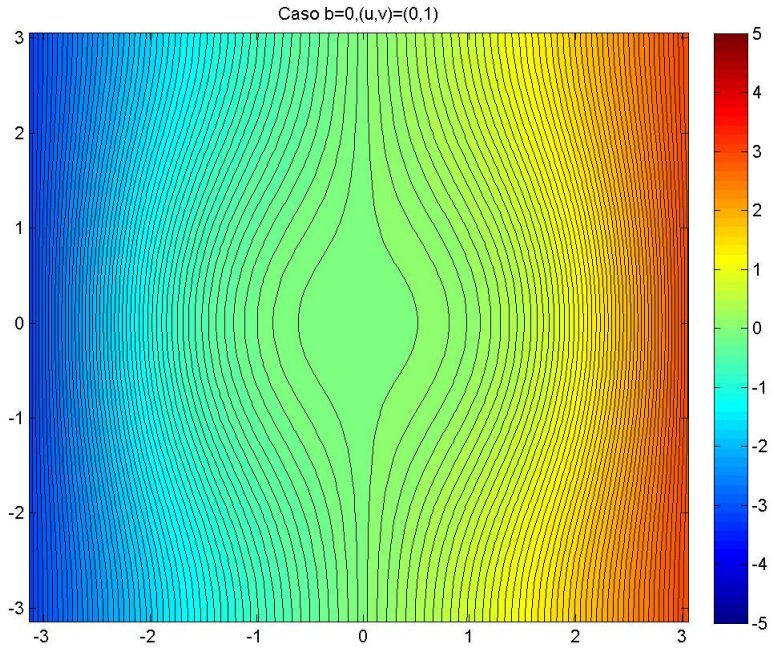

Figure 3.14.: MWN - ((u,v)=(0,1)) - Arakawa

b) Case (u,v)=(1,1)

c) Case (u,v)=(-1,1)

d) Case (u,v)=(1,$\frac{1}{2}$)

e) Case (u,v)=(1,$\frac{1}{4}$)

3D plots comparing analytical and modified wave numbers

For the 3D plot I will show, as example, only the case $(u, v) = (-1, 1)$.

Error comparison for different choices of the parameter

We can summarize the analys defining the four squared domains:

- $A = [-\frac{\pi}{6}, \frac{\pi}{6}] \times [-\frac{\pi}{6}, \frac{\pi}{6}]$
- $B = [-\frac{\pi}{4}, \frac{\pi}{4}] \times [-\frac{\pi}{4}, \frac{\pi}{4}]$
- $C = [-\frac{\pi}{2}, \frac{\pi}{2}] \times [-\frac{\pi}{2}, \frac{\pi}{2}]$
- $D = [-\frac{2\pi}{3}, \frac{2\pi}{3}] \times [-\frac{2\pi}{3}, \frac{2\pi}{3}]$

and the following error limitations on the MWN:

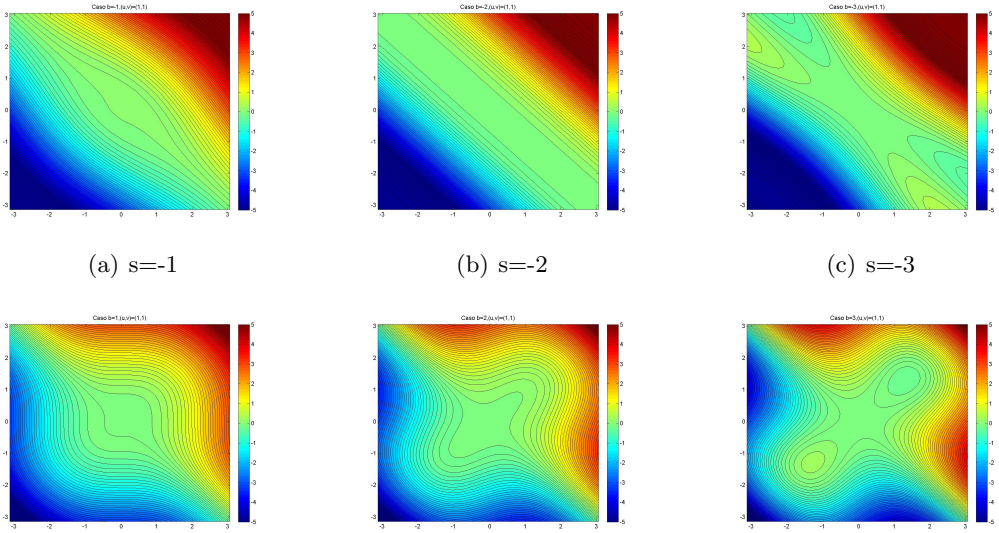

(a) s=-1 (b) s=-2 (c) s=-3

(d) s=1 (e) s=2 (f) s=3

Figure 3.15.: MWN - ((u,v)=(1,1))

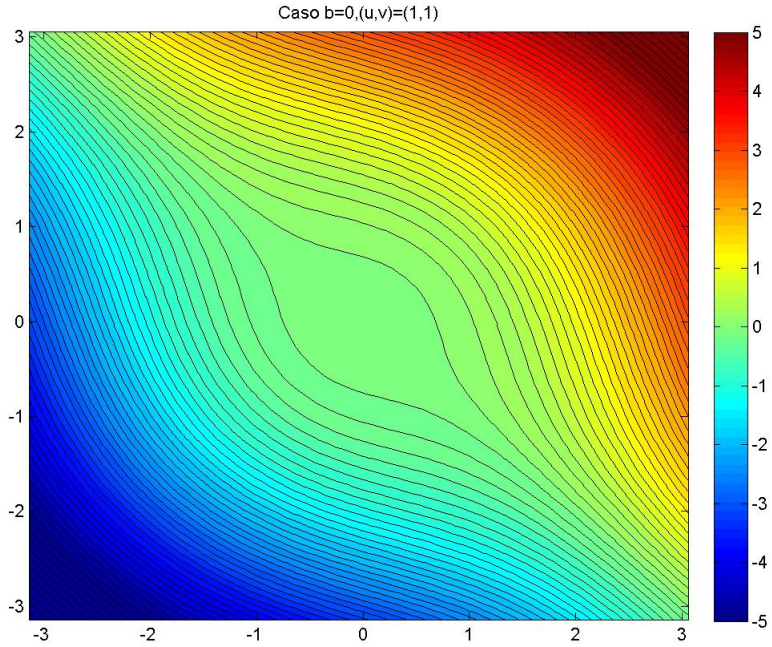

Figure 3.16.: MWN - ((u,v)=(1,1)) - Arakawa

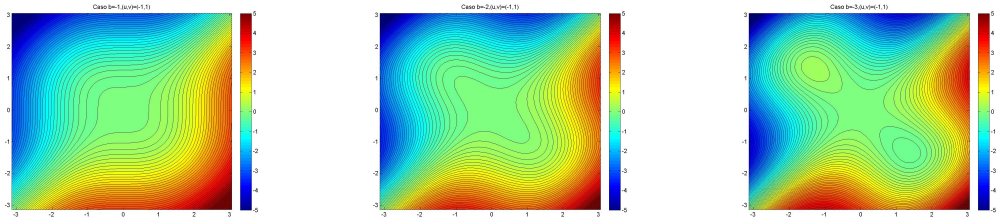

(a) s=-1 (b) s=-2 (c) s=-3

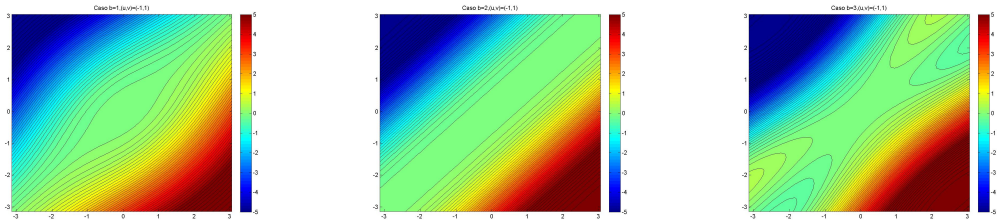

(d) s=1 (e) s=2 (f) s=3

Figure 3.17.: MWN - ((u,v)=(-1,1))

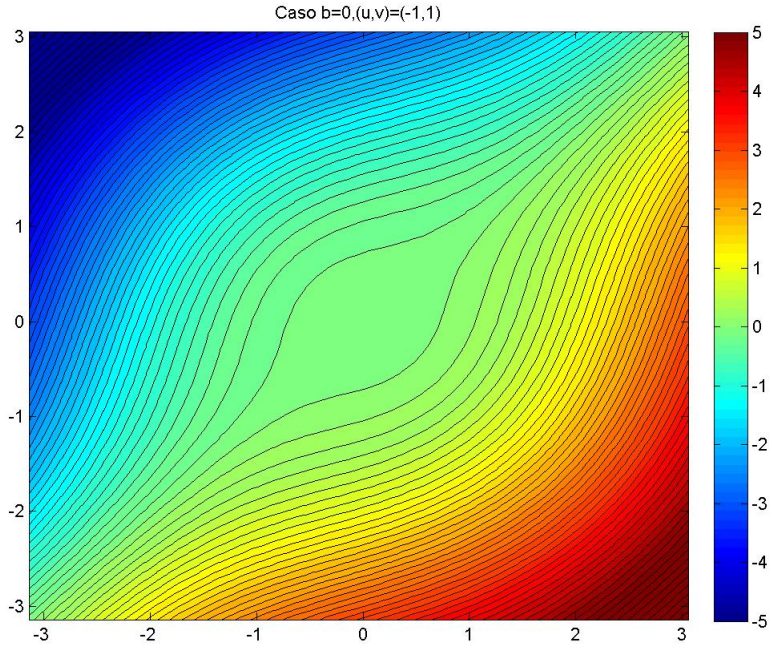

Figure 3.18.: MWN - ((u,v)=(-1,1)) - Arakawa

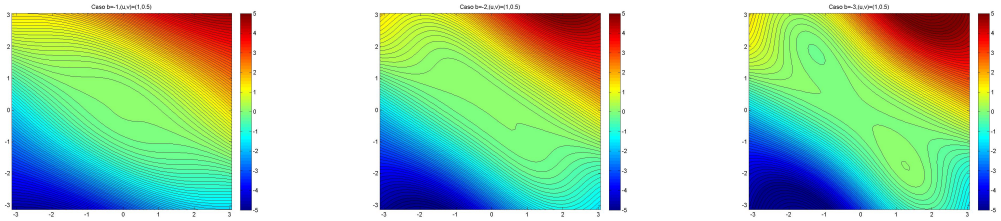

(a) s=-1 (b) s=-2 (c) s=-3

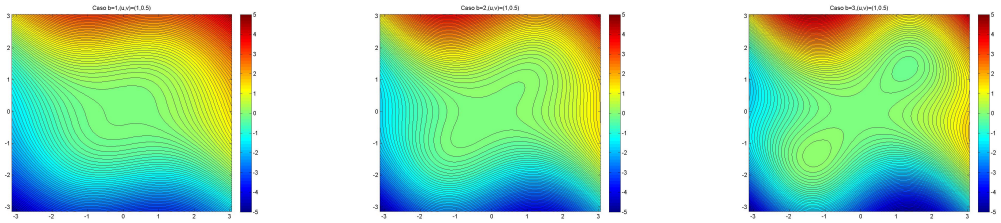

(d) s=1 (e) s=2 (f) s=3

Figure 3.19.: MWN - ((u,v)=$(1,\frac{1}{2})$)

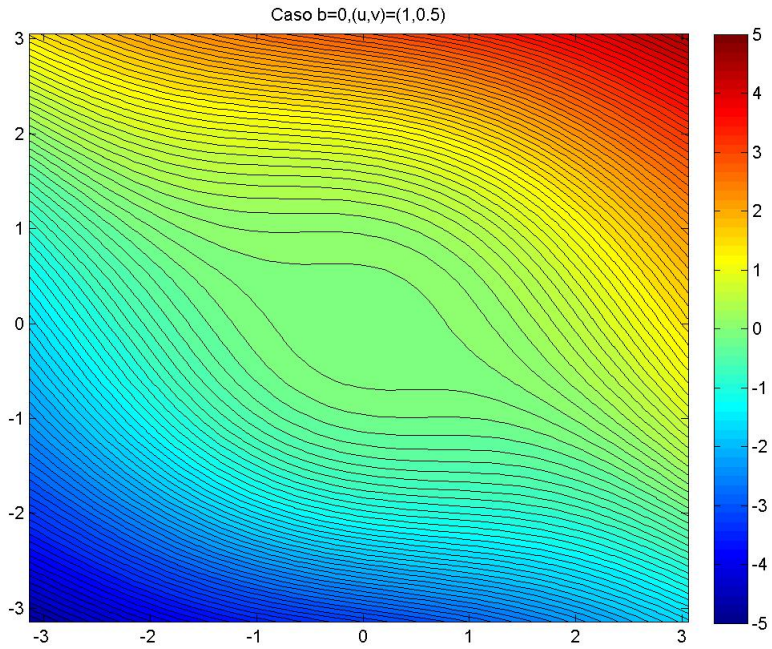

Figure 3.20.: MWN - ((u,v)=$(1,\frac{1}{2})$) - Arakawa

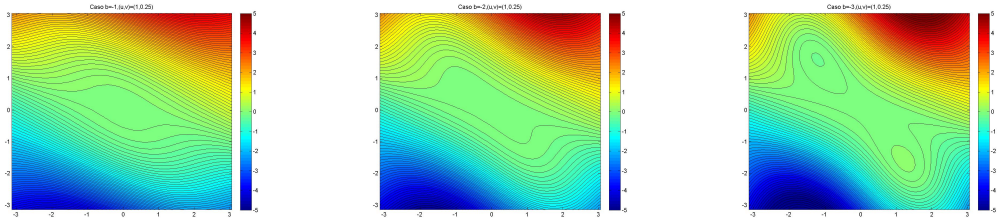

(a) s=-1 (b) s=-2 (c) s=-3

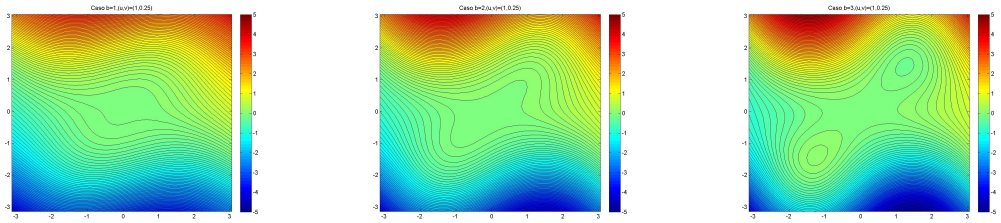

(d) s=1 (e) s=2 (f) s=3

Figure 3.21.: MWN - ((u,v)=$(1,\frac{1}{4})$)

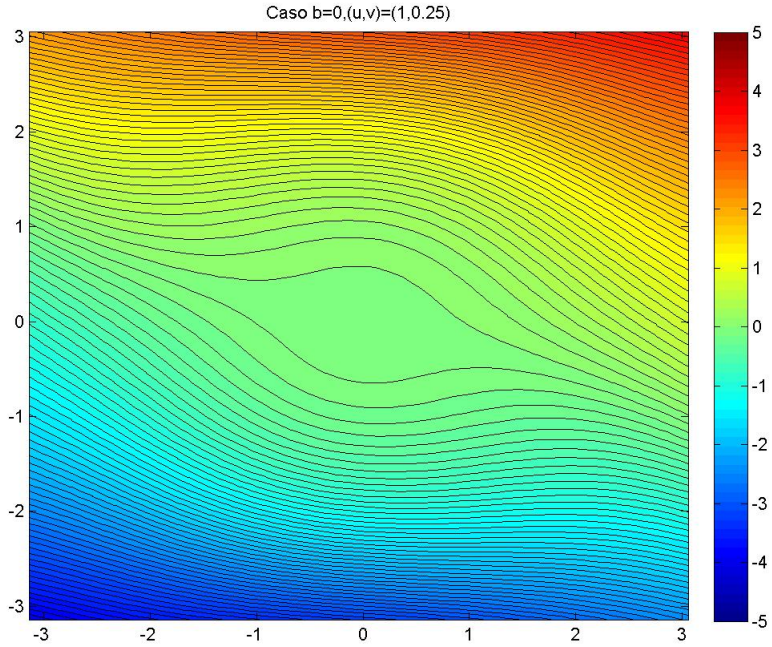

Figure 3.22.: MWN - ((u,v)=$(1,\frac{1}{4})$) - Arakawa

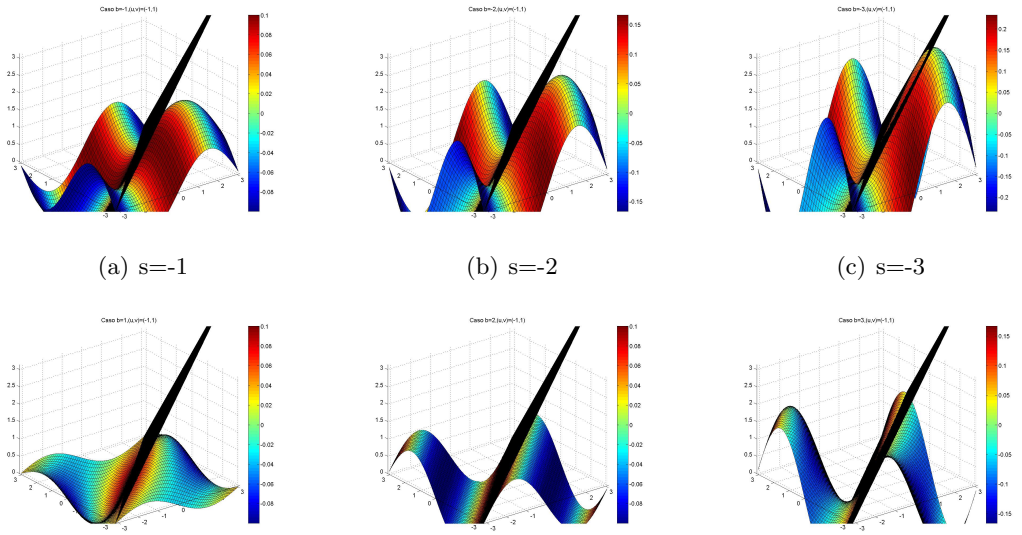

(a) s=-1 (b) s=-2 (c) s=-3

(d) s=1 (e) s=2 (f) s=3

Figure 3.23.: MWN 3D - ((u,v)=(-1,1))

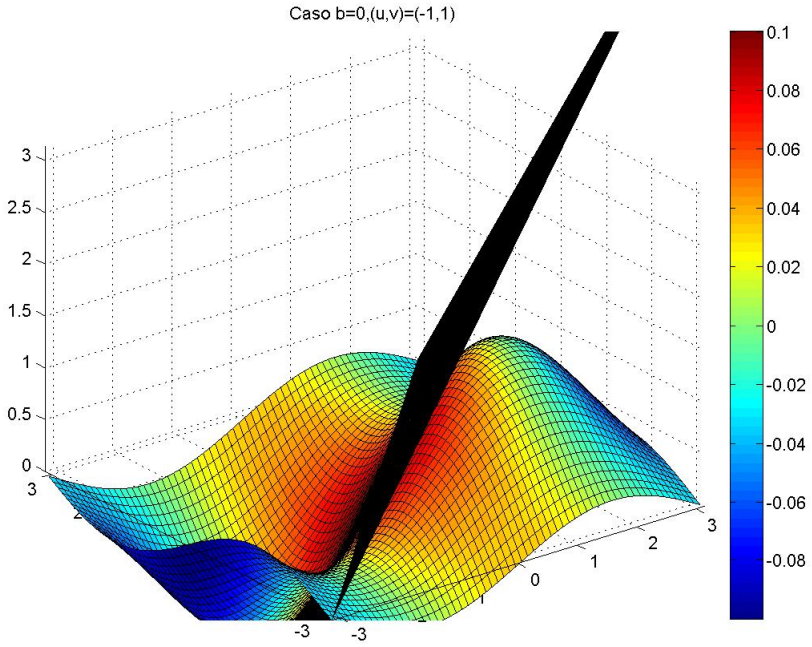

Figure 3.24.: MWN 3D - ((u,v)=(-1,1)) - Arakawa

- Case i) $\Omega - \tilde{\Omega} < a$
  where $a = 1, 2, 15, 30$ is expressed as percentage respect to Ω, for $\vec{x}$ respectively belonging to A, B, C, D;

(u,v)/s	**-5**	**-4**	**-3**	**-2**	**-1**	**0**	**1**	**2**	**3**	**4**	**5**
(1,1)								√	√		
(1,-1)			√	√							
(-1,1)			√	√							
(-1,-1)								√	√		
(0,1)											
(1,0)											
(0,-1)											
(-1,0)											
(1,$\frac{1}{2}$)							√				
(1,-$\frac{1}{2}$)					√						
(-1,$\frac{1}{2}$)					√						
(-1,-$\frac{1}{2}$)							√				
($\frac{1}{2}$,1)							√				
($\frac{1}{2}$,-1)					√						
(-$\frac{1}{2}$,1)					√						
(-$\frac{1}{2}$,-1)							√				

- Case ii) $\Omega - \tilde{\Omega} < b$
  where $b = 2, 3, 20, 35$ is expressed as percentage respect to Ω, for $\vec{x}$ respectively belonging to A, B, C, D;

(u,v)/s	**-5**	**-4**	**-3**	**-2**	**-1**	**0**	**1**	**2**	**3**	**4**	**5**
(1,1)								√	√		
(1,-1)			√	√							
(-1,1)			√	√							
(-1,-1)								√	√		
(0,1)						√					
(1,0)						√					
(0,-1)						√					
(-1,0)						√					
(1,$\frac{1}{2}$)							√	√	√		
(1,-$\frac{1}{2}$)			√	√	√						
(-1,$\frac{1}{2}$)			√	√	√						
(-1,-$\frac{1}{2}$)							√	√	√		
($\frac{1}{2}$,1)							√	√	√		
($\frac{1}{2}$,-1)			√	√	√						
(-$\frac{1}{2}$,1)			√	√	√						
(-$\frac{1}{2}$,-1)							√	√	√		

- Case iii) $\Omega - \tilde{\Omega} < c$
  where $c = 3, 5, 20, 40$ is expressed as percentage respect to Ω, for $\vec{x}$ respectively belonging to A, B, C, D;

(u,v)/s	**-5**	**-4**	**-3**	**-2**	**-1**	**0**	**1**	**2**	**3**	**4**	**5**
(1,1)							√	√	√	√	
(1,-1)		√	√	√	√						
(-1,1)		√	√	√	√						
(-1,-1)							√	√	√	√	
(0,1)					√	√	√				
(1,0)					√	√	√				
(0,-1)					√	√	√				
(-1,0)					√	√	√				
(1,$\frac{1}{2}$)							√	√	√		
(1,-$\frac{1}{2}$)			√	√	√						
(-1,$\frac{1}{2}$)			√	√	√						
(-1,-$\frac{1}{2}$)							√	√	√		
($\frac{1}{2}$,1)							√	√	√		
($\frac{1}{2}$,-1)			√	√	√						
(-$\frac{1}{2}$,1)			√	√	√						
(-$\frac{1}{2}$,-1)							√	√	√		

- Case iv) $\Omega - \tilde{\Omega} < d$
  where $d = 5, 10, 40, 60$ is expressed as percentage respect to Ω, for $\vec{x}$ respectively

belonging to A, B, C, D;

(u,v)/s	**-5**	**-4**	**-3**	**-2**	**-1**	**0**	**1**	**2**	**3**	**4**	**5**
(1,1)							√	√	√	√	√
(1,-1)	√	√	√	√	√						
(-1,1)	√	√	√	√	√						
(-1,-1)							√	√	√	√	√
(0,1)		√	√	√	√	√	√	√	√	√	
(1,0)		√	√	√	√	√	√	√	√	√	
(0,-1)		√	√	√	√	√	√	√	√	√	
(-1,0)		√	√	√	√	√	√	√	√	√	
(1,$\frac{1}{2}$)				√	√	√	√	√	√	√	√
(1,-$\frac{1}{2}$)	√	√	√	√	√	√	√	√			
(-1,$\frac{1}{2}$)	√	√	√	√	√	√	√	√			
(-1,-$\frac{1}{2}$)				√	√	√	√	√	√	√	√
($\frac{1}{2}$,1)				√	√	√	√	√	√	√	√
($\frac{1}{2}$,-1)	√	√	√	√	√	√	√	√			
(-$\frac{1}{2}$,1)	√	√	√	√	√	√	√	√			
(-$\frac{1}{2}$,-1)				√	√	√	√	√	√	√	√

3.2.4. Stability Analysis

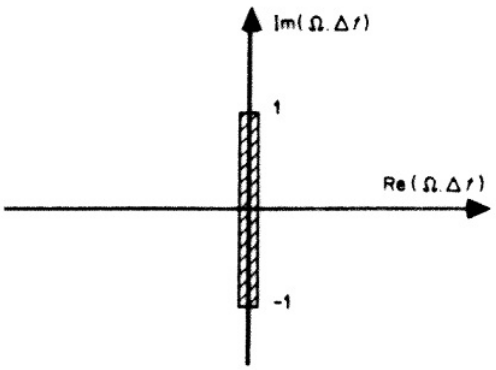

Figure 3.25.: Stability region for the leapfrog scheme

In the next Section we will show some numerical examples to show different behaviours corresponding to different spatial discretization of the Jacobian. We will also need a time integrator, and we will use the Leap-frog scheme. Particular attention must be paid to the choice of time-step in the case where the parameter is not zero. Indeed: let $R = \frac{u}{v}$,

in order to get stability, an analysis on the modified wave number gives us the following estimate (starting from eq. 3.32):

$$\begin{aligned}\Omega &= \tfrac{1}{3h}[-v(2sin(\beta)+sin(\beta)cos(\alpha))-u(2sin(\alpha)+sin(\alpha)cos(\beta)) \\ &\quad +s(v(-sin(\alpha)+sin(\alpha)cos(\beta))-u(sin(\beta)-sin(\beta)cos(\alpha)))] \\ &\leq \tfrac{|v|}{3h}[2+1+|R|(2+1)+|s|(1+1+|R|(1+1))] \\ &= \tfrac{|v|}{3h}[3+3|R|+|s|(2+2|R|)] = \tfrac{|v|}{3h}[(1+|R|)(3+2|s|)]\end{aligned} \tag{3.35}$$

Now, an analysis of the stability region for the Leap-Frog scheme [53], fig. 3.25, leads to:

$$\Delta t \leq \frac{3h}{|v|}[(3+2|s|)(1+|R|)]^{-1} \tag{3.36}$$

in the case s=0 (Arakawa) we get the classical condition:

$$\Delta t \leq \frac{h}{|v|+|u|}. \tag{3.37}$$

3.2.5. Numerical Simulations

3.2.5.1. Two-dimensional advection equation

In order to test the family of schemes that we have found with the general method, we start analyzing an easy, linear, case: the advection equation:

$$\frac{\partial \zeta}{\partial t} + \vec{u} \cdot \vec{\nabla}\zeta = 0 \tag{3.38}$$

We will show different simulations for different values of the parameter and of the velocity field. The boundary conditions are supposed to be biperiodic on the domain $[0,1]\times[0,1]$ and, to integrate over the time, Leap-Frog scheme is used (and already analyzed in the previous section):

$$\zeta_{i,j}^{n+1} = \zeta_{i,j}^{n-1} + 2dtJ_{i,j}(\zeta^n, \psi^n) \tag{3.39}$$

for the first time-step Euler method is used:

$$\zeta_{i,j}^{n+1} = \zeta_{i,j}^{n} + dtJ_{i,j}(\zeta^n, \psi^n). \tag{3.40}$$

We consider two different initial conditions:

$$\zeta(x,y) = exp(-\frac{1}{0.04}[(x-\frac{1}{2})^2+(y-\frac{1}{2})^2]) \tag{3.41}$$

$$\zeta(x,y) = \begin{cases} 1 & \text{if x} \in [\frac{1}{4},\frac{3}{4}]\times[\frac{1}{4},\frac{3}{4}] \\ 0 & \text{otherwise} \end{cases} \tag{3.42}$$

- (u,v)=(1,0)

– TEST 1, initial condition (3.41)

s	**T**	**N**	**CFL**	L^∞	L^1	L^2
0	5	64	0.5	1.2173 e-001	4.2880 e-002	2.5707 e-002
1	5	64	0.5	1.2261 e-001	4.2684 e-002	2.6346 e-002
-1	5	64	0.5	1.2261 e-001	4.2684 e-002	2.6346 e-002

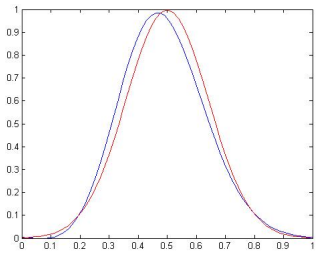

(a) s=0

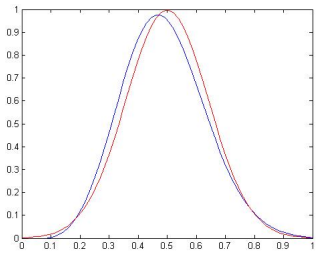

(b) s=1

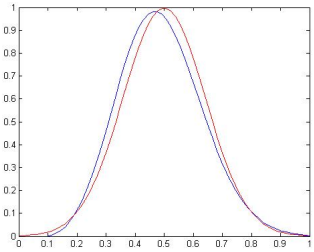

(c) s=-1

Figure 3.26.: TEST 1 - Section

– TEST 2, initial condition 3.42

s	**T**	**N**	**CFL**	L^∞	L^1	L^2
0	1	64	0.5	8.5988e-001	2.8916e-001	1.6600e-001
1	1	64	0.5	8.7407 e-001	3.0204e-001	1.5930e-001
-1	1	64	0.5	8.7407e-001	3.0204e-001	1.5930e-001

- (u,v)=(1,1)

– TEST 3, initial condition (3.41);

s	**T**	**N**	**CFL**	L^∞	L^1	L^2
0	5	64	0.5	1.8564 e-001	4.6229 e-002	3.4902 e-002
1	5	64	0.5	1.3730 e-001	4.0045 e-002	2.7721 e-002
-1	5	64	0.5	2.2337 e-001	5.8602 e-002	4.3846 e-002

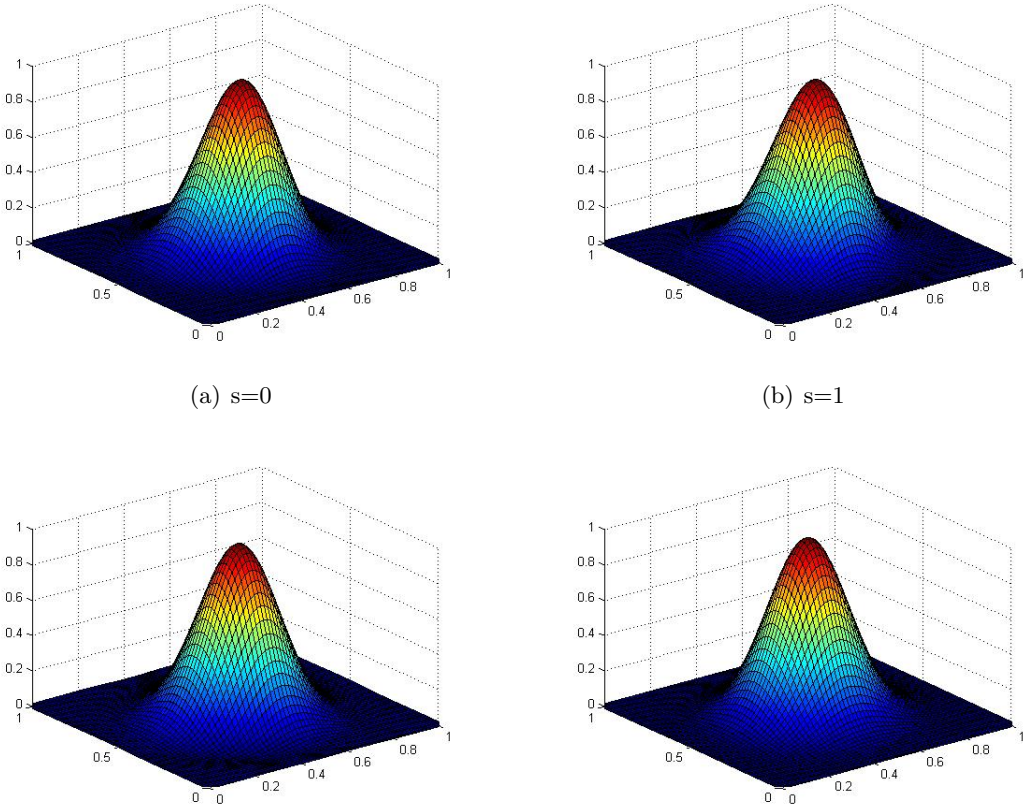

(a) s=0

(b) s=1

(c) s=-1

(d) Soluzione esatta

Figure 3.27.: TEST 1 - 3D

– TEST 4, initial condition (3.41);

s	**T**	**N**	**CFL**	L^∞	L^1	L^2
0	10	64	0.7	3.0168 e-001	8.3144 e-002	6.0423 e-002
1	10	64	0.7	2.1939 e-001	7.3173 e-002	4.9586 e-002
-1	10	64	0.7	3.4885 e-001	9.6304 e-002	7.1262 e-002

- (u,v)=(-1,1)

  – TEST 5, initial condition (3.41);
  For this case we consider also cases with $s > 1$ (paying attenction to the choice of the time step) in order to show results already found by the study of the MWN:

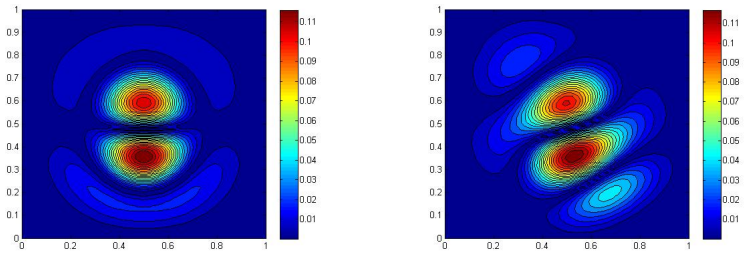

(a) s=0 (b) s=1

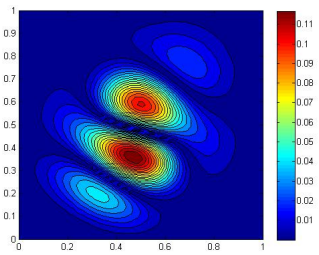

(c) s=-1

Figure 3.28.: TEST 1 - Error

s	**T**	**N**	**CFL**	L^∞	L^1	L^2
-3	5	64	0.5	1.0775 e-001	4.0348 e-002	3.0349 e-002
-2	5	64	0.5	1.0267 e-001	3.8392 e-002	2.5415 e-002
-1	5	64	0.5	1.3730 e-001	4.0045 e-002	2.7721 e-002
0	5	64	0.5	1.8564 e-001	4.6229 e-002	3.4902 e-002
1	5	64	0.5	2.2337 e-001	5.8602 e-002	4.3846 e-002
2	5	64	0.5	2.4628 e-001	7.1161 e-002	5.2478 e-002
3	5	64	0.5	2.5960 e-001	8.2244 e-002	6.1007 e-002

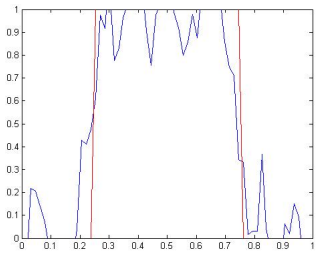

(a) s=0

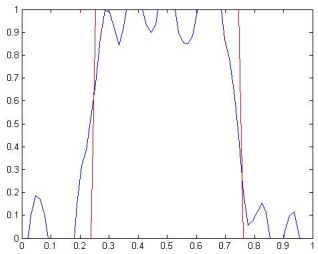

(b) s=1

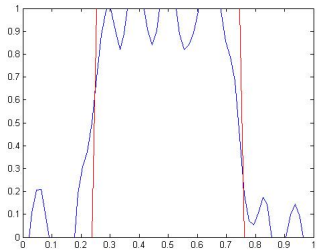

(c) s=-1

Figure 3.29.: TEST 2 - Section

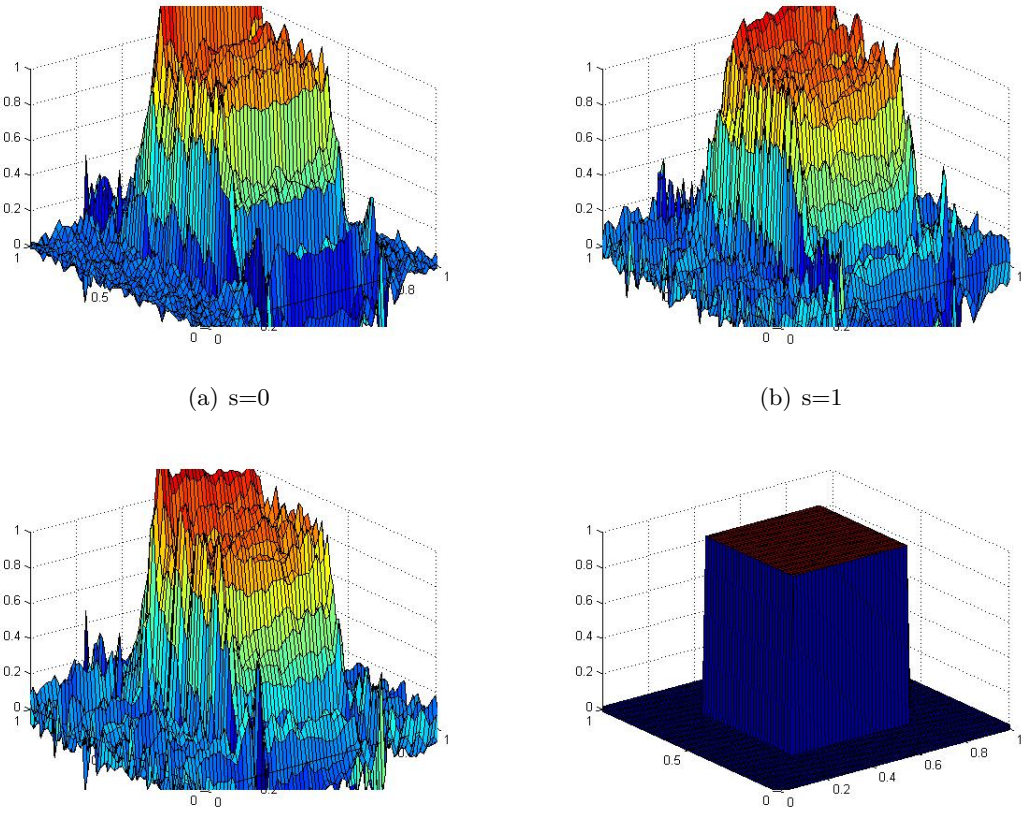

(a) s=0

(b) s=1

(c) s=-1

(d) Soluzione esatta

Figure 3.30.: TEST 2 - 3D

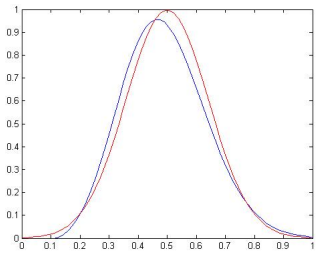

(a) s=0

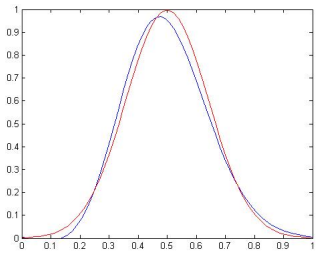

(b) s=1

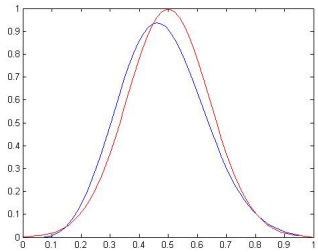

(c) s=-1

Figure 3.31.: TEST 3 - Section

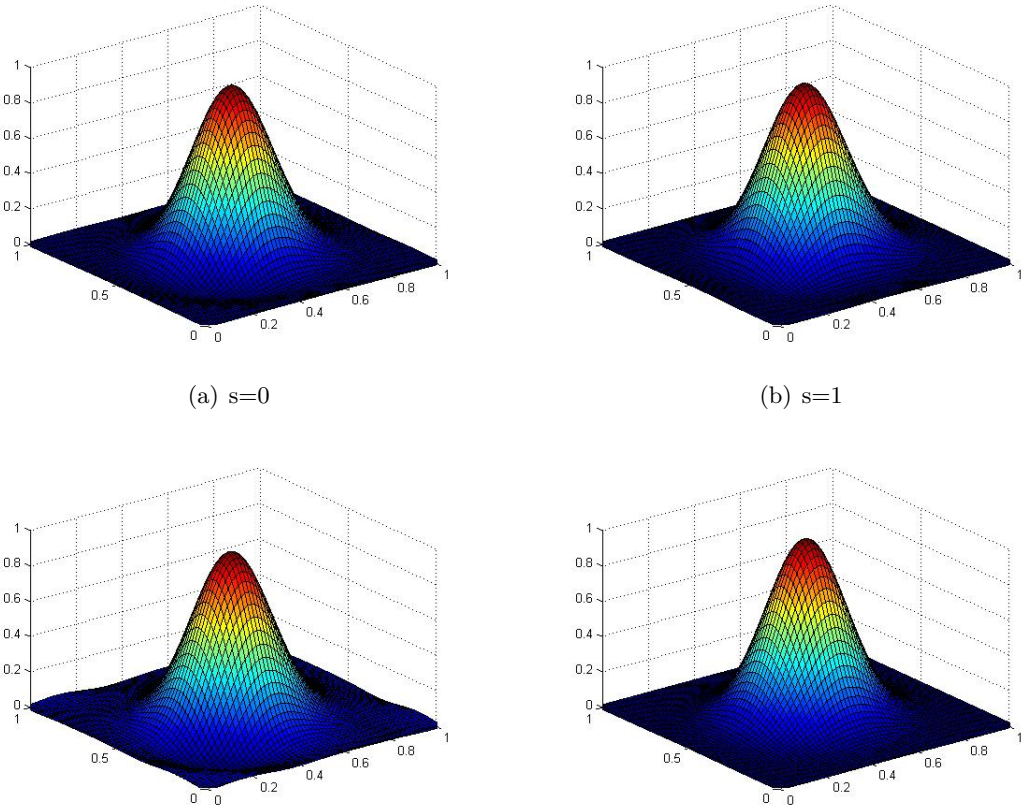

(a) s=0

(b) s=1

(c) s=-1

(d) Soluzione esatta

Figure 3.32.: TEST 3 - 3D

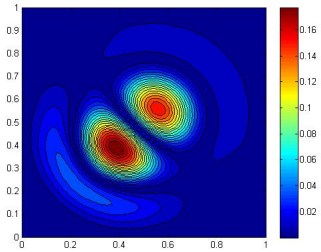

(a) s=0

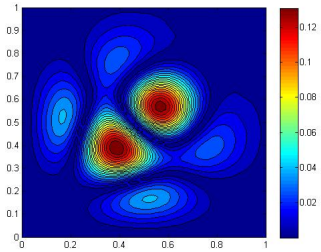

(b) s=1

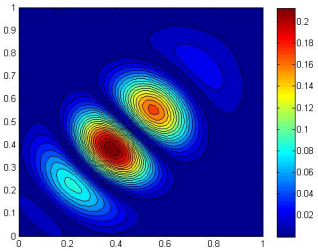

(c) s=-1

Figure 3.33.: TEST 3 - Error

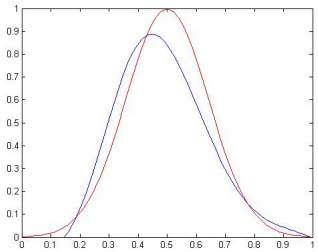

(a) s=0

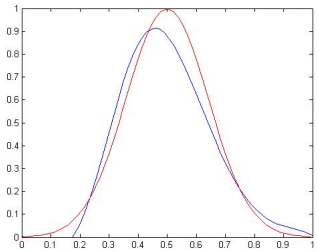

(b) s=1

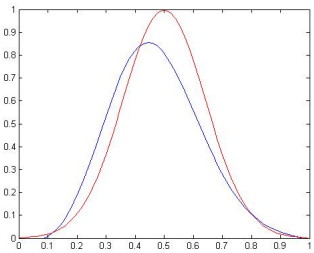

(c) s=-1

Figure 3.34.: TEST 4 - Section

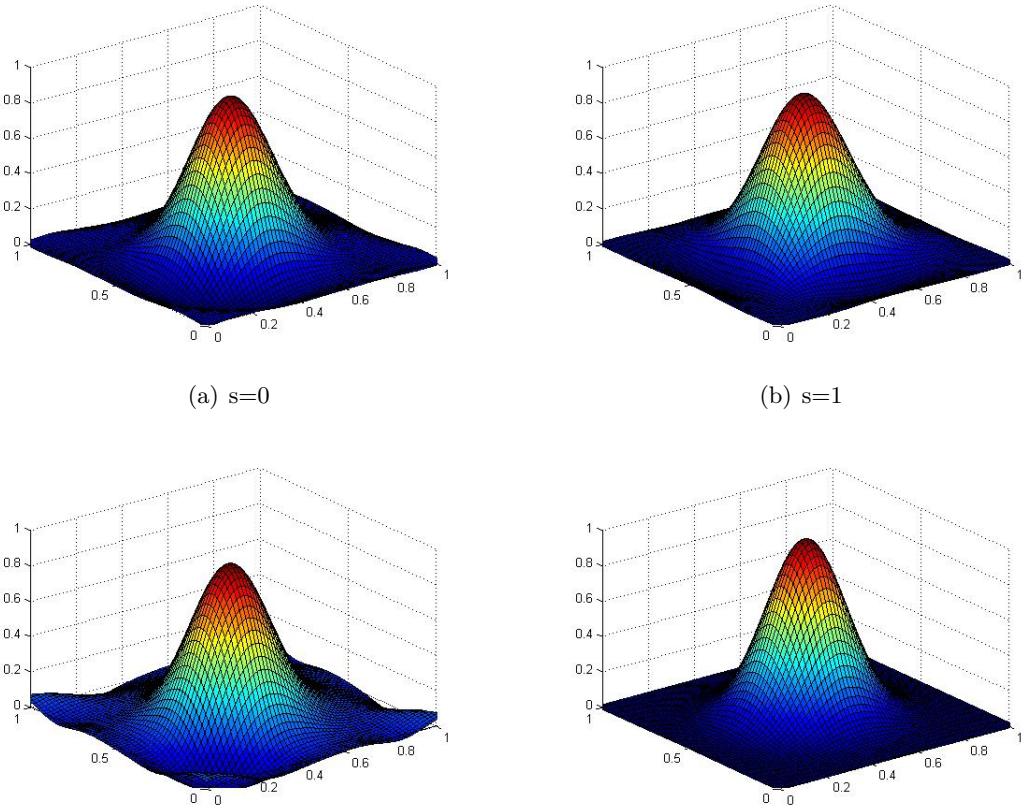

(a) s=0

(b) s=1

(c) s=-1

(d) Soluzione esatta

Figure 3.35.: TEST 4 - 3D

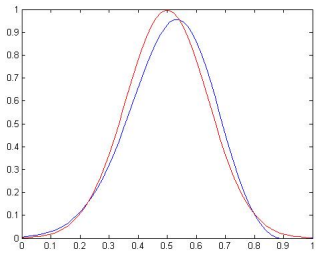

(a) s=0

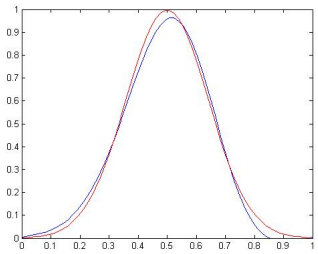

(b) s=-2

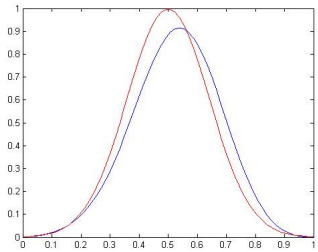

(c) s=2

Figure 3.36.: TEST 5 - Section

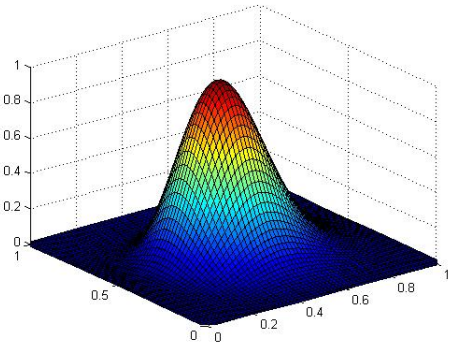

(a) s=0

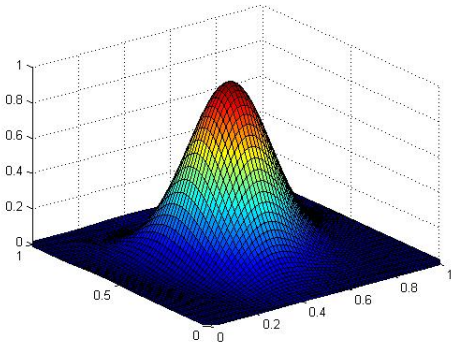

(b) s=-2

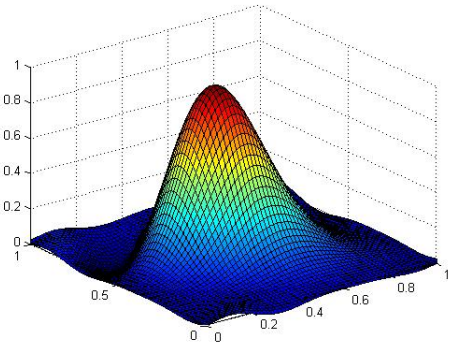

(c) s=2

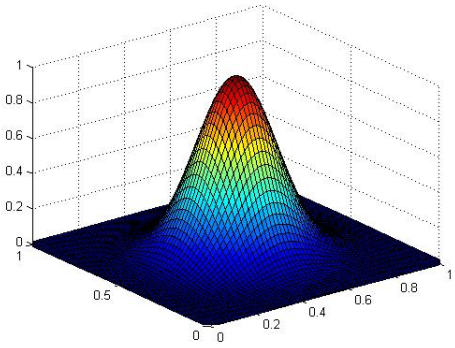

(d) Soluzione esatta

Figure 3.37.: TEST 5 - 3D

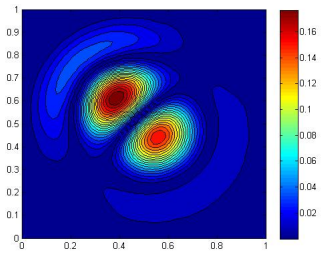

(a) s=0

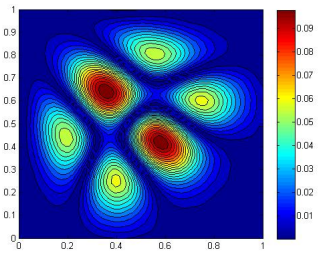

(b) s=-2

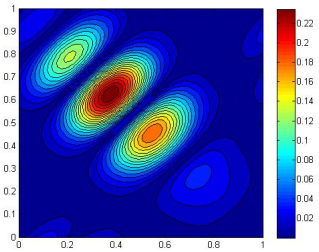

(c) s=2

Figure 3.38.: TEST 5 - Errore

3.2.5.2. The Rankine Vortex

We test now a non-linear example, the Rankine vortex. Now we are back in the formulation where ψ and ζ are related by the Poisson equation $\zeta = \Delta\psi$. It is natural to define the Rankine Vortex in a cylindric coordinate system (r,θ,z). This vortex has a velocity field normal both to the z symmetry axes and to the radial vector r, meaning that the velocity field is parallel to the versor j. The length of the velocity depends only by the radius, in particular the inner part is proportional to r, while the outer is proportional to the inverse of the distance from the centre ($1/r$); the maximum value that the velocity can reach is at the characteristic distance, R, where there's the shift, from the linear to the hyperbolic behaviour. We can analytically define the Rankine Vortex as:

$$\vec{v} = v_r\hat{i} + v_\theta\hat{j} + v_z\hat{k} \tag{3.43}$$

with

$$\begin{cases} \mathrm{v}_r = 0 \\ \mathrm{v}_\theta = \begin{cases} \mathrm{V}_R\frac{r}{R} & if\ 0 \le r < R \\ \mathrm{V}_R\frac{R}{r} & if\ R \le r \end{cases} \\ \mathrm{v}_z = 0 \end{cases} \tag{3.44}$$

V_R is the maximum value of the velocity. It's easy to obtain the vorticity equation for this special field:

$$\vec{\zeta} = \nabla \times \vec{v} = \hat{k}\frac{1}{r}\frac{\partial(rv_\theta)}{\partial r} = \hat{k}(\frac{v_\theta}{r} + \frac{\partial v_\theta}{\partial r}) = \hat{k}\begin{cases} 2\ \frac{V_R}{R} & \text{if } 0 \le r < R \\ 0 & \text{if } \mathrm{R} \le r \end{cases} \tag{3.45}$$

The Rankine Vortex is then characterized by a continuous velocity field but a discontinuous vorticity which, as already seen, will cause problems in the numerical simulations. For the following example we will consider the maximum value $V_R = 1$ and the characteristic distance $R = 1$.

The classic Rankine Vortex

Numerical problems caused by the discontinuities of the vorticity are shown if figures 3.39-3.41; for this reason we are going to construct a similar vortex, which should be yet an analytical solution of the vorticity equation, but we impose it to be smoothed enough in order to avoid numerical problems.

In the following simulation we fix the following data:

- CFL=0.7
- Stream function tolerance = 10^{-11} o $k < 100$
- Domain [-12,12]
- Final time T=235
- Nodes NxN=64x64

Remark 3.3. *A particular attention must be given to the boundary conditions. We are solving the following system:*

$$\begin{cases} \zeta_t = J(\zeta(\vec{x},t),\psi(\vec{x},t)) \\ \zeta = \Delta\psi \\ (solved\ by\ Gauss-Seidel\ algorithm) \\ \\ +\ initial\ conditions\ for\ \zeta \\ \rightarrow initial\ conditions\ for\ \psi\ through\ Gauss-Seidel\ algorithm \\ +\ boundary\ conditions\ for\ \zeta \\ +\ boundary\ conditions\ for\ \psi\ when\ using\ Gauss-Seidel\ algorithm \end{cases} \tag{3.46}$$

The initial condition $\zeta(\vec{x},0) = \zeta_0(\vec{x})$ is given by the analytical Rankine vortex.
In order to fix the boundary conditions correctly, we choose to impose Dirichlet conditions for the ζ, meaning

$$\zeta(\vec{x},t) = 0 \quad if\ \vec{x} \in \partial D$$

and Neumann boundary conditions for the ψ, this is because the most reasonable choice is to impose constant velocity at the boundary (true going to infinity), so we fix

$$\frac{\partial\psi(\vec{x},t)}{\partial \boldsymbol{n}} = f(\vec{x},t) \quad if\ \vec{x} \in \partial D,$$

where $\boldsymbol{n}$ denotes the normal to the boundary.
In our case, then, the function f is fixed calculating the velocity near the boundary.

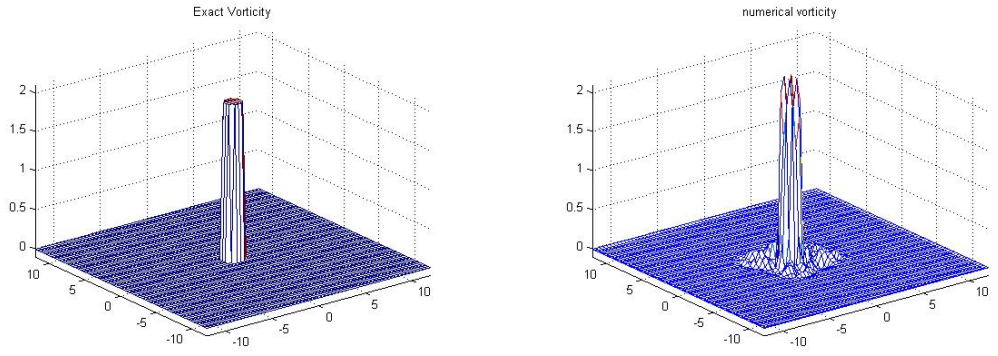

(a) Exact solution (b) Numerical solution at $T = 20$

Figure 3.39.: The classical Rankine Vortex - Vorticity

The smoothed Rankine Vortex

Because of numerical instabilities caused by discontinuities of the vorticity, we look for

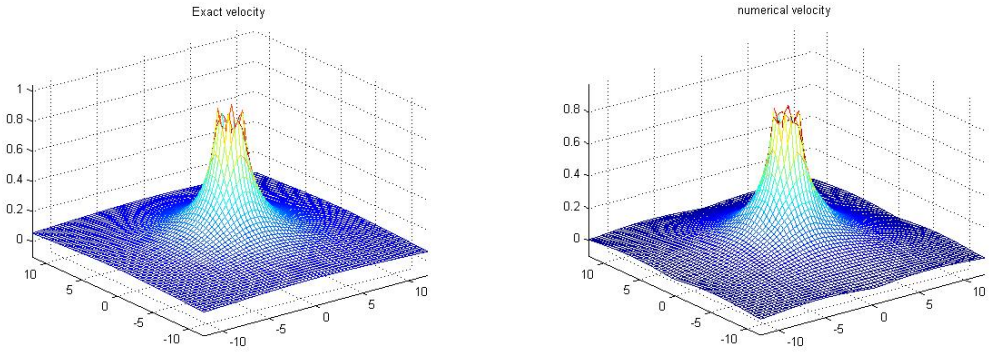

(a) Exact solution (b) Numerical solution at $T = 20$

Figure 3.40.: The classical Rankine Vortex - Velocity

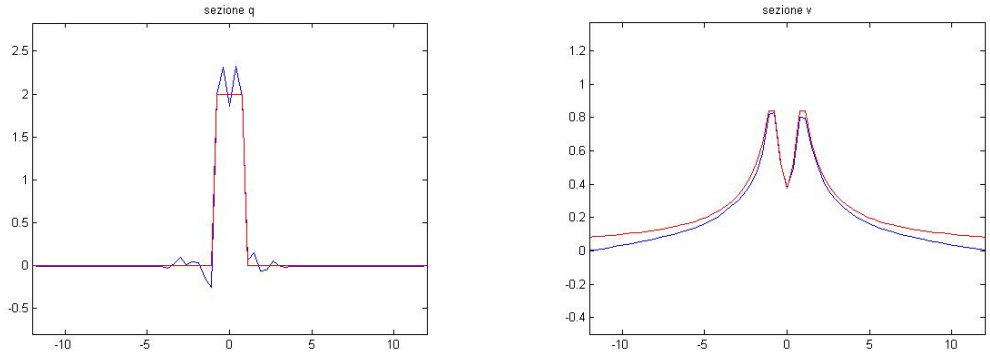

(a) Vorticity section at $T = 20$ compared with the analytical solution

(b) Velocity section at $T = 20$ compared with the analytical solution

Figure 3.41.: The classical Rankine Vortex - Sections

a smoothed version of the Rankine Vortex in order to avoid such problems. We impose:

$$\begin{cases} \mathrm{v}_\theta(r) = r \quad if \quad r < 1 \\ \mathrm{v}_\theta(r) = r^\alpha e^{(1-r)\beta} \quad otherwise \end{cases} \tag{3.47}$$

so that

$$lim_{r\to\infty} v_\theta(r) = 0$$

and

$$v_\theta(1) = 1$$

. The vorticity is then:

$$\vec{\zeta} = \nabla \times \vec{v} = \hat{k}\frac{1}{r}\frac{\partial(rv_\theta)}{\partial r} = \hat{k}(\frac{v_\theta}{r} + \frac{\partial v_\theta}{\partial r}) = \hat{k}\begin{cases}2 & \text{if} \quad r < 1\\ [(\alpha+1)r^{\alpha-1} - \beta r^{\alpha}]e^{(1-r)\beta} & \text{otherwise}\end{cases} \tag{3.48}$$

Now we fix the constants α and β such that

$$lim_{r\to\infty}\zeta(r) = 0$$

and

$$\zeta(1) = 2$$

obtaining

$$\alpha + 1 - \beta = 1 \tag{3.49}$$

meaning the class of solution $\alpha = \beta + 1$.
In the following simulations we consider the case $\alpha = 2$, $\beta = 1$ and we fix the following data:

- CFL=0.7
- Stream function tolerance = 10^{-11} o $k < 100$
- Domain [-12,12]
- Final time T=10
- Nodes NxN=65x65

Scheme parameter s	L^∞	L^1	L^2
0	2.6987e-002	6.5011e-002	3.9821e-002
-1	5.5913e-002	1.1139e-001	7.0287e-002
-2	4.8667e-002	1.3192e-001	9.0814e-002
1	5.5870e-002	1.1372e-001	7.0294e-002
2	4.8610e-002	1.4206e-001	9.0811e-002

In this case, there is no a favorite direction, so the best choice is Arakawa's scheme ($s = 0$).

The smoothed Rankine Vortex with Advection
Now we have a smooth analytical solution for the vorticity equation, so we will add a constant advection in order to compute the error depending on the scheme parameter, s, that we know to have good results with advection. In the following simulations we consider the previous example multiplied by a factor 10^-1 and we consider again the case $\alpha = 2$, $\beta = 1$ and we fix also the following data:

- CFL=0.7
- Stream function tolerance = 10^{-11} o $k < 100$

- Domain [-12,12]
- Final time T=170
- Nodes NxN=129x129
- $(u, v) = (-1, 1)$ constant advection velocity

In these simulations boundary conditions are fixed to be periodic in order to see the vortex turning in our domain. In particular, at the final time the vortex has runned for the whole domain passing through the diagonal ten times, in the following table we can appreciate the error estimates. Energy and enstrophy plots are not showed because, as already proved, these quantities are conserved.

Scheme parameter s	L^∞	L^1	L^2
0	7.5735e-002	2.8436e-001	1.6698e-001
-1	5.7278e-002	2.3686e-001	1.3008e-001
-2	4.0272e-002	1.5199e-001	8.8872e-002
1	1.0773e-001	3.5846e-001	2.3248e-001
2	1.2494e-001	4.4528e-001	2.8537e-001

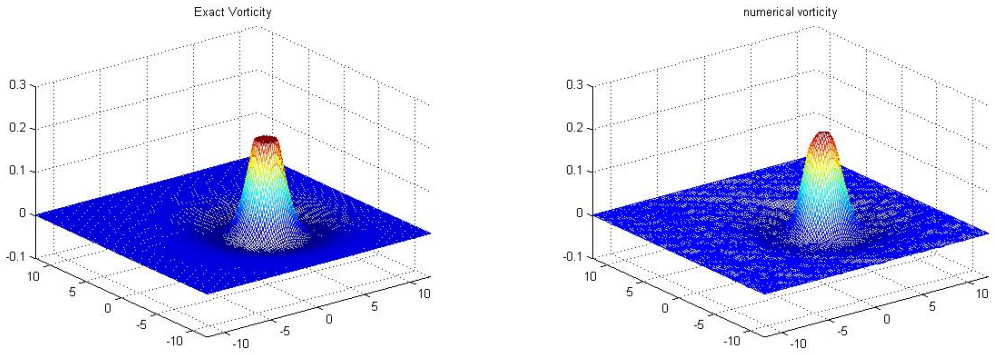

(a) Exact solution (b) $s = -2$

Figure 3.42.: Smoothed Rankine with Advection - Vorticity at final time - Exact solution compared with the best choice of the parameter

In these non-linear examples, we can appreciate what we studied in the easy (linear) advection case, meaning that the parameter s is able to reduce the error when a constant advection field is present (see fig. 3.46-3.49) even if a priori estimate of the best parameter for a general non-linear field is not available.

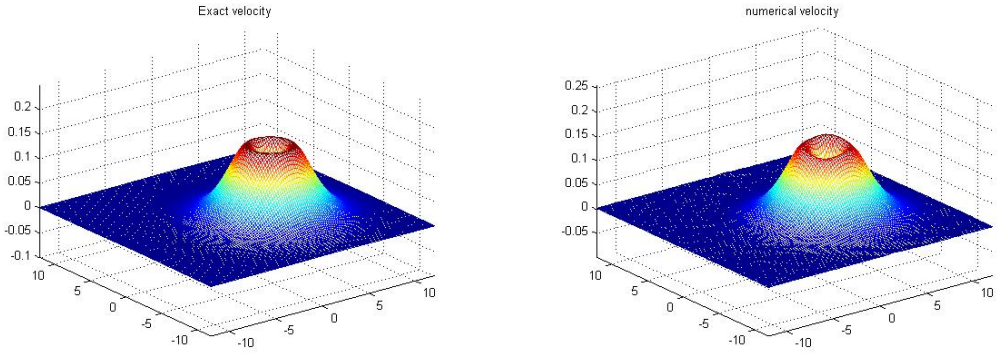

(a) Exact solution (b) $s = -2$

Figure 3.43.: Smoothed Rankine with Advection - Velocity at final time - Exact solution compared with the best choice of the parameter

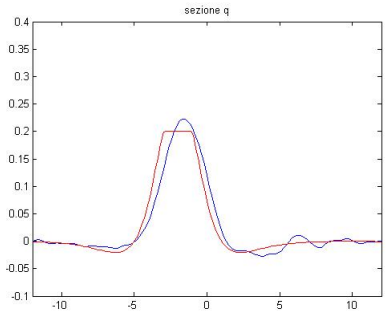

(a) $s = 0$

Figure 3.44.: Smoothed Rankine with Advection - Vorticity at final time -Section

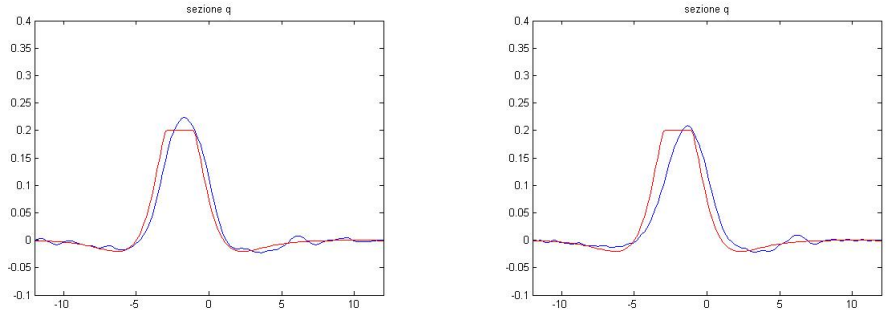

(a) $s = -1$ (b) $s = 1$

Figure 3.45.: Smoothed Rankine with Advection - Vorticity at final time -Section

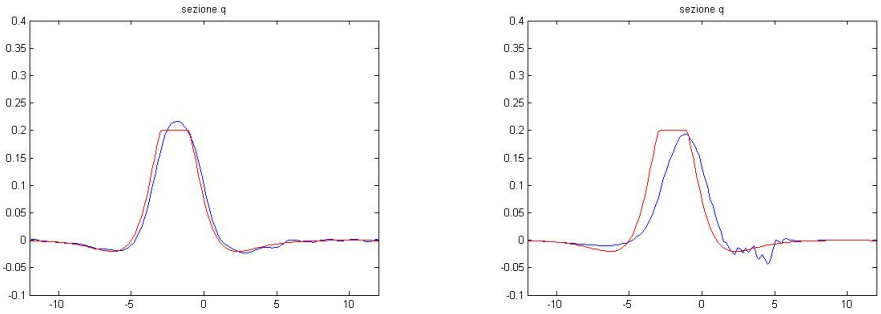

(a) $s = -2$ (b) $s = 2$

Figure 3.46.: Smoothed Rankine with Advection - Vorticity at final time -Section

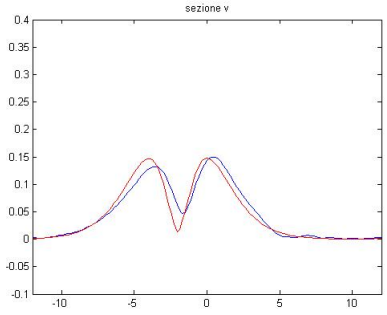

(a) $s = 0$

Figure 3.47.: Smoothed Rankine with Advection - Velocity at final time -Section

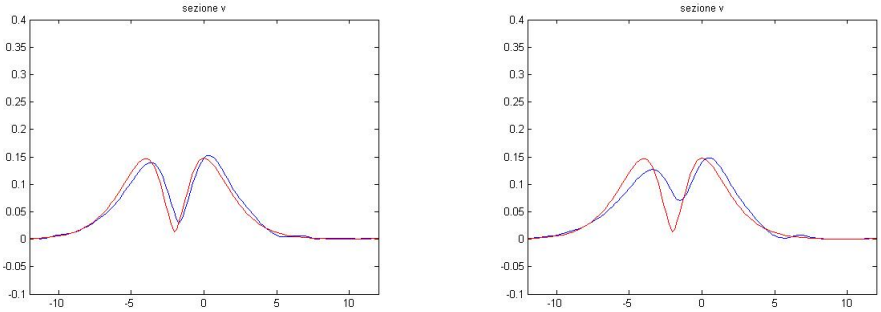

(a) $s = -1$ (b) $s = 1$

Figure 3.48.: Smoothed Rankine with Advection - Velocity at final time -Section

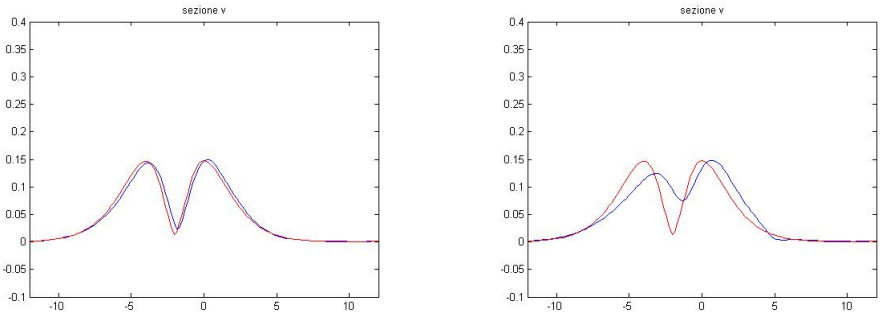

(a) $s = -2$ (b) $s = 2$

Figure 3.49.: Smoothed Rankine with Advection - Velocity at final time -Section

3.2.5.3. A test example to show non-linear numerical instability

In this section we consider a numerical experiment for the vorticity equation in the biperiodic domain $D = [a_x, b_x] \times [a_y, b_y]$ with initial condition:

$$\zeta(x,y) = \sum_{k=4}^{12} \tilde{A} sin(\frac{2\pi kx}{b_x}) sin(\frac{2\pi ky}{b_y}) \tag{3.50}$$

where we fixed $\tilde{A} = 0.15$, $a_x = a_y = 0$, $b_x = b_y = 16$ and N=129 (number of grid points per direction).

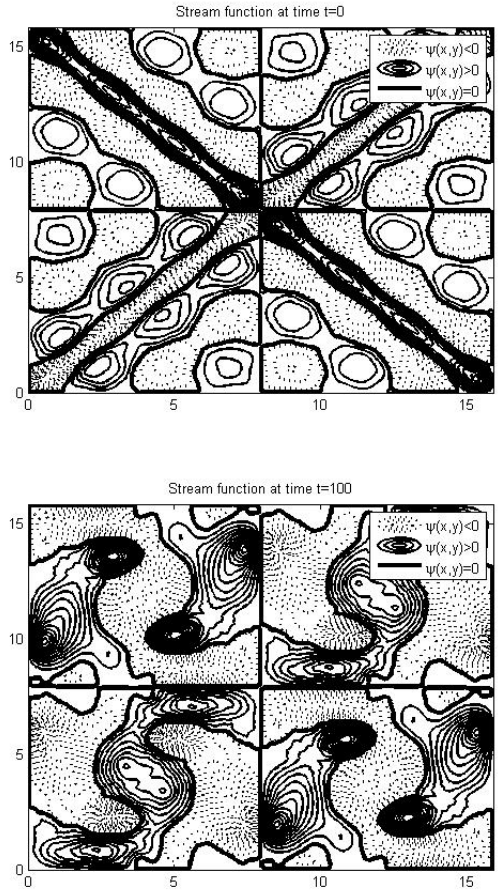

Figure 3.50.: Stream function at different times

In the following experiment we want to show the different behaviors of Jacobians presented in table 3.12. Since some of these, as expected, will not conserve energy and/or enstrophy and the solution will then explode, we decide to fix time-step as independent

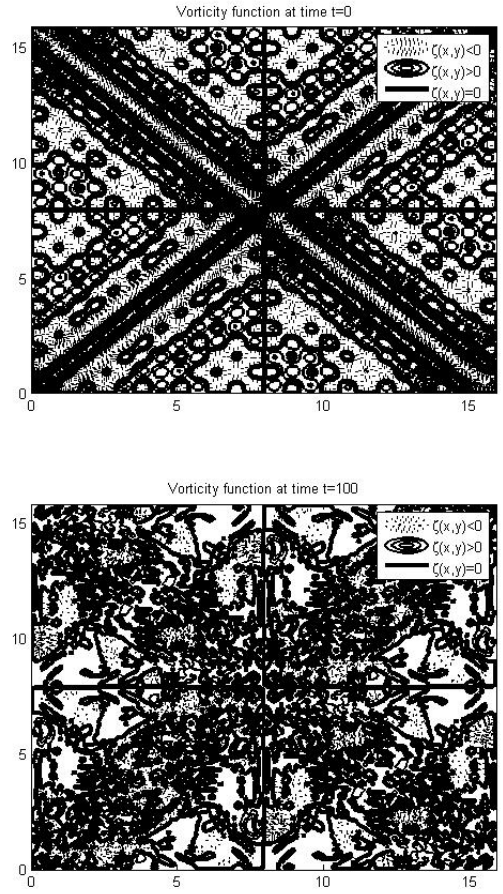

Figure 3.51.: Vorticity function at different times

from the velocity field:

$$\Delta t = \frac{3Ch^2}{3+2|s|} \tag{3.51}$$

and we fix $C = 0.7$. In order to integrate system (2.6), at each time-step we need to solve also the equation for the stream function:

$$\Delta\psi = \zeta \tag{3.52}$$

Gauss-Seidel algorithm is used for equation (3.51). The evolution of the stream function, vorticity and velocity fields are shown in figures (3.50)-(3.51)-(3.52) for the special case $s = 0$. Table (3.52) reports the l_∞-norm of the error of physical constraints $\overline{\zeta J(\zeta,\psi)}$ and $\overline{\psi J(\zeta,\psi)}$ related respectively to the conservation of enstrophy and energy. The behavior of these two quantities is shown in figures (3.53)-(3.54)-(3.55)-(3.56). Figure 3.53 shows the parameter schemes' family (3.12) for s=0, s=0.5, s=-1 and, as expected, both integral

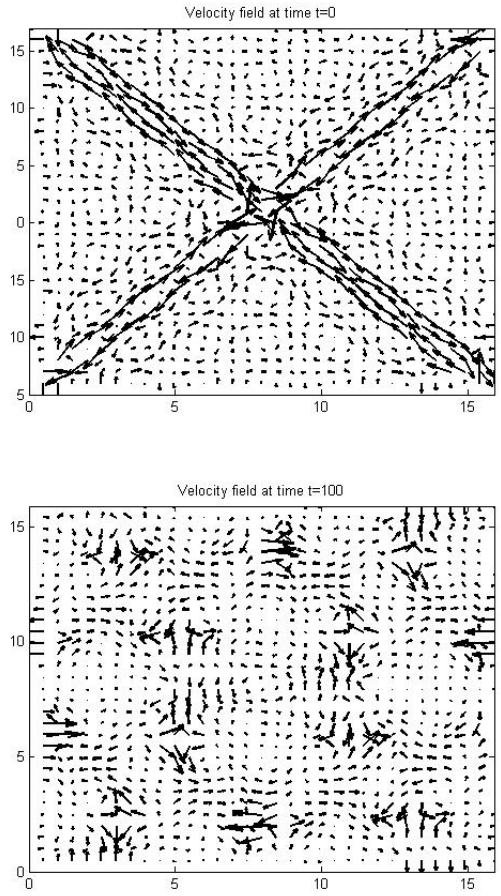

Figure 3.52.: Velocity field at different times

constraints are satisfied. $J^{+\times}$ and $(J^{++} + J^{\times+})/2$ conserve only energy as we can see in figure (3.54) where the enstrophy is going to diverge. The enstrophy-conserving property is a strong requirement as shown in figures (3.55), where $J^{\times+}$ and $(J^{++} + J^{+\times})/2$ do not conserve exactly both physical quantities but only small variations of energy arise. Finally some skew-symmetric cases are shown in figures 3.56: J^{0+} does not conserve either energy or enstrophy but the behavior of J^{0*} is surprising. This Jacobian, also if verifies only the skew-symmetric property, gives rise to a stable simulation. J^{0*} is the combination of $J^{\times+}$ and $J^{+\times}$ which are, respectively, the discretization of the analytic forms $J(\zeta, \psi) = \nabla \cdot (\psi \nabla^{\perp} \zeta)$ and $J(\zeta, \psi) = -\nabla \cdot (\zeta \nabla^{\perp} \psi)$. It's possible to switch from one form to the other, thanks to the fact that the divergence of the curl is always zero, in our case divergence of velocity and of palinstrophy. This correspond to have $\psi_{xy} = \psi_{yx}$ and $\zeta_{xy} = \zeta_{yx}$. By simple inspection of numerical forms $J^{\times+}$ and $J^{+\times}$, it is possible to verify that we go through the same steps in the discrete case while, in general, this is not possible.

Table 3.52.: l_∞-norm error for different Jacobians

Property	Discrete Operator	$\overline{\lvert\psi J(\zeta,\psi)\rvert}$	$\overline{\lvert\zeta J(\zeta,\psi)\rvert}$
General scheme J^s	J^0	1.6650e-003	4.9843e-002
	$\mathrm{J}^{0.5}$	1.6500e-003	5.1186e-002
	J^{-1}	1.6410e-003	5.1133e-002
Energy conserving	$\mathrm{J}^{+\times}$	1.6160e-003	6.6046e-001
	$(\mathrm{J}^{++} + J^{\times+})/2$	1.5840e-003	2.0311e-001
Enstrophy conserving	$\mathrm{J}^{\times+}$	1.5840e-003	4.9843e-002
	$(\mathrm{J}^{++} + J^{+\times})/2$	1.6800e-003	4.9846e-002
Skew symmetric	J^{0+}	$+\infty$	$+\infty$
	J^{0*}	1.6250e-003	4.9843e-002

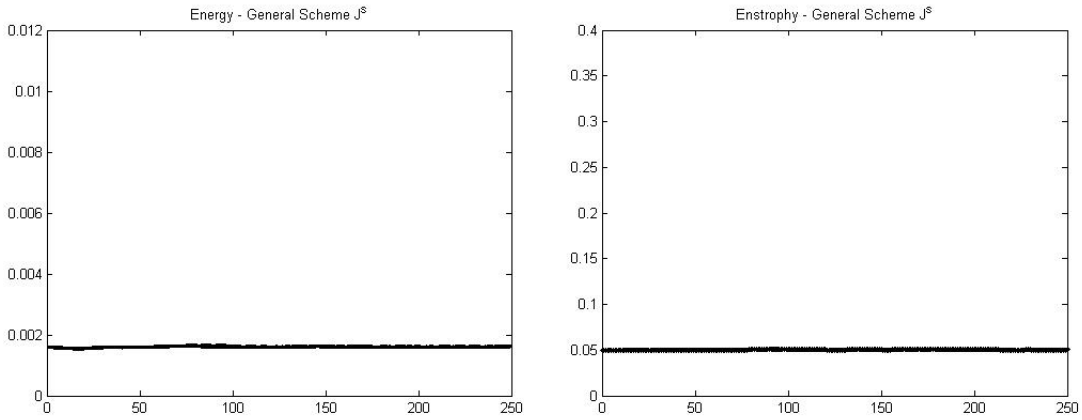

: Mean kinetic energy : Mean square vorticity

Figure 3.53.: J^s with $s = 0$ - - - - - -; $s = 0.5$ ————; $s = -1$ ·····

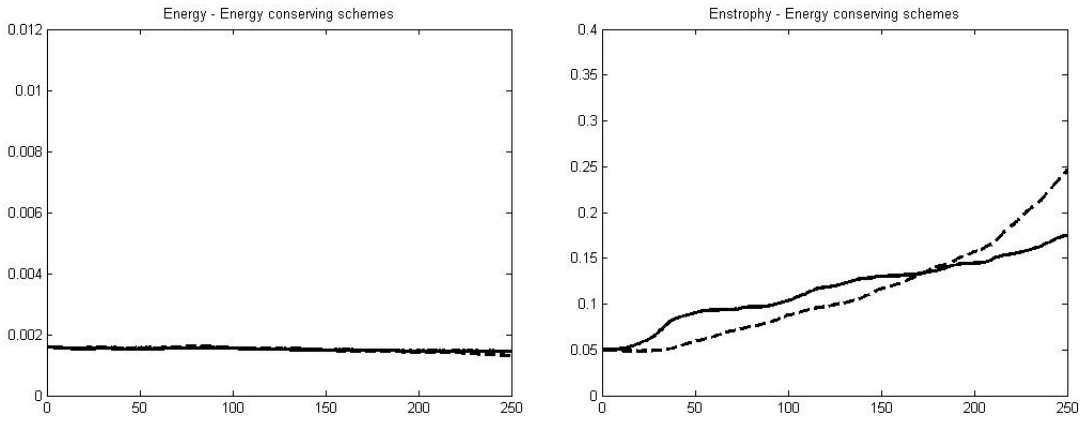

: Mean kinetic energy : Mean square vorticity

Figure 3.54.: $J^{+\times}$ - - - - - - and $(J^{++} + J^{\times+})/2$ ————

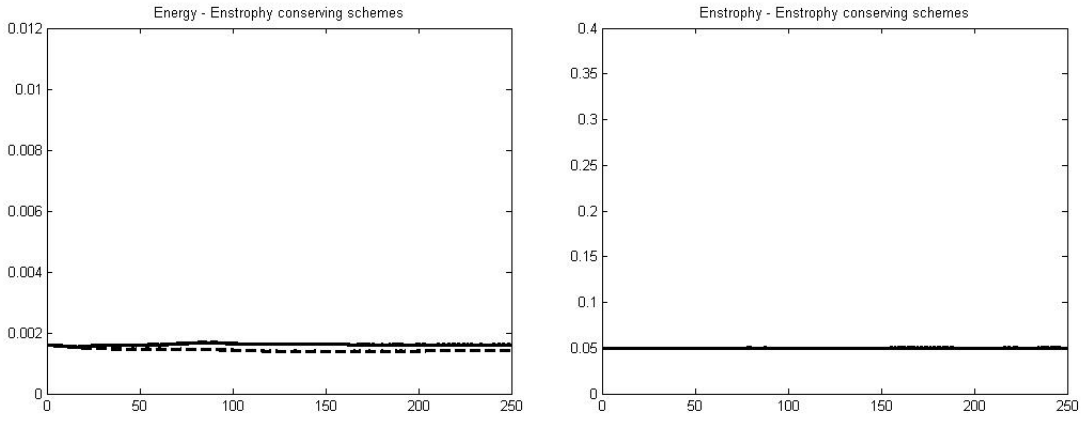

: Mean kinetic energy : Mean square vorticity

Figure 3.55.: $J^{\times+}$ - - - - - - and $(J^{++} + J^{+\times})/2$ ————

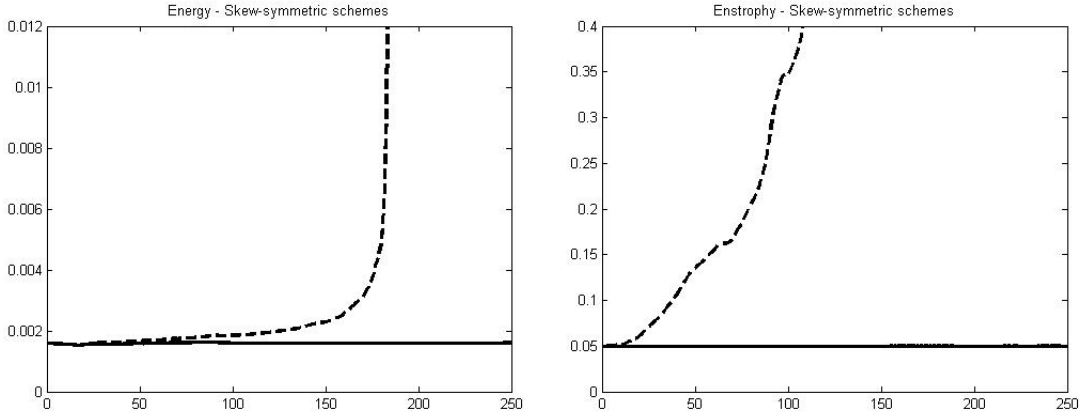

: Mean kinetic energy : Mean square vorticity

Figure 3.56.: J^{0+} - - - - - - and J^{0*} ————

4. SBP formulation

The aim of this section is to propose a new and general solution to the non-linear problem already presented in the first chapter. This new formulation will mix together high order accuracy with mimetic properties re-formulating Arakawa's Jacobian using the summation-by-parts (SBP) operators ([54],[55],[56]). The proficiency of this technique lies in the power of such discretization to simulate integration by parts property which maintains the analytical conservation properties in the discrete space. Moreover, the compact and general form of SBP operators includes any order schemes; as a matter of fact, all mimetic properties are derived thanks to the special discretization matrices structure and they do not depend on a specific numerical discretization as, for example, in Arakawa's solution, where the mimetic properties are proved only for a particular scheme.
Summation-by-parts operators are finite-difference operators which mimic analytical integration by parts. This property results to be very useful in constructing energy-stable discretization of partial differential equations. SBP operators are defined by a weight matrix in combination with a difference operator to approximate any derivative of any order of accuracy. Kreiss and Scherer [57] first suggested the use of SBP spatial operators in relation with second-order central-difference schemes, Strand [58] is a classical reference paper, while in Olsson [19], [20], high order finite difference operators are constructed based on spatial operators of SBP type. Nordström et al. [59] obtained a stable and conservative high order multi-block method for the compressible Navier-Stokes equations. The SBP resulting schemes are strictly stable meaning that the growth rate of the analytic and semi-discrete solution is identical, as we will show explicitly for a particular case in the next section.
The basic idea is that we start from the continuous problem and we want to get an energy estimate in the continuous space as well as in the discrete space, where a proper norm has to be defined; sometimes an adequate split form is necessary for non-linear conservation laws [60], as we already have seen for the vorticity equation with Arakawa's solution, which is the combination of three different (but equal in the analytical space) forms of the Jacobian operator. In [39] Nordstrom showed also how to use artificial dissipation for finite difference approximations (in linear hyperbolic problems) with variable coefficients in order to have the energy estimate and strict stability. Associated to the SBP operators is the simultaneous-approximation-term (SAT) technique for imposing boundary [61] and interface [54] conditions weakly [62], [63], [64]. The SBP-SAT method has been applied to a wide set of problems and has proven to be robust, [65], [66], [67], for this reason, in the next future (not in this work) we will adopt this approach when we will analyze the non-periodic case.
SBP technique has been also applied to discretize in time (for details see [68] and re-

lated bibliography) and we are trying to apply such operators for our simulation (to be completed-november).
I will start with basic notions about SBP theory, I will then show well-posed boundary conditions for a general domain and I will finally reformulate Arakawa's Jacobian with these new operators, proving in this space, the three standard mimetic properties for the Jacobian operator [42]. The last theorem is proved only on a biperiodic domain, but an extension to a general domain will shortly be done.

4.1. Basic Notions

Let the inner product for real valued functions $u, v \in L^2[a, b]$ be defined by

$$(u, v) = \int_a^b uvdx \tag{4.1}$$

and the corresponding norm $\|u\|^2 = (u, u)$. The domain $(a \leq x \leq b)$ is discretized using N equidistant grid points,

$$x_j = a + (j-1)h, \quad j = 1, 2, \ldots, N, \quad h = \frac{b-a}{N-1}.$$

The vector $v^T = [v_1, v_2, \ldots, v_N]$ represents the discrete solution in each grid point x_j. We define the discrete analogous of the inner product for the vector functions $u, v \in \Re^n$ by

$$(u, v)_H = u^T H v \tag{4.2}$$

and the discrete analogous of the norm by

$$\|v\|_H^2 = (v, v)_H \tag{4.3}$$

where $H = H^T$ symmetric-positive-definite.
An SBP operator is basically a finite-difference centered scheme which mimic the behavior of the corresponding continuous operator with regard to the inner product defined by 4.2 because it leads to energy estimates, meaning stability properties. In order to make it clearer, we apply the energy method to the easiest hyperbolic scalar equation:

$$u_t = u_x. \tag{4.4}$$

Multiplying both sides of the continuous equation 4.4 by u, integrating over the interval [a,b] using integration by part property, leads to

$$\frac{\partial}{\partial t} \|u\|^2 = (u, u_x) + (u, u_x) = u^2|_a^b. \tag{4.5}$$

Now we consider the semi-discretization of eq. 4.4, $v_t = D_1 v$ and we give the following definition:

Definition 4.1. *A difference operator $D_1 = H^{-1}Q$ is an SBP operator if H is a symmetric-positive-definite matrix and $Q + Q^T = B$ where B*

$$B = \begin{bmatrix} -1 & 0 & 0 & ... & 0 \\ 0 & 0 & 0 & ... & 0 \\ \vdots & & \vdots & & \vdots \\ 0 & 0 & ... & 0 & 1 \end{bmatrix}. \tag{4.6}$$

If we consider the special case of periodic boundary conditions the matrix B is equal to the zero matrix, meaning that Q is a total skew-symmetric matrix.

Discretizing eq. 4.4 using SBP operators, lead to

$$\frac{\partial}{\partial t} \|v\|_H^2 = (v, H^{-1}Qv)_H + (H^{-1}Qv, v)_H = v^T(Q + Q^T)v = v_N^2 - v_0^2 \tag{4.7}$$

for the general case (of course if we use boundary conditions the RHS is zero both in the continuous case 4.5 and in the discrete one 4.7).
Similarly we can define and work with higher order derivatives [21] and with multi-dimensional problems [59], [69], [63], in particular we are interested in the two-dimensional case.
We recall the definition and the properties of the Kronecker product:

Definition 4.2. *If A is an $m \times n$ matrix and B is a $p \times q$ matrix, then the Kronecker product $A \otimes B$ is the $mp \times nq$ block matrix:*

$$A \otimes B = \begin{bmatrix} a_{11}B & ... & a_{1n}B \\ \vdots & & \vdots \\ a_{m1}B & ... & a_{mn}B \end{bmatrix}. \tag{4.8}$$

Properties:

a) Bilinearity and associativity

The Kronecker product is bilinear and associative:

- $\mathbf{A} \otimes (\mathbf{B} + \mathbf{C}) = \mathbf{A} \otimes \mathbf{B} + \mathbf{A} \otimes \mathbf{C}$,
- $(\mathbf{A} + \mathbf{B}) \otimes \mathbf{C} = \mathbf{A} \otimes \mathbf{C} + \mathbf{B} \otimes \mathbf{C}$,
- $(k\mathbf{A}) \otimes \mathbf{B} = \mathbf{A} \otimes (k\mathbf{B}) = k(\mathbf{A} \otimes \mathbf{B})$,
- $(\mathbf{A} \otimes \mathbf{B}) \otimes \mathbf{C} = \mathbf{A} \otimes (\mathbf{B} \otimes \mathbf{C})$, where A, B and C are matrices and k is a scalar.

b) Non-commutative:

In general $A \otimes B \neq B \otimes A$.
However, $A \otimes B$ and $B \otimes A$ are permutation equivalent, meaning that there exist permutation matrices P and Q (so called commutation matrices) such that

$$\mathbf{A} \otimes \mathbf{B} = \mathbf{P}\,(\mathbf{B} \otimes \mathbf{A})\,\mathbf{Q}.$$

If A and B are square matrices, then $A \otimes B$ and $B \otimes A$ are even permutation similar, meaning that we can take $P = QT$.

c) The mixed-product property and the inverse of a Kronecker product:

If A, B, C and D are matrices of such size that one can form the matrix products AC and BD, then

$$(\mathbf{A} \otimes \mathbf{B})(\mathbf{C} \otimes \mathbf{D}) = (\mathbf{AC}) \otimes (\mathbf{BD}).$$

It follows that $A \otimes B$ is invertible if and only if A and B are invertible, in which case the inverse is given by

$$(\mathbf{A} \otimes \mathbf{B})^{-1} = \mathbf{A}^{-1} \otimes \mathbf{B}^{-1}.$$

d) Transpose:

The transposition and conjugate transposition are distributive over the Kronecker product:

$$(\mathbf{A} \otimes \mathbf{B})^T = \mathbf{A}^T \otimes \mathbf{B}^T$$
$$(\mathbf{A} \otimes \mathbf{B})^* = \mathbf{A}^* \otimes \mathbf{B}^*.$$

e) Determinant:

Let A and B be two squared matrices of size n and p respectively. Then

$$|\mathbf{A} \otimes \mathbf{B}| = |\mathbf{A}|^p |\mathbf{B}|^n.$$

For the bidimensional case, we introduce the computational grid, $x_i = ih_x$, $i \in 0, 1, 2, ..., N$ and $y_j = jh_y$, $j \in 0, 1, 2, ..., M$ where h_x and $h_y > 0$ are the spatial step in the two dimensions.
A general function $f(x, y)$ will be represented in the discrete space as a matrix $\mathbf{F}$ of size $N \times M$, where the generic element $f_{i,j}$ is the representation of the function f calculated in the grid point (x_i, y_j). In order to simplify the notation and to introduce the bidimensional SBP operator, our function will not be represented as a matrix, but as a vector, defined as:
$\mathbf{f} = (f_{11}, ..., f_{1M}, f_{21}..., f_{2M}, ..., f_{N1}, ..., f_{NM})$.
On this vector we will apply SBP operators, where the partial derivatives are approximated by

$$\frac{\partial f}{\partial x} \approx (P_x^{-1} Q_x \otimes I_y)\mathbf{f} \quad \text{and} \quad \frac{\partial f}{\partial y} \approx (I_x \otimes P_y^{-1} Q_y)\mathbf{f} \tag{4.9}$$

The $P_{x,y}$ are diagonal positive definite operators such that $(P_x \otimes P_y)$ define a two-dimensional L^2 norm by

$$\|\mathbf{f}\|^2_{(P_x \otimes P_y)} = \mathbf{f}^T (P_x \otimes P_y)\mathbf{f}.$$

While $Q_{x,y}$ are periodic operators satisfying

$$Q_{x,y} + Q_{x,y}^T = 0$$

(again, the non-periodic case will define matrices $Q_{x,y}$ such that $Q_{x,y}+Q_{x,y}^T = B$, defined in 4.6).

4.2. Re-formulation of Arakawa's Jacobian

In this section, we will use the notation already introduced in the previous paragraph 4.1.
In order to define a discrete non-linear operator, we need to define an analogous of the product between two functions; to do it, we go through the definition of the operator $diag(\cdot)$, which turns vectors into matrices with special properties. For any vector $\mathbf{a} = (a_1, ..., a_N)$, let the matrix $diag(a)$ be

$$diag(a) = \begin{bmatrix} a_1 & 0 & 0 & ... & 0 \\ 0 & a_2 & 0 & ... & 0 \\ \vdots & & \vdots & & \vdots \\ 0 & 0 & ... & 0 & a_N \end{bmatrix}. \tag{4.10}$$

and the vector $\mathbf{1} = (1, \cdots, 1)^T$ be of the same length as $\mathbf{a}$. Then we have

$$diag(a)\mathbf{1} = \mathbf{a} \quad \text{and} \quad \mathbf{1}^T diag(a) = \mathbf{a}^T \tag{4.11}$$

with properties:

$$Ddiag(a) = diag(Da) \tag{4.12}$$

$$a^T B = (B^T a)^T = 1^T diag(B^T a) \tag{4.13}$$

for any diagonal matrix D, and for any vector $\mathbf{a}$ of length N and $N \times N$ matrix B. Eq. (4.13) follows from (4.11).
In the SBP notation, the definition (4.11) is used as follows to define the vectors:

$$D_x\mathbf{f} = (P_x^{-1}Q_x \otimes I_y)\mathbf{f} = diag(P_x^{-1}Q_x \otimes I_y\mathbf{f})\mathbf{1} \tag{4.14}$$

$$D_y\mathbf{f} = (I_x \otimes P_y^{-1}Q_y)\mathbf{f} = diag(I_x \otimes P_y^{-1}Q_y\mathbf{f})\mathbf{1} \tag{4.15}$$

Now we can define the corresponding SBP discretization of the analytical Jacobian adopting the previous definition for each non-linear term of the analytical Jacobian (see

Chapter 1):

$$\begin{aligned} J(\psi,\zeta) &= \frac{1}{3}\left(\frac{\partial\psi}{\partial x}\frac{\partial\zeta}{\partial y}-\frac{\partial\psi}{\partial y}\frac{\partial\zeta}{\partial x}\right) \\ &+ \frac{1}{3}\left(\frac{\partial}{\partial x}\left(\psi\frac{\partial\zeta}{\partial y}\right)-\frac{\partial}{\partial y}\left(\psi\frac{\partial\zeta}{\partial x}\right)\right) \\ &+ \frac{1}{3}\left(\frac{\partial}{\partial x}\left(\zeta\frac{\partial\psi}{\partial y}\right)-\frac{\partial}{\partial y}\left(\zeta\frac{\partial\psi}{\partial x}\right)\right). \end{aligned} \tag{4.16}$$

In the discrete space, the analogous of an Arakawa-like Jacobian operator is a vector of size NM defined as the combination of the three following:

$$\begin{aligned} J_1 &= \left\{\left[diag(P_x^{-1}Q_x\otimes I_y\psi)diag(I_x\otimes P_y^{-1}Q_y\zeta)\right]\mathbf{1}\right. \\ &- \left.\left[diag(I_x\otimes P_y^{-1}Q_y\psi)diag(P_x^{-1}Q_x\otimes I_y\zeta)\right]\mathbf{1}\right\} \end{aligned} \tag{4.17}$$

$$\begin{aligned} J_2 &= \left\{(P_x^{-1}Q_x\otimes I_y)\left[diag(\psi)diag(I_x\otimes P_y^{-1}Q_y\zeta)\right]\mathbf{1}\right. \\ &- \left.(I_x\otimes P_y^{-1}Q_y)\left[diag(\psi)diag(P_x^{-1}Q_x\otimes I_y\zeta)\right]\mathbf{1}\right\} \end{aligned} \tag{4.18}$$

$$\begin{aligned} J_3 &= \left\{(I_x\otimes P_y^{-1}Q_y)\left[diag(\zeta)diag(P_x^{-1}Q_x\otimes I_y\psi)\right]\mathbf{1}\right. \\ &- \left.(P_x^{-1}Q_x\otimes I_y)\left[diag(\zeta)diag(I_x\otimes P_y^{-1}Q_y\psi)\right]\mathbf{1}\right\}. \end{aligned} \tag{4.19}$$

where ζ and ψ are the vectors of size NM.
The following theorem refers to mimetic properties of the discrete scheme obtained by the linear combination of J_1, J_2 and J_3; in particolar theorem (4.2.1) and the existence of high-order SBP operators prove that the Arakawa-like scheme (4.20) is a mimetic arbitrary high-order accurate finite difference approximation of the non-linear Jacobian operator (4.16). Moreover, with the same techniques used to prove theorem 4.2.1, we can prove one specific property for each discrete Jacobian: J_1 is only skew-symmetric, J_2 conserves enstrophy and J_3 conserves kinetic energy.

Theorem 4.2.1. *The linear combination*

$$J^* = \frac{1}{3}J_1 + \frac{1}{3}J_2 + \frac{1}{3}J_3 \tag{4.20}$$

is skew-symmetric, conserves enstrophy and conserves kinetic energy.

Proof. The proof is divided in three parts:

a) *Skew-symmetry*
We start noting that J_1 is itself skew-symmetric, by definition (4.17):

$$J_1(a,b) = -J_1(b,a) \tag{4.21}$$

while J_2 and J_3 are not their-selves skew-symmetric, but, using definitions (4.18)-(4.19) they satisfy:

$$J_2(a,b) = -J_3(b,a). \tag{4.22}$$

The linear combination J^* satisfies then:

$$\begin{aligned} J^*(a,b) &= \tfrac{1}{3}[J_1(a,b)+J_2(a,b)+J_3(a,b)] \\ &= \tfrac{1}{3}[-J_1(b,a)-J_3(b,a)-J_2(b,a)] \\ &= -J^*(b,a) \end{aligned} \tag{4.23}$$

b) *Conservation of enstrophy*
Consider the semi-discretization

$$\frac{\partial \zeta}{\partial t} + J^*(\psi,\zeta) = 0. \tag{4.24}$$

By multipling (4.24) by $\zeta^T(P_x \otimes P_y)$ we have

$$\begin{aligned} \zeta^T(P_x\otimes P_y)\frac{\partial\zeta}{\partial t} &= \frac{1}{2}\frac{\partial}{\partial t}\|\zeta\|^2_{(P_x\otimes P_y)} \\ = -\frac{1}{3}\zeta^T(P_x\otimes P_y)\{&[diag(P_x^{-1}Q_x\otimes I_y\psi)diag(I_x\otimes P_y^{-1}Q_y\zeta)]\mathbf{1} \\ &-[diag(I_x\otimes P_y^{-1}Q_y\psi)diag(P_x^{-1}Q_x\otimes I_y\zeta)]\mathbf{1}\} \\ -\frac{1}{3}\zeta^T(P_x\otimes P_y)\{&(P_x^{-1}Q_x\otimes I_y)[diag(\psi)diag(I_x\otimes P_y^{-1}Q_y\zeta)]\mathbf{1} \\ &-(I_x\otimes P_y^{-1}Q_y)[diag(\psi)diag(P_x^{-1}Q_x\otimes I_y\zeta)]\mathbf{1}\} \\ -\frac{1}{3}\zeta^T(P_x\otimes P_y)\{&(I_x\otimes P_y^{-1}Q_y)[diag(\zeta)diag(P_x^{-1}Q_x\otimes I_y\psi)]\mathbf{1} \\ &-(P_x^{-1}Q_x\otimes I_y)[diag(\zeta)diag(I_x\otimes P_y^{-1}Q_y\psi)]\mathbf{1}\}. \end{aligned} \tag{4.25}$$

In the first term on the RHS of (4.25) we use (4.11) and the commutative property of diagonal matrices to write

$$\zeta^T(P_x\otimes P_y) = \mathbf{1}^T diag(\zeta)(P_x\otimes P_y) = \mathbf{1}^T(P_x\otimes P_y)diag(\zeta).$$

In the second and third term we use $Q_{x,y} = -Q_{x,y}^T$, (4.11), (4.12) and (4.13) as follows

$$\begin{aligned} \zeta^T(P_x\otimes P_y)(P_x^{-1}Q_x\otimes I_y) &= \zeta^T(Q_x\otimes P_y) \\ &= -\zeta^T(Q_x^TP_x^{-1}\otimes I_y)(P_x\otimes P_y) \\ &= -[(P_x\otimes P_y)(P_x^{-1}Q_x\otimes I_y)\zeta]^T \\ &= -\mathbf{1}^T diag[(P_x\otimes P_y)(P_x^{-1}Q_x\otimes I_y)\zeta] \\ &= -\mathbf{1}^T(P_x\otimes P_y)diag(P_x^{-1}Q_x\otimes I_y\zeta) \end{aligned} \tag{4.26}$$

and

$$\begin{aligned}\zeta^T(P_x\otimes P_y)(I_x\otimes P_y^{-1}Q_y) &= \zeta^T(P_x\otimes Q_y)\\ &= -\zeta^T(I_x\otimes Q_y^TP_y^{-1})(P_x\otimes P_y)\\ &= -[(P_x\otimes P_y)(I_x\otimes P_y^{-1}Q_y)\zeta]^T\\ &= -\mathbf{1}^Tdiag[(P_x\otimes P_y)(I_x\otimes P_y^{-1}Q_y)\zeta]\\ &= -\mathbf{1}^T(P_x\otimes P_y)diag(I_x\otimes P_y^{-1}Q_y\zeta).\end{aligned} \tag{4.27}$$

Next, by extracting $diag(\psi)$ and $diag(\zeta)$ from the second and the third term respectively, (4.25) becomes

$$\begin{aligned}&\frac{1}{2}\frac{\partial}{\partial t}\|\zeta\|^2_{(P_x\otimes P_y)}\\ &= -\frac{1}{3}\mathbf{1}^T(P_x\otimes P_y)diag(\zeta)\\ &\quad\left\{\left[diag(P_x^{-1}Q_x\otimes I_y\psi)diag(I_x\otimes P_y^{-1}Q_y\zeta)\right]\mathbf{1}\right.\\ &\quad\left.-\left[diag(I_x\otimes P_y^{-1}Q_y\psi)diag(P_x^{-1}Q_x\otimes I_y\zeta)\right]\mathbf{1}\right\}\\ &\quad+\frac{1}{3}\mathbf{1}^T(P_x\otimes P_y)diag(\psi)\\ &\quad\left\{-diag(P_x^{-1}Q_x\otimes I_y\zeta)\left[diag(I_x\otimes P_y^{-1}Q_y\zeta)\right]\mathbf{1}\right.\\ &\quad\left.+\,diag(I_x\otimes P_y^{-1}Q_y\zeta)\left[diag(P_x^{-1}Q_x\otimes I_y\zeta)\right]\mathbf{1}\right\}\\ &\quad+\frac{1}{3}\mathbf{1}^T(P_x\otimes P_y)diag(\zeta)\\ &\quad\left\{diag(I_x\otimes P_y^{-1}Q_y\zeta)\left[diag(P_x^{-1}Q_x\otimes I_y\psi)\right]\mathbf{1}\right.\\ &\quad\left.-\,diag(P_x^{-1}Q_x\otimes I_y\zeta)\left[diag(I_x\otimes P_y^{-1}Q_y\psi)\right]\mathbf{1}\right\}\end{aligned} \tag{4.28}$$

Note that the first term on the RHS of eq. (4.28) is the same of the third term with opposite sign, thanks to the commutative property of diagonal matrices. The same property is applied to the second term and finally, by summation, we have

$$\frac{1}{2}\frac{\partial}{\partial t}\|\zeta\|^2_{(P_x\otimes P_y)} = 0.$$

c) *Conservation of kinetic energy*

We multiply (4.24) by $\psi^T(P_x \otimes P_y)$ and we obtain

$$\begin{aligned}
\psi^T(P_x \otimes P_y)\frac{\partial \zeta}{\partial t} &= \frac{1}{2}\frac{\partial}{\partial t}\|(\nabla\psi)^2\|^2_{(P_x\otimes P_y)} \\
= -\frac{1}{3}\psi^T(P_x \otimes P_y)\big\{\big[diag(P_x^{-1}Q_x \otimes I_y\psi)diag(I_x \otimes P_y^{-1}Q_y\zeta)\big]\,\mathbf{1} \\
- \big[diag(I_x \otimes P_y^{-1}Q_y\psi)diag(P_x^{-1}Q_x \otimes I_y\zeta)\big]\,\mathbf{1}\big\} \\
-\frac{1}{3}\psi^T(P_x \otimes P_y)\big\{(P_x^{-1}Q_x \otimes I_y)\big[diag(\psi)diag(I_x \otimes P_y^{-1}Q_y\zeta)\big]\,\mathbf{1} \\
- (I_x \otimes P_y^{-1}Q_y)\big[diag(\psi)diag(P_x^{-1}Q_x \otimes I_y\zeta)\big]\,\mathbf{1}\big\} \\
-\frac{1}{3}\psi^T(P_x \otimes P_y)\big\{(I_x \otimes P_y^{-1}Q_y)\big[diag(\zeta)diag(P_x^{-1}Q_x \otimes I_y\psi)\big]\,\mathbf{1} \\
- (P_x^{-1}Q_x \otimes I_y)\big[diag(\zeta)diag(I_x \otimes P_y^{-1}Q_y\psi)\big]\,\mathbf{1}\big\}.
\end{aligned} \tag{4.29}$$

Similar to the procedure above for the first term on the RHS of (4.29) we rewrite

$$\psi^T(P_x \otimes P_y) = \mathbf{1}^T diag(\psi)(P_x \otimes P_y) = \mathbf{1}^T(P_x \otimes P_y)diag(\psi).$$

In the second and third term we again apply $Q_{x,y} = -Q_{x,y}^T$, (4.12) and (4.13) obtaining, with analogous steps of (4.26) and (4.27),

$$\psi^T(P_x \otimes P_y)(P_x^{-1}Q_x \otimes I_y) \;=\; -\mathbf{1}^T(P_x \otimes P_y)diag(P_x^{-1}Q_x \otimes I_y\psi)$$

and

$$\psi^T(P_x \otimes P_y)(I_x \otimes P_y^{-1}Q_y) \;=\; -\mathbf{1}^T(P_x \otimes P_y)diag(I_x \otimes P_y^{-1}Q_y\psi).$$

Then, by extracting from the second and the third term $diag(\psi)$ and $diag(\zeta)$,

respectively, (4.29) becomes

$$\begin{aligned}
&\frac{1}{2}\frac{\partial}{\partial t}\|(\nabla\psi)\|^2_{(P_x\otimes P_y)} \\
&\qquad = \; -\frac{1}{3}\mathbf{1}^T(P_x\otimes P_y)diag(\psi) \\
&\qquad\quad \left\{\left[diag(P_x^{-1}Q_x\otimes I_y\psi)diag(I_x\otimes P_y^{-1}Q_y\zeta)\right]\mathbf{1}\right. \\
&\qquad\quad \left. -\left[diag(I_x\otimes P_y^{-1}Q_y\psi)diag(P_x^{-1}Q_x\otimes I_y\zeta)\right]\mathbf{1}\right\} \\
&\qquad\quad +\frac{1}{3}\mathbf{1}^T(P_x\otimes P_y)diag(\psi) \\
&\qquad\quad \left\{diag(P_x^{-1}Q_x\otimes I_y\psi)\left[diag(I_x\otimes P_y^{-1}Q_y\zeta)\right]\mathbf{1}\right. \\
&\qquad\quad \left. -\, diag(I_x\otimes P_y^{-1}Q_y\psi)\left[diag(P_x^{-1}Q_x\otimes I_y\zeta)\right]\mathbf{1}\right\} \\
&\qquad\quad +\frac{1}{3}\mathbf{1}^T(P_x\otimes P_y)diag(\zeta) \\
&\qquad\quad \left\{-diag(I_x\otimes P_y^{-1}Q_y\psi)\left[diag(P_x^{-1}Q_x\otimes I_y\psi)\right]\mathbf{1}\right. \\
&\qquad\quad \left. +\, diag(P_x^{-1}Q_x\otimes I_y\psi)\left[diag(I_x\otimes P_y^{-1}Q_y\psi)\right]\mathbf{1}\right\}
\end{aligned} \tag{4.30}$$

Note again that the first term on the RHS of eq. (4.30) is the same of the second term with opposite sign, thanks to the commutative property of diagonal matrices. The same property is applied to the last term and finally, by summation, we have

$$\frac{1}{2}\frac{\partial}{\partial t}\|(\nabla\psi)\|^2_{(P_x\otimes P_y)} = 0.$$

□

5. A physical application: study of the energy spectra for a quasi-geostrophic model

This section focuses on the devolopment and the study of an atmospheric model, the quasi-geostrophic model. Quasi-geostrophic (QG) theory is based on the assumption of rapid rotation (small Rossby number) and thinness (10 km vertical vs 20000 km horizontal). The underlying physics involves a velocity equation and a temperature equation, and 1st-order perturbation expansion around the Rossby number. The vertical velocity is constrained, for this reason 2D and QG theories are related also if they are not isomorphic in terms of physics [70].
In particular, I will focus on the numerical model, for this reason I'll try to give a short introduction to the geophysical problem, even if an infinite bibliography is available on this topic. A good introduction to the Geophysical fluid dynamics is given by Pedlosky [44], a very useful PhD dissertation on the theoretical study of the cascades of 3D, 2D, and QG turbulence is given by Eleftherios Gkioulekas [71], a collection on the available informations of the bidimensional turbulence is given by Tabeling [72], and many other more specific references will be discussed in the next sections.
The physical problem highlights the need of a numerical method able to respect physical properties as energy/enstrophy conservation and a correct simulation of the energy spectrum. For this reason I will start with a short introduction of the turbulence dynamics and the related energy spectrum, I will show how it is possible to derive the quasi-geostrophic model and, in the last section, I will present the numerical results that we obtained using mimetic finite difference operators for a two-layer QG model. Again, we will deal with the non-linearity of equations: this will cause an energy transfer between different scales, so we have to be very careful in the treatment of numerical experiments.
This work has been done in collaboration with ENEA UTMEA -Unitá Tecnica Modellistica Energetica Ambientale- laboratories, Anguillara.

5.1. The turbulence

One of the main properties of turbulence, lies in its capability to transfer energy between different scales of motion; this mechanism begins when big vorteces spring up at the integral scale, where the fluid kinetic energy is conveyed, and, due to the high instability tipical of these vortex structures, there is a fragmentation phenomenon which gives rise to smaller vorteces causing an energy cascade toward the inertial scale. The trasferred

kinetic energy is finally dissipated at smallest scales through a viscous term - heat - (Kolmogorov scale).
Atmospheric turbulence near the Earth's surface differs from that at higher levels. At low levels (within a few hundred metres of the surface), when solar radiation heats the surface, the air above it becomes warmer and more buoyant, and cooler, denser air descends to displace it. The resulting vertical movement of air, together with flow variations around surface obstacles, makes low-level winds extremely irregular. At night the surface cools rapidly, chilling the air near the ground; when that air becomes cooler than the air above it, a stable temperature inversion is created, and the wind speed decreases sharply. At altitudes of several thousand meters or more, frictional effects of surface topography on the wind are greatly reduced, and the small-scale turbulence characteristic of the lower atmosphere is absent. Generally upper-level winds are usually relatively regular, but this is not always true.
The transfer between different scales is due to non linear processes, as we have seen for an easy 1D model in 1.2, for this reason the energy cascade will depend on the equations considered: a brief description of the turbulence is given, trying to focusing on the differences between 2D and 3D model dynamics.

5.1.1. 3D and 2D Turbulence

In this section I will show turbulence behavior depending on the model considered and I will show the main differences between a 2D and a 3D modeling.
Let's start again applying the curl to the momentum equation for an incompressible flow,

$$\frac{\partial \omega}{\partial t} + u \cdot \nabla \omega = \nu \nabla^2 \omega + \nabla \times f + \frac{\nabla \rho \times \nabla p}{\rho^2} + \omega \cdot \nabla u \tag{5.1}$$

Let's suppose that f can be written as the gradient of a scalar function and that $\nabla\rho \times \nabla p = 0$, in this case the equation (5.1) reduces to:

$$\frac{\partial \omega}{\partial t} + u \cdot \nabla \omega = \nu \nabla^2 \omega + \omega \cdot \nabla u \tag{5.2}$$

On the LHS we can see the terms composing the material derivative of ω, they quantify the vorticity variation of a fluid particle, measured moving on the particle. The terms on the RHS represent the reason of such variation, the first term is the diffusion and the second is the vortex stretching. In order to better understand the action of the last term, we write component by component (for example the x component in a cartesian system):

$$(\omega \cdot \nabla u) \cdot \widehat{x} = \omega_x \frac{\partial u_x}{\partial x} + \omega_y \frac{\partial u_x}{\partial y} + \omega_z \frac{\partial u_x}{\partial z} \tag{5.3}$$

The term $\omega_x \frac{\partial u_x}{\partial x}$ operates when the velocity gradient has the same direction of the vorticity and will stretch the fluid; due to the angular momentum conservation, the rotational velocity must increase and so does the vorticity. This is a self-amplification mechanism and it is caused by the velocity gradient and it doesn't need any external

sources. The other two terms acts in order to rotate the existent vorticity because of the cross velocity gradients.
In the 3-dimensional vorticity dynamic there is an amplification mechanism associated to the increasingly smaller scales of motion; this growth is stopped at the characteristic scale $r_B = (\frac{\nu^3}{\epsilon})^{\frac{1}{4}}$ (Kolmogorov scale) where vortex stretching and diffusion cancel out each other.
We cannot use the same arguments of 3D dynamics in the 2-dimensional flows because it results $\omega \cdot \nabla u = 0$ and the vortex-stretching is zero, changing the dynamic at all; 2-D flows tend to well approximate large-scale flows in thin fluid shells, such as planetary atmospheres and the ocean, so it seems reasonable to study bidimensional dynamics. In 2D flows, the vector ω has only the component normal to the plane of motion, them, without viscous terms, equation (5.2) becomes

$$\frac{D\omega}{Dt} = 0 \tag{5.4}$$

This equation states that each single fluid particle vorticity is conserved along its trajectory; multiplying such equation with ω^n we can see that any power of the vorticity will still be conserved. We can integrate equation (5.4) on the plane of motion, obtaining the conservation of the circulation

$$\Gamma = \int_S \omega dS, \tag{5.5}$$

of the enstrophy

$$\Omega = \int_S \frac{\omega^2}{2} dS, \tag{5.6}$$

and of all velocity's powers.
All these conservation properties cause deep differences with the 3D case, first of all the energy transfer between different scales. In the next section we will explore physical and theorical results for the energy spectra of 2D and quasi-geostrophic models.

5.2. KLB theory and Tung-Orlando-Gkouliekas extension

KLB (Kraichnan [73]-[74], Leith [75], Batchelor [76]) theory for the 2D turbulence claims there is only one energy flux (energy upscale cascade) and one entrophy flux (enstrophy downscale cascade); these two cascades live on disjointed spectral interval. The union set of these processes is called *dual-pure cascade*. Kraichnan, Leith e Batchelor use a scale analysis to show that the energy spectrum, respectively in the upper scales for the energy cascade and in the lower scales for the enstrophy cascade, is given by:

$$\begin{aligned} E(k) &= C_1 \epsilon^{2/3} k^{-\frac{5}{3}} \\ E(k) &= C_2 \eta^{\frac{2}{3}} k^{-3} \end{aligned} \tag{5.7}$$

where ϵ and η respectively represent the energy and the entrophy injection rates, fig. 5.1.

These expression hold only under the hypotesis of disjointed intervals for the two cas-

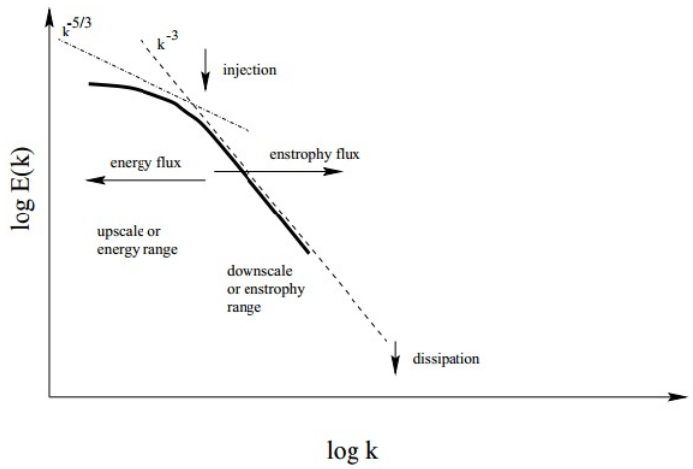

Figure 5.1.: The Kraichnan-Leith-Batchelor scenario of a dual-pure cascade.

cades. Moreover, for the numerical point of view there is the limit of an unrepresentable infinite domain, even if, recently, it was shown that it is possible to obtain the enstrophy cascade in agreement with the KLB theory [77],[78],[79].
Charney [80] states that quasi-geostrophic model is isomorphic to the 2D turbulence, so initially one would execpt the Q.G. behavior to be similar to the 2D case. This is not really true (as argued in [81]), and anyway a different dynamic appears when we consider a two-layer Q.G. model [70]. In this case, the stratification leads to a situation where Danilov inequality is not valid [82]-[83] and in the inertial range can coexist energy and enstrophy fluxes. In order to break Danilov inequality, the quasi-geostrophic system needs to have a sufficently big asymmetry between the two layers, meaning that the system has to be baroclinic. This is obtained putting a suitable Ekman damping in the lower layer [84].
Moreover, against KLB theory, Gkioulekas and Tung ([85]) conjectured that intervals can overlap each other giving rise to a double energy/enstrophy cascade in both directions. In particular they derive a useful expression for the energy cascade using a linear combination of the flux spectrum related to the energy (k^{-3}), and to the enstrophy ($k^{-\frac{5}{3}}$) proving how these two fluxes can coexist; the transition from -3 slope to $-5/3$ slope occurs at the transition wavenumber k_t. The order of magnitude of k_t can be estimated by dimensional analysis and it is given by $k_t \approx \sqrt{\eta/\epsilon}$.
What if we compare modeling theories with experimental results? In 1984 Nastrom and Gage [86] proposed the (renowned) energy spectrum for the atmospheric turbulence obtained from more then 6000 commercial aircraft flights made during the GASP (Global Atmospheric Sampling Program). In figure 5.2, we can see two different slopes: between

3000 km and 800 km (large scales) the slope behaves like k^{-3} whilst for small scales, around 600 km and 1 km, the slope is like $k^{-5/3}$. The transition region appears for the scales between 600 km and 800 km. Nastrom and Gage analysis showed that only little variability respect to latitude, season etc. appears, except for the temperature amplitudes, which result to be much larger in the stratosphere than in the troposphere.
So far we have seen two different approaches to explain the Nastrom-Gage spectrum: the

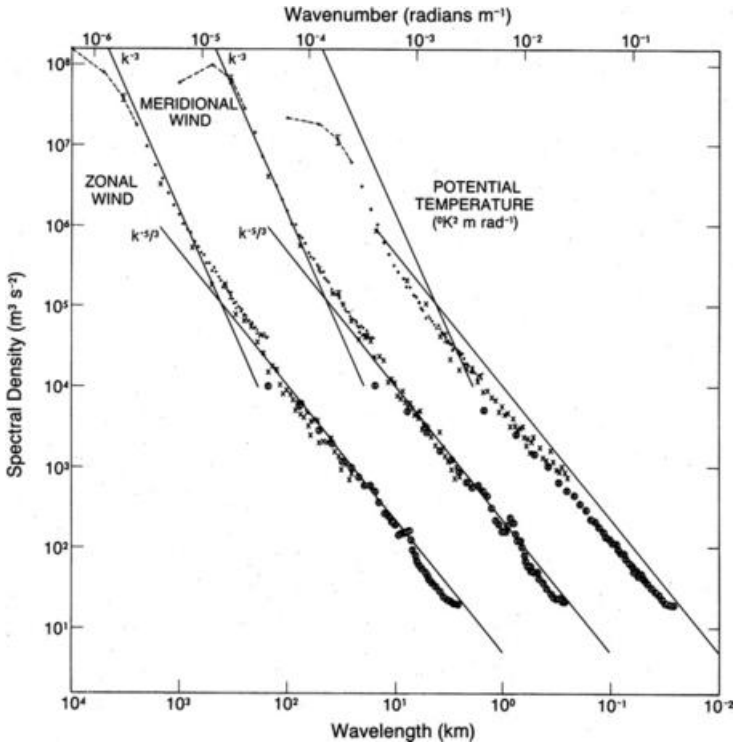

Figure 5.2.: Nastrom-Gage Spectrum

dual pure cascade (KLB theory) vs the double energy cascade (Gkioulekas and Tung); the dual pure cascade was supported also by Fjortoft [87], who proved that in the 2D turbulence cannot exist a downscale energy cascade, but this proof was argued to be incorrect [70] by Tung and Orlando, which contributed to support the double energy cascade theory. They proved that in 2D turbulence, as well as in Q.G. dynamics, the energy downscale cascade is not prohibited, but the downscale energy cascade in 2D does not appear due to the absence of anomalous dissipation when the viscosity coefficient vanishes. In the Q.G. dynamic this prohibition does not hold, so a downscale energy cascade is possible. Another important difference between Q.G. and 2D turbulence is the QG-contained mechanism of baroclinic instability as the source of energy and enstrophy injection [88].
Tung and Orlando claim that the quasi-geostrophic model is sufficient to reproduce Nastrom-Gage spectrum, and showed it using spectral methods [89], see figure **??**. They

used a two-layer Q.G. model without any forcing other than self-excited baroclinic instability, or other (e.g., unbalanced) dynamics, and this does not appear to present any difficulty for the model in producing the right amount of turbulent energy in all scales of motion. The subgrid dissipation used, albeit small, appears to be sufficient to ensure a downscale energy flux throughout the subsynoptic and mesoscales. Also the transition between the two slopes $k = -3$ and $k = -5/3$ is in agreement with the one obtained by observations.

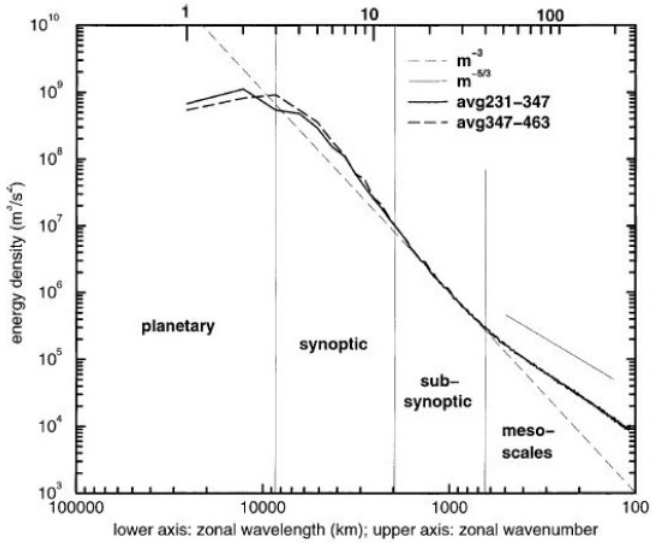

Figure 5.3.: Numerical Tung-Orlando spectrum

For the reasons presented, the Q.G. model seems to be an easy but good model to represent the atmospheric dynamic; in the next section I'll give a full derivation of the quasi-geostrophic equation and in the last section I will show numerical results of such model using mimetic finite difference discretization.

5.3. The quasi-geostrophic model

The main idea of the quasi-geostrophic model is to re-scale motion equations for the synoptic scale, using a Taylor expansion respect to an adimensional parameter (the Rossby number). The main steps can be summarized as follows:

a) **Euler equations**
Let's consider the conservation equations:

$$\rho \frac{D\underline{u}}{Dt} = -\nabla p + \rho \nabla \phi + \underline{F} \tag{5.8}$$

$$\frac{D\rho}{Dt} + \rho\nabla \cdot \underline{u} = 0 \tag{5.9}$$

$$\rho\frac{De}{Dt} = -p\rho\frac{D}{Dt}\rho^{-1} + k\nabla^2 T + \chi + \rho Q \tag{5.10}$$

where, by $\frac{D}{Dt} = \partial_t + \underline{u}\cdot\nabla$ we denote the material derivative, while other terms are:

- $\underline{u} = (u, v, w)$, the velocity vector
- ρ, the density
- p, the pressure
- e, the internal energy per mass unit
- ϕ, the conservative forces potential (tipically this corresponds to the gravity)
- $\underline{F}$, the non-conservative forces
- T, the temperature
- Q, the heat
- k, the thermal conductivity coefficient
- χ, the heat due to viscous dissipation

b) **Equation of state and potential temperature**
We consider the ideal gas law:

$$\rho = \frac{p}{RT} \tag{5.11}$$

where the internal energy depends only by the temperature, $e = e(T)$, and we assume this relation to be linear. We define, respectively, C_v when the volume is constant and C_p when the pressure is constant as:

$$C_v = \frac{de}{dt} \tag{5.12}$$

$$C_p = \frac{d(e + p/\rho)}{dT}, \tag{5.13}$$

They are related by:

$$C_p = C_v + R, \tag{5.14}$$

We can write (linear dependence):

$$e = C_v T. \tag{5.15}$$

Now we can introduce the specific entropy $s = s(p, T)$, related to the other termodynamic variable by:

$$Tds = de + pd(\rho^{-1}) \tag{5.16}$$

We can substitute the specific entropy in the equation (5.10), obtaining:

$$T\frac{Ds}{Dt} = \frac{k}{\rho}\nabla^2 T + Q \tag{5.17}$$

while, deriving the equation of state:

$$\frac{dT}{T} = \frac{dp}{p} - \frac{d\rho}{\rho} \tag{5.18}$$

This, together with (5.16), divide by T, yields:

$$ds = C_v \frac{dT}{T} + \frac{p}{T} d(\frac{1}{\rho}) = C_v \frac{dT}{T} - \frac{R\rho}{\rho^2} d\rho) = C_v \frac{dT}{T} + R(\frac{dT}{T} - \frac{dp}{p}). \tag{5.19}$$

Finally, using the relation (5.14), we obtain:

$$ds = C_p \frac{dT}{T} - R\frac{dp}{p}. \tag{5.20}$$

$$s = C_p ln(T) - Rln(p) = ln(\frac{T^{C_p}}{p^R}). \tag{5.21}$$

If we consider a constant entropy transformation, starting with initial temperature T_0 and initial pressure p_0 we'll get:

$$C_p ln(\frac{T}{T_0}) = Rln(\frac{p}{p_0}) \tag{5.22}$$

$$\frac{T}{T_0} = (\frac{p}{p_0})^{\frac{R}{C_p}}. \tag{5.23}$$

Then we obtain the definition of potential temperature θ:

$$\theta = T(\frac{p_0}{p})^{\frac{R}{C_p}} \tag{5.24}$$

The potential temperature is the temperature that the parcel would acquire if adiabatically brought to a standard reference pressure. Using the ideal gas law, equation (5.24) can be written as:

$$\rho = \frac{p_0}{R\theta}(\frac{p}{p_0})^{\frac{1}{\gamma}} \tag{5.25}$$

with $\gamma = \frac{C_p}{C_v}$.
Let's consider now figure (5.4), where a fluid particle A is brought from height z to height $z + dz$ at the same level of another fluid particle B.

Then, at $z + dz$, the density variation of A is:

$$d\rho_A = \frac{1}{\gamma} \frac{p_0}{R\theta} (\frac{p}{p_0})^{\frac{1}{\gamma}} \frac{\partial p}{\partial z} \frac{dz}{p} \tag{5.26}$$

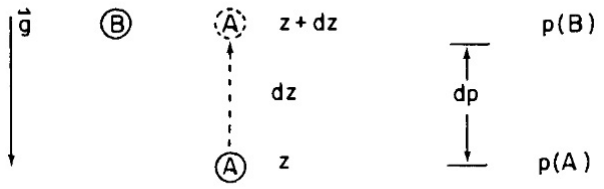

Figure 5.4.: Static Stability

then we can write the density at $z + dz$ as

$$\rho_A + d\rho_A = \rho_A(z) + \frac{1}{\gamma}\frac{\rho}{p}\frac{\partial p}{\partial z}dz. \tag{5.27}$$

Particle B density is:

$$\rho_B = \rho_A(z) + \frac{\partial \rho}{\partial z}dz \tag{5.28}$$

then:

$$\rho_A + d\rho_A - \rho_B = (\frac{1}{\gamma}\frac{\rho}{p}\frac{\partial p}{\partial z} - \frac{\partial \rho}{\partial z})dz. \tag{5.29}$$

This gap gives rise to a buoyancy force equal to

$$\frac{g}{\rho}(\rho_A + d\rho_A - \rho_B) = g(\frac{1}{\gamma}\frac{1}{p}\frac{\partial p}{\partial z} - \frac{1}{\rho}\frac{\partial \rho}{\partial z})dz = \frac{g}{\theta}\frac{\partial \theta}{\partial z}dz \tag{5.30}$$

This means that, if $\frac{\partial \theta}{\partial z} > 0$, the buoyancy force pushes the particle back to the starting point z and the atmosphere is said to be stable. For this reason, the quantity $\frac{1}{\theta}\frac{\partial \theta}{\partial z}$ is called static stability coefficient. Moreover, due to the fact that the force is proportional to the change of position, the fluid particle oscillation frequency around his equilibrium point is given by:

$$N = (\frac{g}{\theta}\frac{\partial \theta}{\partial z})^{\frac{1}{2}} \tag{5.31}$$

which is called Brunt-Vaisala frequency. We consider again the temperature and, using the hydrostatic balance, we can write the stability coefficient as:

$$\frac{1}{\theta}\frac{\partial \theta}{\partial z} = \frac{1}{T}[\frac{\partial T}{\partial z} + \frac{g}{C_p}] \tag{5.32}$$

then, even if $\frac{\partial T}{\partial z} < 0$, the atmosphere will be stable until the adiabatic lapse rate $(-\frac{\partial T}{\partial z})$ is not bigger than $\frac{g}{C_p}$.

Finally, we observe:

$$\frac{D}{\theta}\frac{\partial\theta}{\partial z} = \frac{N^2 D}{g} = O(10^{-1}) \tag{5.33}$$

where D is the vertical spatial scale.
Let's go back to the potential temperature (5.24), if we derive:

$$\begin{aligned} d\theta &= dT(\frac{p_0}{p})^{\frac{R}{C_p}} + Tp_0^{\frac{R}{C_p}}\frac{R}{C_p}\frac{1}{p}^{\frac{R}{C_p}-1}(-\frac{dp}{p^2}) \\ &= dT(\frac{p_0}{p})^{\frac{R}{C_p}} + T\frac{p_0}{p}^{\frac{R}{C_p}}\frac{R}{C_p}(-\frac{dp}{p}) \\ = dT(\frac{\theta}{T})^{\frac{R}{C_p}} - \theta\frac{R}{C_p}(\frac{dp}{p}) &= \frac{\theta}{C_p}(C_p\frac{dT}{T} - R\frac{dp}{p}) = \frac{\theta}{C_p}ds. \end{aligned} \tag{5.34}$$

Using θ instead of e, we write equation (5.17) obtaining a potential temperature equation:

$$\frac{d\theta}{dt} = \frac{\theta}{C_p T}(\frac{k}{\rho}\nabla^2 T + Q) \tag{5.35}$$

c) **Rotational coordinate system**
In order to take care of the Earth's rotation, we consider a rotational coordinate system assuming the Earth to be a sphere turning around his own rotating axis with constant angular velocity Ω. Let $\underline{r} = (r_x, r_y, r_z)$ be the position vector in the inertial system $(\widehat{i}, \widehat{j}, \widehat{k})$ and $\underline{r'} = (r'_x, r'_y, r'_z)$ be the position vector in the rotating coordinate system $(\widehat{i'}, \widehat{j'}, \widehat{k'})$; regarding velocity and acceleration we have:

$$\underline{v} = \underline{v'} + \Omega \times \underline{r'} \tag{5.36}$$

$$\frac{d\underline{v}}{dt} = \frac{d\underline{v'}}{dt} + 2\Omega \times \underline{v'} + \Omega \times (\Omega \times r') \tag{5.37}$$

Assuming $\Omega = (0, 0, \Omega)$, and substituting this relation in equation (5.8), we obtain (from now on I will obmit the quotes because we will always refer to the non-inertial coordinate system):

$$\frac{\partial u}{\partial t} + u\frac{\partial u}{\partial x} + v\frac{\partial u}{\partial y} + w\frac{\partial u}{\partial z} = -\frac{1}{\rho}\frac{\partial p}{\partial x} + v2\Omega sin(\varphi) \tag{5.38}$$

$$\frac{\partial v}{\partial t} + u\frac{\partial v}{\partial x} + v\frac{\partial v}{\partial y} + w\frac{\partial v}{\partial z} = -\frac{1}{\rho}\frac{\partial p}{\partial y} - u2\Omega sin(\varphi) \tag{5.39}$$

$$\frac{\partial w}{\partial t} + u\frac{\partial w}{\partial x} + v\frac{\partial w}{\partial y} + w\frac{\partial w}{\partial z} = -\frac{1}{\rho}\frac{\partial p}{\partial z} - g \tag{5.40}$$

$2\Omega sin(\varphi) = f$ is the Coriolis parameter.

d) **Hydrostatic approximation** When the atmosphere is at rest, the gravity bal-

ances the vertical component of the pressure gradient (hydrostatic balance):

$$\frac{\partial p_s(z)}{\partial z} = -\rho_s(z)g \tag{5.41}$$

Due to the smallness of velocity components, it is useful to write p and ρ as the sum of hte basic state plus a small deviation due to the motion:

$$p = p_s(z) + p'(x, y, z, t) \tag{5.42}$$

$$\rho = \rho_s(z) + \rho'(x, y, z, t). \tag{5.43}$$

e) **Scaling and adimensional equations**
We are looking for motions acting on the following scales:

- $T \approx 10^5\ s$, temporal scale
- $L \approx 10^6\ m$, horizontal spatial scale
- $D \approx 10^4\ m$, depth scale
- $U \approx 10\ m/s$, horizontal velocity scale
- $W \approx 10\ cm/s$, vertical velocity scale
- $f_0 U \approx 10^{-3} m/s^2$
- $\frac{\delta P}{\rho} \approx 10^3 m^2/s^2$ scale of the fluctuations of the horizontal pressure
- $\frac{P}{\rho D} \approx 10\ m/s^2$, scale of the vertical pressure gradient
- $\Omega \approx 10^{-4}/sec$, angular velocity of the Earth
- $G \approx 10\ m/s^2$, gravity scale

Now it is useful to introduce a dimensionless parameter, the Rossby number:

$$R_0 = \frac{U}{fL}. \tag{5.44}$$

We write different fields in such a way that it is easy to compare similar scales: $u = U\overline{u}$, $t = \frac{L}{U}\overline{t}$, $p = P\overline{p}$, etc..
Thanks to (5.42)-(5.43), we re-write equation (5.9) as:

$$\frac{\partial \rho'}{\partial t} + w\frac{\partial \rho_s}{\partial z} + U \cdot \nabla \rho' + (\rho_s + \rho')\nabla \cdot U \tag{5.45}$$

Moreover, we observe:

$$p = p_s(z) + \rho_s U f_0 L \overline{p}' \tag{5.46}$$

$$\rho = \rho_s(z)[1 + R_0 F \overline{\rho}'] \tag{5.47}$$

where $F = \frac{f_0^2 L^2}{gD}$, eq. (5.45), divided by ρ_s, becomes:

$$\begin{aligned} &\frac{W}{D}(\overline{w}\frac{1}{\rho_s}\frac{\partial \rho_s}{\partial \overline{z}} + \frac{\partial \overline{w}}{\partial \overline{z}}) + \frac{U}{L}(\frac{\partial \overline{u}}{\partial \overline{x}} + \frac{\partial \overline{v}}{\partial \overline{y}}) \\ &+\frac{R_0 F U}{L}(\frac{\partial \overline{\rho}'}{\partial \overline{t}} + \overline{u}\frac{\partial \overline{\rho}'}{\partial \overline{x}} + \overline{v}\frac{\partial \overline{\rho}'}{\partial \overline{y}} + \overline{\rho}'\frac{\partial \overline{u}}{\partial \overline{x}} + \overline{\rho}'\frac{\partial \overline{v}}{\partial \overline{y}}) \\ &+\frac{R_0 F W}{D}(\overline{w}\frac{\partial \overline{\rho}'}{\partial \overline{z}} + \overline{\rho}'\frac{\partial \overline{w}}{\partial \overline{z}}) = 0 \end{aligned} \tag{5.48}$$

We can analyze the different scales:

- $A = \frac{W}{D} \approx \frac{10^{-6}}{s}$
- $B = \frac{U}{L} \approx \frac{10^{-5}}{s}$
- $C = \frac{F R_0 U}{L} \approx \frac{10^{-7}}{s}$
- $D = \frac{R_0 F W}{D} \approx \frac{10^{-8}}{s}$

Because of $B >> A >> C >> D$, we choose to keep only A and B:

$$\frac{W}{D}(\overline{w}\frac{1}{\rho_s}\frac{\partial \rho_s}{\partial \overline{z}} + \frac{\partial \overline{w}}{\partial \overline{z}}) + \frac{U}{L}(\frac{\partial \overline{u}}{\partial \overline{x}} + \frac{\partial \overline{v}}{\partial \overline{y}}) = 0 \tag{5.49}$$

Regarding the potential temperature, similar to what we have already done with p and ρ, we obtain the following decomposition:

$$\theta = \theta_s(z)[1 + R_0 F \overline{\theta}'(x, y, z, t)]. \tag{5.50}$$

where

$$ln(\theta_s(z)) = \frac{1}{\gamma} ln(p_s(z)) - ln(\rho_s(z)) + cost, \quad \gamma = \frac{C_p}{C_v} \tag{5.51}$$

Using the decomposition (5.50), we can write dimensionless eq. (5.35):

$$\frac{\partial \overline{\theta}'}{\partial \overline{t}} + \overline{u}\frac{\partial \overline{\theta}'}{\partial \overline{x}} + \overline{v}\frac{\partial \overline{\theta}'}{\partial \overline{y}} + \frac{\overline{w}}{R_0 F \theta_s}\frac{\partial \theta_s}{\partial \overline{z}}(1 + R_0 F \overline{\theta}') = (\frac{H_*}{C_p T})\frac{gD}{U^2 f_0} \tag{5.52}$$

with

$$H_* = \frac{k}{\rho}\nabla^2 T + Q. \tag{5.53}$$

and $H_* \leq O(U^2 f_0)$. We define also:

$$H = H_* \frac{gD}{C_p T f_0 U^2} \tag{5.54}$$

and the stratification parameter $S(z)$:

$$S(z) = \frac{F^{-1}}{\theta_s}\frac{\partial \theta_s}{\partial z} \tag{5.55}$$

so that eq. (5.52) is now:

$$\frac{\partial\overline{\theta}'}{\partial\overline{t}} + \overline{u}\frac{\partial\overline{\theta}'}{\partial\overline{x}} + \overline{v}\frac{\partial\overline{\theta}'}{\partial\overline{y}} + \frac{\overline{w}}{R_0}S(1 + R_0F\overline{\theta}') = H \tag{5.56}$$

First two equations of the motion are easy to handle, while the third one:

$$\begin{aligned}\frac{WU}{L}\frac{\partial\overline{w}}{\partial\overline{t}} + \frac{UW}{L}\overline{u}\frac{\partial\overline{w}}{\partial\overline{x}} + \frac{UW}{L}\overline{v}\frac{\partial\overline{w}}{\partial\overline{y}} + \frac{W^2}{D}\overline{w}\frac{\partial\overline{w}}{\partial\overline{z}} \\ = -\frac{P}{D\rho_s(1 + R_0F\overline{\rho})}\frac{\partial(p_s + \rho_sUfL\overline{p})}{\partial\overline{z}} - g\end{aligned} \tag{5.57}$$

but

- $A = \frac{WU}{L} \approx 10^{-7}\frac{m}{s^2}$
- $B = \frac{W^2}{D} \approx 10^{-8}\frac{m}{s^2}$
- $C = \frac{P}{D\rho_s} \approx g \approx 10\frac{m}{s^2}$

so that $C >> A >> B$ and then:

$$0 = -\frac{P}{D\rho_s(1 + R_0F\overline{\rho})}\frac{\partial(p_s + \rho_sUfL\overline{p})}{\partial\overline{z}} - g \tag{5.58}$$

Finally we are able to write the whole system:

$$\frac{U^2}{L}\frac{\partial\overline{u}}{\partial\overline{t}} + \frac{U^2}{L}\overline{u}\frac{\partial\overline{u}}{\partial\overline{x}} + \frac{U^2}{L}\overline{v}\frac{\partial\overline{u}}{\partial\overline{y}} + \frac{UW}{D}\overline{w}\frac{\partial\overline{u}}{\partial\overline{z}} = -\frac{P}{\rho_sL}\frac{\partial\overline{p}}{\partial\overline{x}} + 2U\Omega sin(\varphi)\overline{v} \tag{5.59}$$

$$\frac{U^2}{L}\frac{\partial\overline{v}}{\partial\overline{t}} + \frac{U^2}{L}\overline{u}\frac{\partial\overline{v}}{\partial\overline{x}} + \frac{U^2}{L}\overline{v}\frac{\partial\overline{v}}{\partial\overline{y}} + \frac{UW}{D}\overline{w}\frac{\partial\overline{v}}{\partial\overline{z}} = -\frac{P}{\rho_sL}\frac{\partial\overline{p}}{\partial\overline{y}} - 2U\Omega sin(\varphi)\overline{u} \tag{5.60}$$

$$0 = -\frac{P}{D\rho_s(1 + R_0F\overline{\rho})}\frac{\partial(p_s + \rho_sUfL\overline{p})}{\partial\overline{z}} - g \tag{5.61}$$

$$\frac{W}{D}(\overline{w}\frac{1}{\rho_s}\frac{\partial\rho_s}{\partial\overline{z}} + \frac{\partial\overline{w}}{\partial\overline{z}}) + \frac{U}{L}(\frac{\partial\overline{u}}{\partial\overline{x}} + \frac{\partial\overline{v}}{\partial\overline{y}}) = 0 \tag{5.62}$$

$$R_0[\frac{\partial\overline{\theta}'}{\partial\overline{t}} + \overline{u}\frac{\partial\overline{\theta}'}{\partial\overline{x}} + \overline{v}\frac{\partial\overline{\theta}'}{\partial\overline{y}}] + \overline{w}S^{-1}(1 + R_0F\overline{\theta}') = HR_0 \tag{5.63}$$

f) **Series Expansion respect to the Rossby number**
We consider now the series expansion of primitive variable respect to the Rossby number

$$R_0 = \frac{U}{fL}$$

:

$$u = u^{(0)} + R_0u^{(1)} + R_0^2u^{(2)} + .. \tag{5.64}$$

$$v = v^{(0)} + R_0 v^{(1)} + R_0^2 v^{(2)} + .. \tag{5.65}$$

and so on.

- $\frac{\partial u}{\partial z} = \frac{\partial v}{\partial z} = 0$, indeed, studying the vorticity equation $\omega = \nabla \times u$:

$$\frac{d\omega}{dt} = \omega_a \cdot \nabla u - \omega_a \nabla \cdot u + \frac{\nabla\rho \times \nabla p}{\rho^2} + \nabla \times \frac{F}{\rho} \tag{5.66}$$

  with $\omega_a = \omega + 2\Omega$, we get the vorticity equation for large scale motions:

$$(2\Omega \cdot \nabla)u - 2\Omega\nabla \cdot u = -\frac{\nabla\rho \times \nabla p}{\rho^2} \tag{5.67}$$

  Recalling that Ω has got only the component parallel to the z axis, then we write eq. (5.67) for each component:

$$2\Omega\frac{\partial u}{\partial z} = -\frac{1}{\rho^2}(\frac{\partial p}{\partial z}\frac{\partial \rho}{\partial y} - \frac{\partial p}{\partial y}\frac{\partial \rho}{\partial z}) \tag{5.68}$$

$$2\Omega\frac{\partial v}{\partial z} = \frac{1}{\rho^2}(\frac{\partial p}{\partial z}\frac{\partial \rho}{\partial x} - \frac{\partial p}{\partial x}\frac{\partial \rho}{\partial z}) \tag{5.69}$$

$$2\Omega(\frac{\partial u}{\partial x} + \frac{\partial v}{\partial y}) = -\frac{1}{\rho^2}(\frac{\partial p}{\partial x}\frac{\partial \rho}{\partial y} - \frac{\partial p}{\partial y}\frac{\partial \rho}{\partial x}) \tag{5.70}$$

  We are supposing the density horizontal variations to be negligible, which means $\rho = \rho(z)$, then the last equation is:

$$2\Omega(\frac{\partial u}{\partial x} + \frac{\partial v}{\partial y}) = 0 \tag{5.71}$$

  Putting together this equation with the barotropic model $\nabla\rho \times \nabla p = 0$, we get:

$$\frac{\partial u}{\partial z} = \frac{\partial v}{\partial z} = 0.$$

- Looking at eqs. (5.46),(5.47),(5.50), the ρ and p expansions are:

$$\rho = \rho_s[1 + R_0 F(\overline{\rho}^{(0)} + R_0\overline{\rho}^{(1)} + ..)] \tag{5.72}$$

$$p = p_s + \rho_s U f L(\overline{p}^{(0)} + R_0\overline{p}^{(1)} + ..) \tag{5.73}$$

$$\theta = \theta_s(z)[1 + R_0 F(\overline{\theta}'^{(0)} + R_0\overline{\theta}'^{(1)} + ..)]. \tag{5.74}$$

- β-plane approximation:
  With this assumption, we suppose the Coriolis parameter to change linearly respect to the latitude,

$$f \approx f_0 + \beta_0 y, \tag{5.75}$$

  with $\beta_0 = \frac{2\Omega}{a} cos(\theta_0)$. In principle $\frac{L}{a}$ can be small or big and gives rise to

different developments of the quasi-geostrophic theory. We consider only the special case where $\frac{L}{a} \approx O(R_0)$ which is the situation where the relative vorticity is comparable with the planetary vorticity, this means that we impose the ratio between $\frac{U}{L^2}$ and β_0 to be O(1):

$$O(1) = O(R_0^0) = \frac{U}{L^2\beta_0} = \frac{1}{\beta} \quad \Rightarrow \quad \beta = O(1) \tag{5.76}$$

Starting back from fv expansion:

$$fv = f_0 U\overline{v} + \beta\frac{U^2}{L}\overline{y}\ \overline{v} \tag{5.77}$$

$$fv = \overline{v} + \beta R_0\overline{y}\ \overline{v} \tag{5.78}$$

We put all this works inside eqs. (5.59)-(5.63) factorizing respect to the Rossby number:

$$\begin{aligned} R_0[\frac{\partial}{\partial t}(u^{(0)} + R_0u^{(1)}) + (u^{(0)} + R_0u^{(1)})(\frac{\partial}{\partial x}(u^{(0)} + R_0u^{(1)}))+ \\ (v^{(0)} + R_0v^{(1)})\frac{\partial}{\partial y}(u^{(0)} + R_0u^{(1)})] \end{aligned} \tag{5.79}$$

$$= -\frac{\partial}{\partial x}(p^{(0)} + R_0p^{(1)}) + v^{(0)} + \beta R_0yv^{(0)} + R_0v^{(1)} + \beta R_0^2yv^{(1)}$$

$$\begin{aligned} R_0[\frac{\partial}{\partial t}(v^{(0)} + R_0v^{(1)}) + (u^{(0)} + R_0u^{(1)})(\frac{\partial}{\partial x}(v^{(0)} + R_0v^{(1)}))+ \\ (v^{(0)} + R_0v^{(1)})\frac{\partial}{\partial y}(v^{(0)} + R_0v^{(1)})] \end{aligned} \tag{5.80}$$

$$= -\frac{\partial}{\partial y}(p^{(0)} + R_0p^{(1)}) - u^{(0)} - \beta R_0yv^{(0)} - R_0v^{(1)} - \beta R_0^2yv^{(1)}$$

$$\rho_s(\rho^{(0)} + R_0\rho^{(1)}) = -\frac{\partial(\rho_sp^{(0)})}{\partial z} - R_0\frac{\partial(\rho_sp^{(1)})}{\partial z} \tag{5.81}$$

$$\begin{aligned} \frac{\partial(u^{(0)} + R_0u^{(1)})}{\partial x} + \frac{\partial(v^{(0)} + R_0v^{(1)})}{\partial y} \\ +R_0[(w^{(0)} + R_0w^{(1)})\frac{1}{\rho_s}\frac{\partial\rho_s}{\partial z} + \frac{\partial(w^{(0)} + R_0w^{(1)})}{\partial z}] = 0 \end{aligned} \tag{5.82}$$

$$\begin{aligned} R_0[\frac{\partial(\theta^{(0)} + R_0\theta^{(1)})}{\partial t} + (u^{(0)} + R_0u^{(1)})\frac{\partial(\theta^{(0)} + R_0\theta^{(1)})}{\partial x} \\ +(v^{(0)} + R_0v^{(1)})\frac{\partial(\theta^{(0)} + R_0\theta^{(1)})}{\partial y}] \\ +(w^{(0)} + R_0w^{(1)})S(1 + R_0F(\theta^{(0)} + R_0\theta^{(1)})) = HR_0 \end{aligned} \tag{5.83}$$

In eq. (5.81), we used the hydrostatic balance (5.41).

$$\begin{aligned} & R_0[\frac{\partial u^{(0)}}{\partial t} + u^{(0)}\frac{\partial u^{(0)}}{\partial x} + v^{(0)}\frac{\partial u^{(0)}}{\partial y} + \frac{\partial p^{(1)}}{\partial x} - \beta y v^{(0)} - v^{(1)}] \\ +R_0^2[&\frac{\partial u^{(1)}}{\partial t} + u^{(0)}\frac{\partial u^{(1)}}{\partial x} + u^{(1)}\frac{\partial u^{(0)}}{\partial x} + v^{(0)}\frac{\partial u^{(1)}}{\partial y} + v^{(1)}\frac{\partial u^{(0)}}{\partial y} - \beta y v^{(1)}] \\ & +R_0^3[u^{(1)}\frac{\partial u^{(1)}}{\partial x} + v^{(1)}\frac{\partial u^{(1)}}{\partial y}] \\ & = -\frac{\partial p^{(0)}}{\partial x} + v^{(0)} \end{aligned} \tag{5.84}$$

$$\begin{aligned} & R_0[\frac{\partial v^{(0)}}{\partial t} + u^{(0)}\frac{\partial v^{(0)}}{\partial x} + v^{(0)}\frac{\partial v^{(0)}}{\partial y} + \frac{\partial p^{(1)}}{\partial y} + \beta y u^{(0)} + u^{(1)}] \\ +R_0^2[&\frac{\partial v^{(1)}}{\partial t} + u^{(0)}\frac{\partial v^{(1)}}{\partial x} + u^{(1)}\frac{\partial v^{(0)}}{\partial x} + v^{(0)}\frac{\partial v^{(1)}}{\partial y} + v^{(1)}\frac{\partial v^{(0)}}{\partial y} + \beta y u^{(1)}] \\ & +R_0^3[u^{(1)}\frac{\partial v^{(1)}}{\partial x} + v^{(1)}\frac{\partial v^{(1)}}{\partial y}] \\ & = -\frac{\partial p^{(0)}}{\partial y} - u^{(0)} \end{aligned} \tag{5.85}$$

$$\rho_s\rho^{(0)} + \frac{\partial(\rho_s p^{(0)})}{\partial z} + R_0[\rho_s\rho^{(1)} + \frac{\partial(\rho_s p^{(1)})}{\partial z}] = 0 \tag{5.86}$$

$$\begin{aligned} & \frac{\partial u^{(0)}}{\partial x} + \frac{\partial v^{(0)}}{\partial y} \\ +R_0[&\frac{\partial u^{(1)}}{\partial x} + \frac{\partial v^{(1)}}{\partial y} + w^{(0)}\frac{1}{\rho_s}\frac{\partial \rho_s}{\partial z} + \frac{\partial w^{(0)}}{\partial z}] \\ & +R_0^2[w^{(1)}\frac{1}{\rho_s}\frac{\partial \rho_s}{\partial z} + \frac{\partial w^{(1)}}{\partial z}] = 0 \end{aligned} \tag{5.87}$$

$$\begin{aligned} & Sw^{(0)} + R_0[\frac{\partial\theta^{(0)}}{\partial t} + u^{(0)}\frac{\partial\theta^{(0)}}{\partial x} + v^{(0)}\frac{\partial\theta^{(0)}}{\partial y} + Sw^{(1)} + Sw^{(0)} - H] \\ +R_0^2[&\frac{\partial\theta^{(1)}}{\partial t} + u^{(0)}\frac{\partial\theta^{(1)}}{\partial x} + v^{(0)}\frac{\partial\theta^{(1)}}{\partial y} + u^{(1)}\frac{\partial\theta^{(0)}}{\partial x} + v^{(1)}\frac{\partial\theta^{(0)}}{\partial y} \\ & +SFw^{(0)}\theta^{(1)} + SFw^{(1)}\theta^{(0)}] \\ & +R_0^3[u^{(1)}\frac{\partial\theta^{(1)}}{\partial x} + v^{(1)}\frac{\partial\theta^{(1)}}{\partial y} + SFw^{(1)}\theta^{(1)}] = 0 \end{aligned} \tag{5.88}$$

g) **Hierarchy of primitive variables equations**
Now we are able to select any possible scale, starting from the $O(1) = O(R_0^0)$ order we obtain the geostrophic equations:

- $O(1) = O(R_0^0)$**, geostrophic equations**

$$v^{(0)} = \frac{\partial p^{(0)}}{\partial x} \tag{5.89}$$

$$u^{(0)} = -\frac{\partial p^{(0)}}{\partial y} \tag{5.90}$$

$$\rho^{(0)} = -\frac{1}{\rho_s}\frac{\partial}{\partial z}(\rho_s p^{(0)}) \tag{5.91}$$

$$\frac{\partial u^{(0)}}{\partial x} + \frac{\partial v^{(0)}}{\partial y} = 0 \tag{5.92}$$

$$w^{(0)} = 0 \tag{5.93}$$

Remark: From the definition of θ it follows that:

$$\begin{aligned} ln(\theta) &= [\frac{1}{\gamma}ln(p_s) - ln(\rho_s)] + \frac{1}{\gamma}ln(1 + R_0\frac{f_0^2 L^2 p}{p_s/\rho_s}) - ln(1 + R_0 F\rho) \\ &= \frac{1}{\gamma}ln(p_s) - ln(\rho_s) + \frac{1}{\gamma}R_0\frac{f_0^2 L^2 p}{p_s/\rho_s} - R_0 F\rho + O(R_0^2 F) \end{aligned} \tag{5.94}$$

which means that we can write $\theta^{(0)}$ respect to the pressure and the density:

$$\theta^{(0)} = -\rho^{(0)} + \frac{1}{\gamma}(\frac{\rho_s g D}{p_s})p^{(0)} = \frac{\partial p^{(0)}}{\partial z} - p^{(0)}\frac{1}{\theta_s}\frac{\partial \theta_s}{\partial z} \tag{5.95}$$

Thanks to the estimate (5.33), we know that $\frac{1}{\theta_s}\frac{\partial \theta_s}{\partial z} = O(R_0)$ which allows us to write:

$$\theta^{(0)} = \frac{\partial p^{(0)}}{\partial z} \tag{5.96}$$

This equation, together with eqs. (5.89)-(5.90):

$$\frac{\partial u^{(0)}}{\partial z} = -\frac{\partial \theta^{(0)}}{\partial y} \tag{5.97}$$

$$\frac{\partial v^{(0)}}{\partial z} = \frac{\partial \theta^{(0)}}{\partial x}. \tag{5.98}$$

- $O(R_0)$**, quasi-geostrofic equations**
  We introduce the notation $\frac{d_0}{dt} = \partial_t + u^{(0)}\partial_x + v^{(0)}\partial_y$:

$$\frac{d_0}{dt}u^{(0)} = -\frac{\partial}{\partial x}p^{(1)} + v^{(1)} + \beta v^{(0)} y \tag{5.99}$$

$$\frac{d_0}{dt}v^{(0)} = -\frac{\partial}{\partial y}p^{(1)} - u^{(1)} - \beta u^{(0)} y \tag{5.100}$$

$$\rho^{(1)} = -\frac{1}{\rho_s}\frac{\partial}{\partial z}(\rho_s p^{(1)}) \tag{5.101}$$

$$\frac{\partial u^{(1)}}{\partial x} + \frac{\partial v^{(1)}}{\partial y} = 0 \tag{5.102}$$

$$\frac{d_0\theta^{(0)}}{dt} + w^{(1)}S = H \tag{5.103}$$

h) **The potential vorticity**
We want to take care of another variable, the vorticity, $\zeta = \frac{\partial v}{\partial x} - \frac{\partial u}{\partial y}$ and we need to change variables $height \rightarrow pressur$. We recall the hydrostatic balance:

$$\frac{\partial p}{\partial z} = -\rho g \tag{5.104}$$

where $g = \nabla\phi$,

$$\phi = gz \rightarrow \partial\phi = g\partial z$$

to obtain, thank to the equation of state

$$\partial p = -\frac{p}{RT}g\partial z \tag{5.105}$$

$$\frac{\partial p}{p} = -\frac{g}{RT}\partial z \quad \Rightarrow \partial\phi = -RT\frac{\partial p}{p} \tag{5.106}$$

Here we introduce the new vertical variable $Z := -ln(\frac{p}{p_0})$ and:

$$\partial Z = -\frac{g}{RT}\partial z \tag{5.107}$$

We want to switch from *height levels* to *pressure levels*.
We would like to write the whole system using the new coordinates, but we need first to transform also the derivative operators, meaning that, using the pressure as the vertical coordinate, the horizontal partial derivatives must be calculated at constant p and no more constant z. Looking at the fig. (5.5):

$$[\frac{(p_0+\delta p)-p_0}{\delta x}]_z = [\frac{(p_0+\delta p)-p_0}{\delta z}]_x(\frac{\delta z}{\delta x})_p \tag{5.108}$$

where the subscript means the variable to be constant. Going to the limit $\delta z \rightarrow 0$, $\delta x \rightarrow 0$ and using the hydrostatic equation:

$$-\frac{1}{\rho}(\frac{\partial p}{\partial x})_z = -g(\frac{\partial z}{\partial x})_p = -(\frac{\partial\phi}{\partial x})_p \tag{5.109}$$

Similarly for y:

$$-\frac{1}{\rho}(\frac{\partial p}{\partial y})_z = -(\frac{\partial\phi}{\partial y})_p \tag{5.110}$$

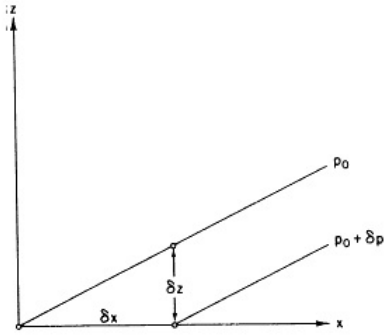

Figure 5.5.: Slope of pressure surfaces in the x, z plane.

We can finally write the whole system in the new coordinates:

$$\frac{\partial u}{\partial t} + u\frac{\partial u}{\partial x} + v\frac{\partial u}{\partial y} + W\frac{\partial u}{\partial Z} = -\frac{\partial \phi}{\partial x} + fv \tag{5.111}$$

$$\frac{\partial v}{\partial t} + u\frac{\partial v}{\partial x} + v\frac{\partial v}{\partial y} + W\frac{\partial v}{\partial Z} = -\frac{\partial \Phi}{\partial y} - fu \tag{5.112}$$

$$\frac{\partial \phi}{\partial Z} = RT \tag{5.113}$$

$$-Z + \frac{\partial u}{\partial x} + \frac{\partial v}{\partial y} + \frac{\partial W}{\partial Z} = 0 \tag{5.114}$$

$$\frac{D}{Dt}\frac{\partial \phi}{\partial Z} + W\frac{\partial}{\partial Z}(\frac{\partial \phi}{\partial Z} + k\phi) = kQ \tag{5.115}$$

with $W = \frac{DZ}{Dt}$ e $k = \frac{R}{C_p}$.

As already seen with the primitive variables and applying similar steps, we can

write an equation for the vorticity at order 0:

$$\begin{aligned}\frac{d_0}{dt}(\frac{\partial v^{(0)}}{\partial x}-\frac{\partial u^{(0)}}{\partial y}) &= -\frac{\partial u^{(1)}}{\partial x}-\frac{\partial v^{(1)}}{\partial y}-\frac{\partial(\beta y u^{(0)})}{\partial x}-\frac{\partial(\beta y v^{(0)})}{\partial y}\\ &= -\frac{\partial u^{(1)}}{\partial x}-\frac{\partial v^{(1)}}{\partial y}-\beta y\frac{\partial(u^{(0)})}{\partial x}-\beta y\frac{\partial(v^{(0)})}{\partial y}-\beta v^{(0)}\\ &= -\frac{\partial u^{(1)}}{\partial x}-\frac{\partial v^{(1)}}{\partial y}-\beta y\frac{\partial(\phi^{(0)})}{\partial x\partial y}-\beta y\frac{\partial(\phi^{(0)})}{\partial y\partial x}-\beta v^{(0)}\\ &= -\frac{\partial u^{(1)}}{\partial x}-\frac{\partial v^{(1)}}{\partial y}-\beta v^{(0)}\end{aligned} \tag{5.116}$$

where by $\frac{d_0}{dt}$ we denote the material derivative respect the the velocity at order 0.

$$\frac{d_0\zeta}{dt} = -\nabla\cdot\mathbf{u}^{(1)}-\beta v^{(0)} \tag{5.117}$$

If we observe that $(u^{(0)},v^{(0)}) = (-\frac{\partial\phi^{(0)}}{\partial y},\frac{\partial\phi^{(0)}}{\partial x})$ we can write the equation for the stream function ϕ:

$$\frac{\partial}{\partial t}\nabla^2\phi^{(0)}+J(\phi^{(0)},\nabla^2\phi^{(0)}+\beta y) = -\nabla\cdot\mathbf{u}^{(1)} \tag{5.118}$$

where $J(A,B)$ is the Jacobian operator:

$$J(A,B) = \frac{\partial A}{\partial x}\frac{\partial B}{\partial y}-\frac{\partial A}{\partial y}\frac{\partial B}{\partial x}.$$

In order to close the system, we need to estimate $\nabla\cdot\mathbf{u}^{(1)}$, to do this, we need dimensionless thermodynamic equations. Let's consider eq. (5.115) and $\frac{\partial\phi}{\partial Z} = RT$, $\phi = gZ$, $\frac{\partial}{\partial x} = \frac{g}{RT}\frac{\partial}{\partial Z}$:

$$\frac{\partial}{\partial Z}(\frac{\partial\phi}{\partial Z}+k\phi) = \frac{RT}{g}\frac{\partial}{\partial z}(RT+\frac{R}{C_p}gZ) = \frac{R^2T}{g}(\frac{\partial T}{\partial z}+\frac{g}{C_p}) \tag{5.119}$$

We introduce a new dimensionless parameter, the Richardson number:

$$R_i = \frac{R^2T_{RC}}{gU^2}(\frac{\partial T_{RC}}{\partial z}+\frac{g}{C_p}). \tag{5.120}$$

We can factorize ϕ in the sum of a radiative-convective part (depending only from the pressure) and part depending from the deviations due to the motion:

$$\phi = \phi_{RC}(Z)+f_0LU\phi'(x,y,Z,t) \tag{5.121}$$

Putting eq. (5.121) into eq. (5.115), we obtain:

$$fU^2(\frac{\partial}{\partial\overline{t}}+\overline{u}\frac{\partial}{\partial\overline{x}}+\overline{v}\frac{\partial}{\partial\overline{y}})\frac{\partial}{\partial\overline{Z}}\overline{\phi'}+\frac{U}{L}\overline{W}\frac{\partial}{\partial\overline{Z}}[(\frac{\partial}{\partial\overline{Z}}\phi_{RC}+k\phi_{RC})+fLU(\frac{\partial}{\partial\overline{Z}}\phi'+k\phi')] = kQ \tag{5.122}$$

Considering the order 1 and dividing everything by Uf^2L (in order to see the Rossby number), we obtain:

$$R_0\frac{d}{dt}\frac{\partial\phi^{(0)}}{\partial Z}+R_0^2R_iR_0W^{(1)}=0 \tag{5.123}$$

The static stability is defined as $S(Z)=R_0^2R_i$, so that

$$W^{(1)}=-\frac{1}{S(Z)}\frac{d}{dt}\frac{\partial}{\partial Z}\phi^{(0)}. \tag{5.124}$$

Now we put the following equation

$$\frac{\partial}{\partial Z}W^{(1)}-W^{(1)}=-\nabla\cdot u^{(1)} \tag{5.125}$$

into the vorticity equation, to obtain:

$$\frac{d\zeta}{dt}=\frac{\partial}{\partial Z}W^{(1)}-W^{(1)}=\frac{1}{p}\frac{\partial}{\partial Z}[pW^{(1)}] \tag{5.126}$$

$$\frac{\partial}{\partial t}\nabla^2\phi^{(0)}+J(\phi^{(0)},\nabla^2\phi^{(0)}+\beta y)=-\frac{1}{p}\frac{\partial}{\partial Z}[\frac{p}{S(Z)}\frac{d}{dt}\frac{\partial\phi^{(0)}}{\partial Z}]. \tag{5.127}$$

The last equation can be written in conservative form:

$$\frac{d_0}{dt}q=0 \tag{5.128}$$

with

$$q=\nabla^2\phi^{(0)}+\beta y+\frac{1}{p}\frac{\partial}{\partial Z}[\frac{p}{S(Z)}\frac{d}{dt}\frac{\partial\phi^{(0)}}{\partial Z}]. \tag{5.129}$$

5.4. Numerical Results

Following [44] for a rigourus derivation of a general N-layer QG model, and in particular adopting the model proposed by Haidvogel and Held [90], we consider a horizontally uniform temperature-gradient in a two-layer quasi-geostrophic model on a β-plane:

$$\frac{\partial Q_1}{\partial t} + J(\Psi_1, Q_1) = -\nu\nabla^6\Psi_1 \tag{5.130}$$

$$\frac{\partial Q_2}{\partial t} + J(\Psi_2, Q_2) = -k\Delta\Psi_2 - \nu\nabla^6\Psi_2 \tag{5.131}$$

where the subscripts 1 and 2 refer to the upper and lower layers respectively. The two layers are assumed to have equal depths when at rest. The potential vorticities are related to the stream-functions through the relations

$$Q_i = \Delta\Psi_i + \beta y + \frac{1}{2R_d^2}(\Psi_j - \Psi_i) \tag{5.132}$$

for $i, j = 1, 2$ and $i \neq j$, $R_d = (g'\frac{\Delta\theta}{\theta_0}\frac{H}{2f_0^2})^{\frac{1}{2}}$ is the Rossby radius of deformation, H is the resting depth, g' is the reduced gravity ($g' = \frac{g(\rho_2-\rho_1)}{\rho_1}$) and f_0 is the Coriolis parameter.
Here we consider a horizontally uniform temperature-gradient, meaning:

$$\begin{aligned} \Psi_1(x, y, t) &= -Uy + \psi_1(x, y, t) \\ \Psi_2(x, y, t) &= \psi_2(x, y, t) \end{aligned} \tag{5.133}$$

where ψ_i is the deviation of the stream-function from its time-average. Nondimensionalizing, the quasi-geostrophic voritcity equations become:

$$\frac{\partial q_1}{\partial t} + J(\psi_1, q_1) = -\tilde{\nu}\nabla^6\psi_1 + F_1 \tag{5.134}$$

$$\frac{\partial q_2}{\partial t} + J(\psi_2, q_2) = -\tilde{k}\Delta\psi_2 - \tilde{\nu}\nabla^6\psi_2 + F_2 \tag{5.135}$$

where the eddy potential vorticities are:

$$q_i = \Delta\psi_i + \frac{1}{2}(\psi_j - \psi_i) \tag{5.136}$$

for $i, j = 1, 2$ and $i \neq j$. The forcing terms F_1 and F_2 represent the effects of the mean temperature and planetary vorticity gradients

$$\begin{aligned} F_1 &= -\frac{\partial q_1}{\partial x} - (\tilde{\beta} + 1/2)\frac{\partial \psi_1}{\partial x} \\ F_2 &= -(\tilde{\beta} - 1/2)\frac{\partial \psi_2}{\partial x} \end{aligned} \tag{5.137}$$

All variables are nondimensional and $\tilde{\beta} = \beta R_d^2/U$, $\tilde{\nu} = \nu/R_d^2 U$, $\tilde{k} = kR_d/U$.
We distinguish physical and numerical parameters:

- Physical parameters:

  - $\tilde{\beta}$, this is a non-dimensional measure of the planetary vorticity gradient
  - $\tilde{k}$, this is a non-dimensional measure of the bottom friction
- Numerical parameters:
  - L, N defining the resolution and then the maximum wavenumber $k_{max} = N/2L$,
  - $\tilde{\nu}$, the artificial viscosity.

In the following simulations we will consider a squared biperiodic domain of size $L \times L$ with initial condition given by:

$$q_i(x,y) = \sum_{k=1}^{4} a_{i,k} sin(\frac{2\pi k}{L}x) sin(\frac{2\pi k}{L}y), \tag{5.138}$$

which represents the composition of different waves with random amplitude $a_{i,k}$.

Spatial Integration

The most important part of the discretization, lies in the spatial integration of the non linear term, the Jacobian operator, widely presented in the previous chapter. In order to conserve enstrophy and energy we choose the mimetic scheme of Arakawa. Dissipative and forcing terms are always discretized using central finite differences.

Time Integration

To integrate over the time, we choose the Leap-Frog scheme in combination with Matsuno scheme, this is a common choice in atmospheric simulations because Leap-Frog scheme could result unstable for long time iteration, then applying Matsuno scheme at constant interval steps will avoid this problem. At the first time-step we apply Eulero scheme again. We recall, for the PDE

$$\frac{\partial u}{\partial t} = f(u)$$

- Eulero scheme:

$$u^{n+1} = u^n + dtf(u^n) \tag{5.139}$$

- Leap-frog scheme:

$$u^{n+1} = u^{n-1} + 2dtf(u^n) \tag{5.140}$$

- Matsuno scheme:

$$\begin{aligned} u^{int} &= u^n + dtf(u^n) \\ u^{n+1} &= u^n + dtf(u^{int}) \end{aligned} \tag{5.141}$$

Inversion of the biperiodic Laplacian Operator
In order to solve the Poisson equation for the stream function (see equation 5.136), we use the iterative method of Gauss-Seidel [91] in combination with a Multigrid algorithm [92] in order to accelerate the convergence.

5.4.1. Analyzed quantities

- i-layer kinetic energy: $K_i = \frac{1}{2}\overline{|\nabla\psi_i|^2}$
- potential energy: $P = \frac{1}{2}\overline{\frac{\psi_1-\psi_2}{2}^2}$
- total energy: $E = K_1 + K_2 + P$
- zonal spectra: for every fixed y, we consider the one-dimensional Fourier transform in x-direction, then we average over the N-transforms and then we average again over time (we could analogously define the meridional spectra with the switched directions but we will omit them because they look approximately the same).

5.4.2. Physical Parameters

5.4.2.1. Bottom Friction

In the following tests we can compare the different behaviors depending on different values of k; as pointed out in [90], one expects the strength of this drag to affect the energy level of the large scale-flow. Reducing k means reducing the bottom friction of the lower layer and then we enforce the kinetic energy of layer 2. For very small k, the system tends to be barotropic and the difference between two layers seems to disappear. Also the energy spectra of two layers reflect this behavior, as we can see by the comparison in fig. 5.9. This behavior leads to a system which loses the original turbulence, and a big vortex of the size of the grid is created (see fig. **Test 3**).

Test 1 $512 \times 32;\ k = 0,6;\ \beta = 0,25$

Test 2 $512 \times 32;\ k = 0,35;\ \beta = 0,25$

Test 3 $512 \times 32;\ k = 0,005;\ \beta = 0,25$

5.4.2.2. Planetary vorticity gradient

The simulations are carried out with a resolution of 64×16.
As we have seen, β is related to the Coriolis parameter through the relation 5.75. The advantage of the β-plane approximation over more accurate formulations is

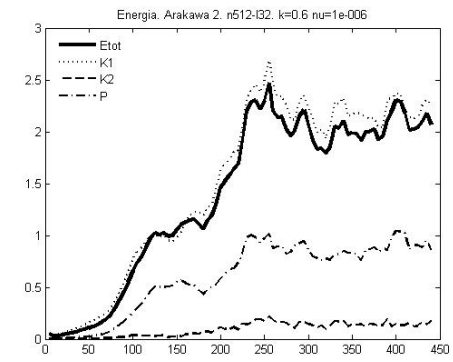

(a) Energy

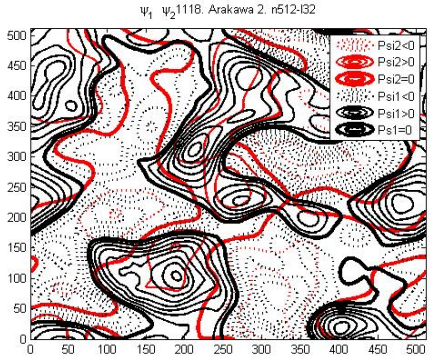

(b) Stream functions ψ_1 and ψ_2

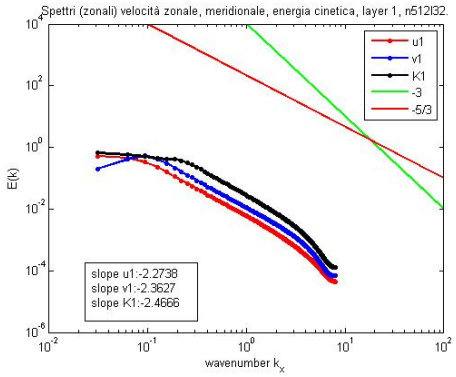

(c) Zonal spectra layer 1

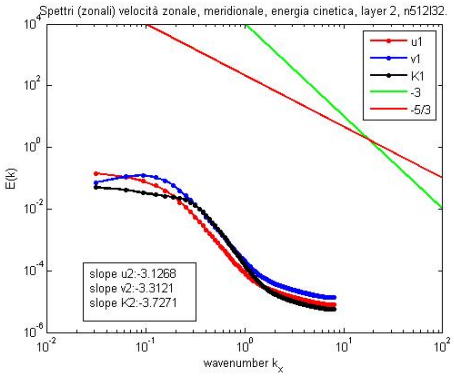

(d) Zonal spectra layer 2

Figure 5.6.: **Test 1**

that it does not contribute nonlinear terms to the dynamical equations; such terms make the equations harder to solve. Anyhow, as we can see in fig. 5.11, also the parameter β affects the large scales and the amount of energy 5.10 and increasing β is not physically reasonable.

5.4.3. Numerical Parameters

5.4.3.1. Artificial Viscosity

The simulations are carried out with a resolution of 88×16.
Fig. 5.12 clearly shows numerical instabilities in the initial part of the simulation when the parameter ν increases. These problems arise only in the beginning of the simulation and doesn't affect the long time behavior of the spectra, as we can appreciate in fig. 5.13. Anyway a possible explanation for instabilities problems can be found in the following remark:

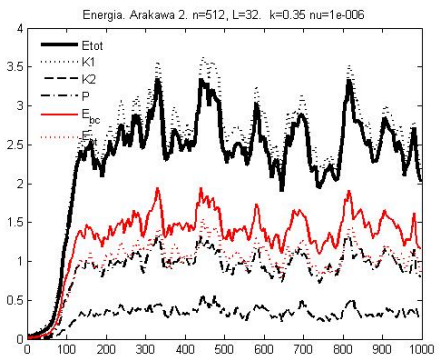

(a) Energy

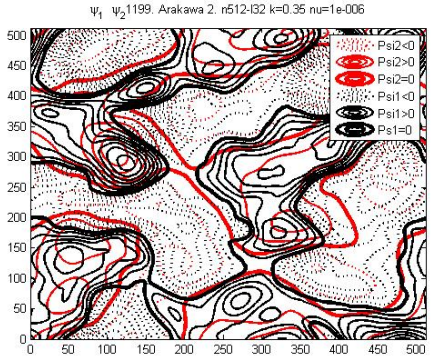

(b) Stream functions ψ_1 and ψ_2

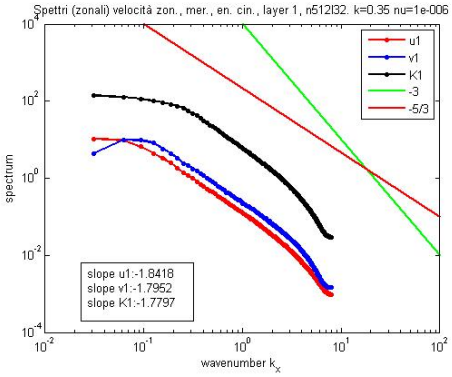

(c) Zonal spectra layer 1

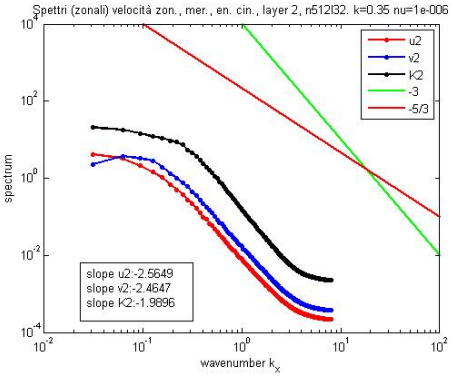

(d) Zonal spectra layer 2

Figure 5.7.: **Test 2**

Remark 5.1. *We are solving a system of non-linear partial differential equation; for each equation we can focus on two main terms: a convective term (the non-linear Jacobian) and a dissipative term* $\nu\nabla^6\psi$*. The last term is proportional to a second derivative, so it has the same properties of a even derivative. We can associate a 1D easier problem, in order to better understand the problems that may arise, so we consider the equation*

$$u_t + au_x = \nu u_{xx} \tag{5.142}$$

Applying Von Neumann analysis to the diffusion equation (ignoring the convective term) it can be proved that a central finite difference discretization results to be stable if the following condition is satisfied

$$dt = \frac{dx^2}{2\nu} \tag{5.143}$$

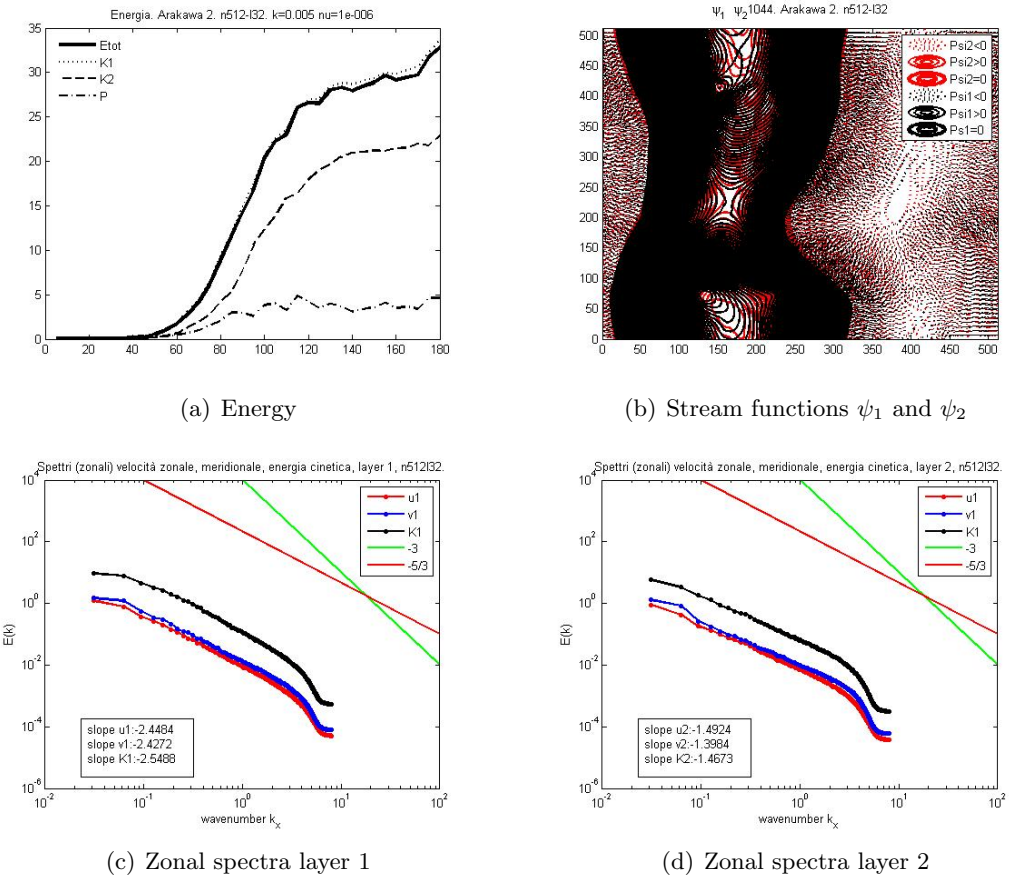

(a) Energy

(b) Stream functions ψ_1 and ψ_2

(c) Zonal spectra layer 1

(d) Zonal spectra layer 2

Figure 5.8.: **Test 3**

whilst in our simulation, we are fixing the time-step using the classical CFL condition for the convection equation $dt = \frac{dt}{a}$.

This could explain why our simulations result to be unstable when the viscosity term increases. To confirm this hypothesis we repeat a simulation with a smaller value of dt and we compare the energy behaviors 5.14:

5.4.3.2. High-resolution simulations

Once we have fixed the correct time-step, we can study the energy spectra for higher resolution in order to figure out if the discrepancy with the theoretical spectrum can be explained by an insufficient resolution. In particular we show the case

$$1000 \times 32, k = 0.5; \beta = 0.25.$$

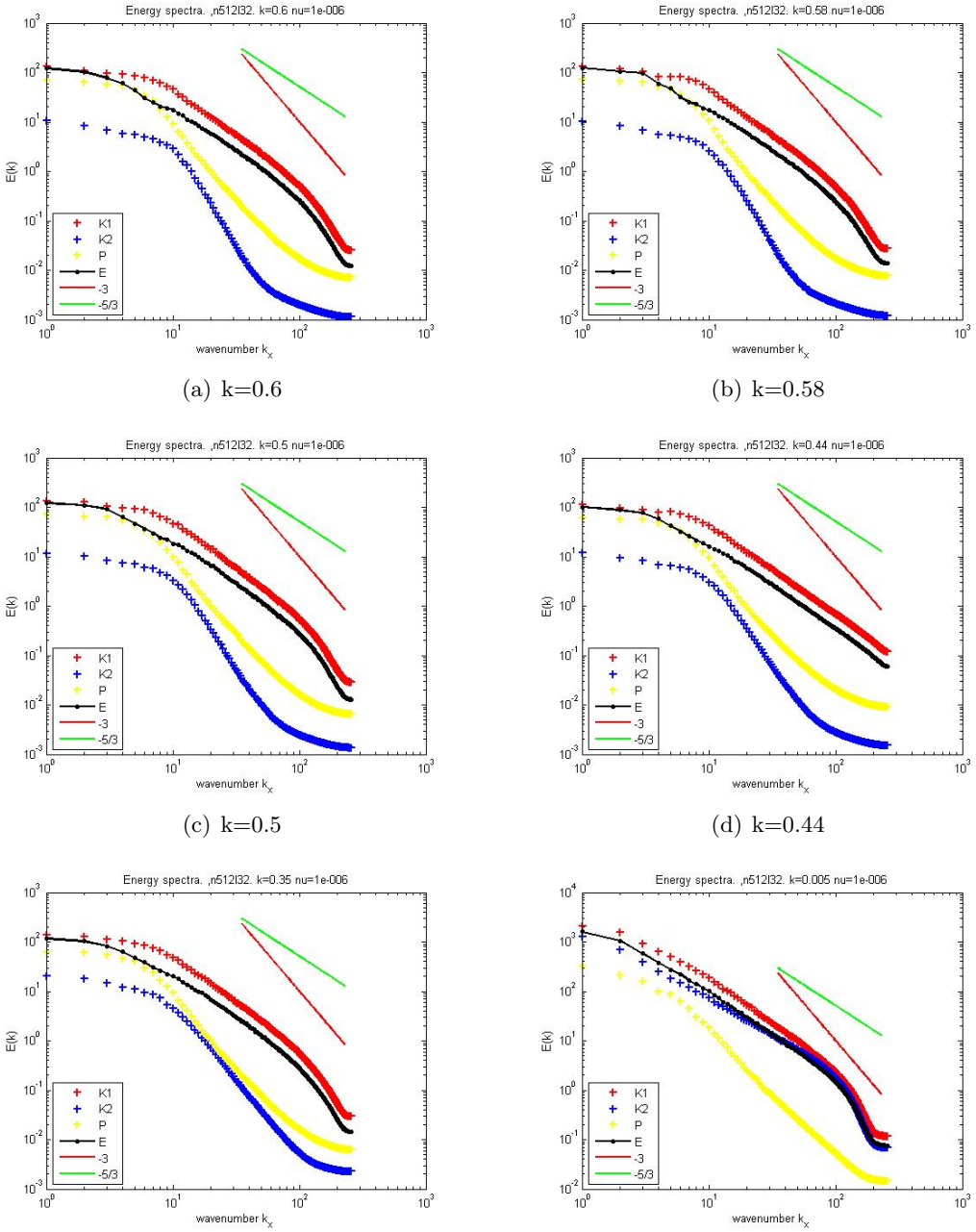

(a) k=0.6 (b) k=0.58

(c) k=0.5 (d) k=0.44

(e) k=0.35 (f) k=0.005

Figure 5.9.: Comparing energy spectra for different k

We cannot infer a clear spectral behavior, nor with the $-5/3$ slope, nor with the -3 one. If the problem would be yet a too low resolution, we should be able at least to clearly see the -3 slope of synoptic scales. Moreover, we cannot see much difference

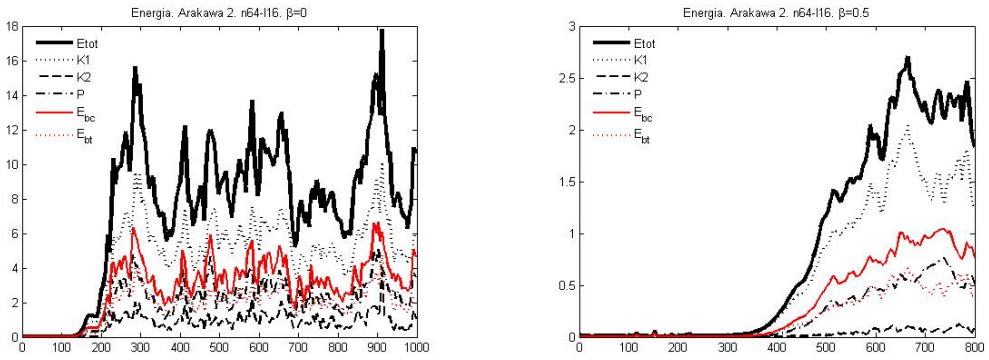

(a) $\beta = 0$ (b) $\beta = 0.5$

Figure 5.10.: Comparing energy for different β

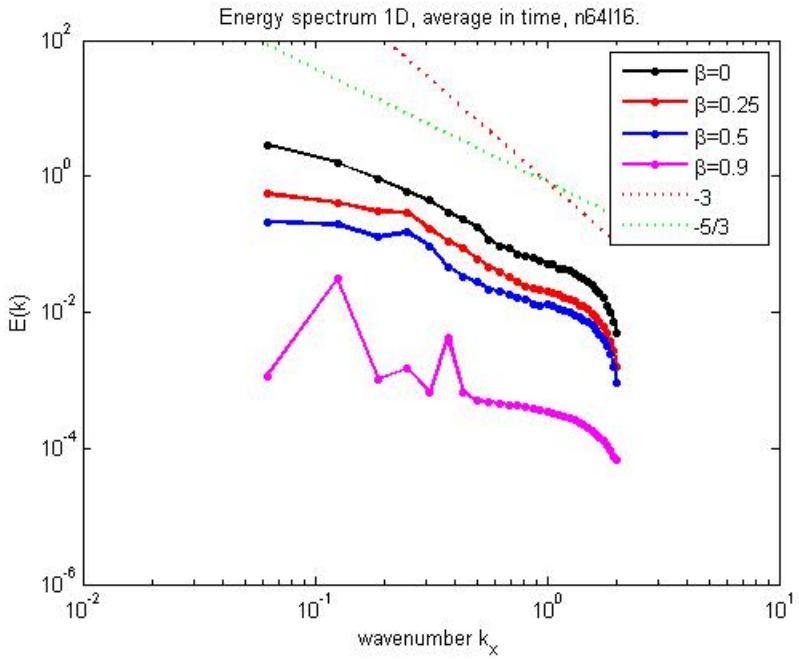

Figure 5.11.: Comparing energy spectra for different β

in the spectra with the simulation with a small and a big k (fig. 5.9), whilst we should see different behaviors for the *barotropic* and the *baroclinic* systems.
What we can see is a different behavior in the two layers: the upper layer looks like a -3 spectrum, while the lower layer like the $-5/3$ (the last part of the spectrum with a different slope is not physical). So the situation seems to be baroclinic enough, but yet the lower layer is slowed down by the bottom friction and seems

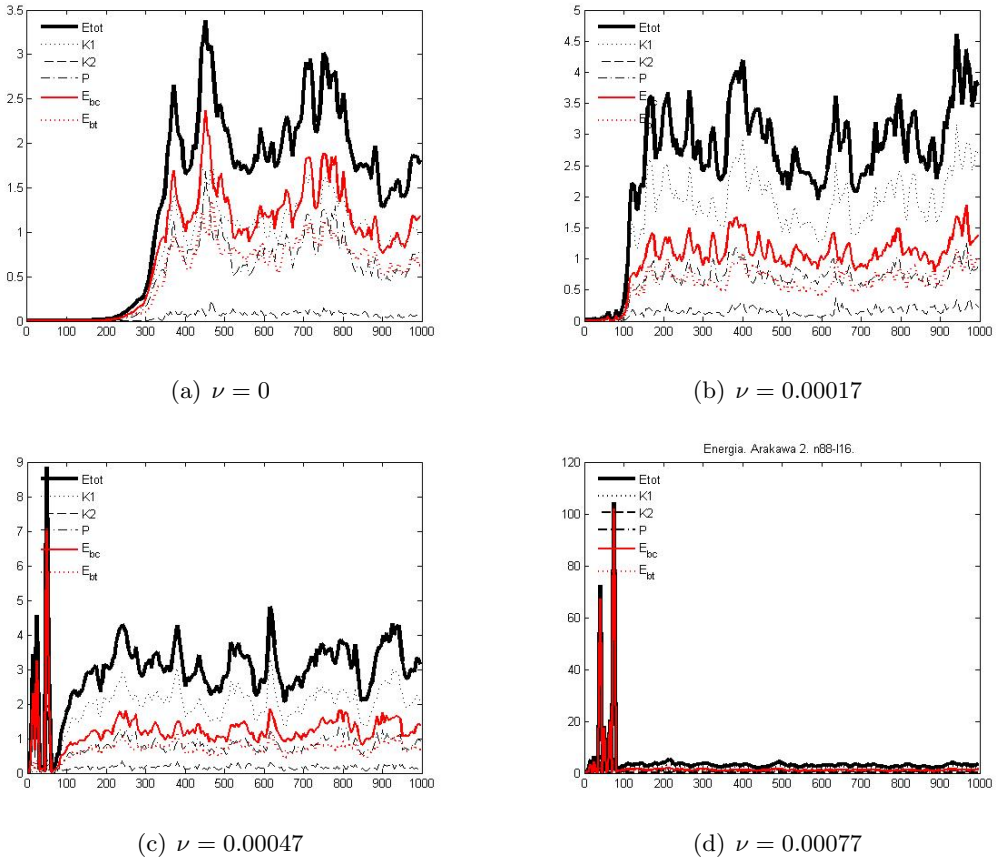

(a) $\nu = 0$

(b) $\nu = 0.00017$

(c) $\nu = 0.00047$

(d) $\nu = 0.00077$

Figure 5.12.: Comparing energy for different ν

to have not enough energy to dominate the smallest wave numbers (this would give the transition $-5/3 \to -3$).
Possible causes of this result could be: a wrong energy injection which could imply that we are not in a stationary condition or maybe, also the biperiodic boundary conditions could comprimise the simulations, as pointed out in [].
Moreover, we underline that Tung and Orlando obtained the energy spectrum 5.3 using a spectral method: maybe a second order finite difference scheme is not enough to study and resolve spectral quantities. For this reason we are going to raise the order of accuracy of the scheme to conclude if the model is unable to reproduce the Nastrom-Gage spectrum, or we just need a higher-order scheme.

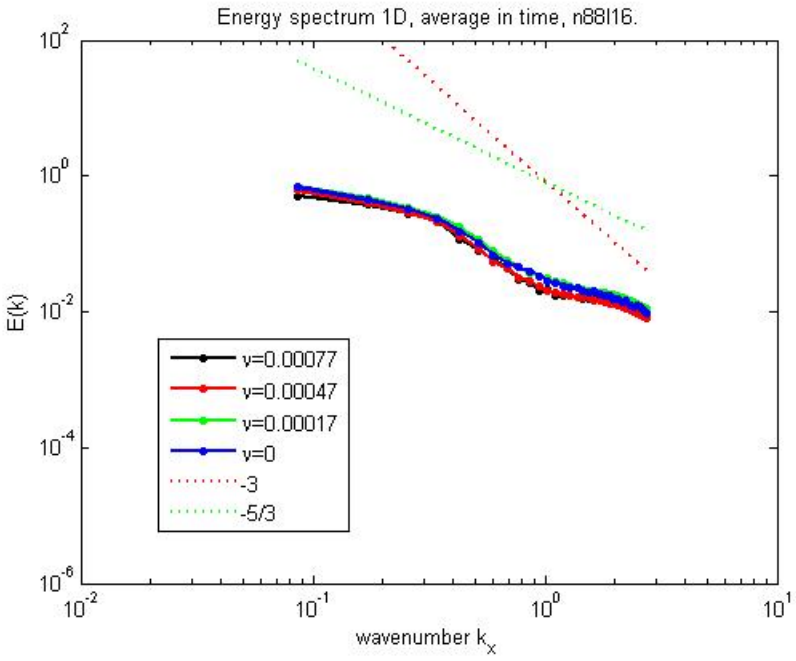

Figure 5.13.: Comparing energy spectra for different ν

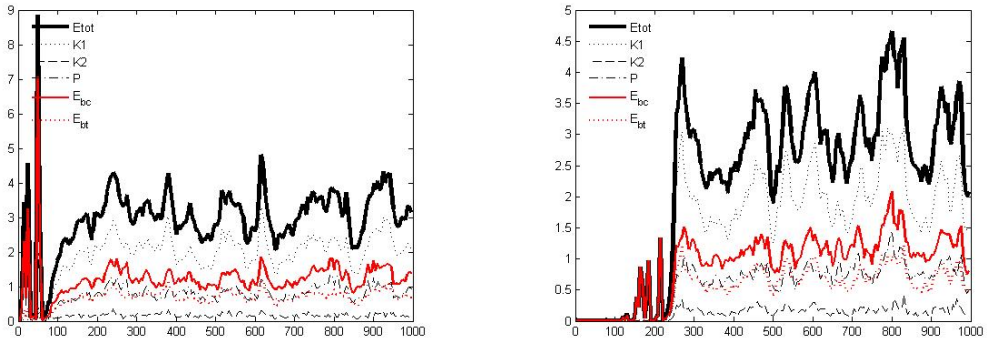

(a) dt (b) $10^{-1}dt$

Figure 5.14.: Comparing energy for different dt

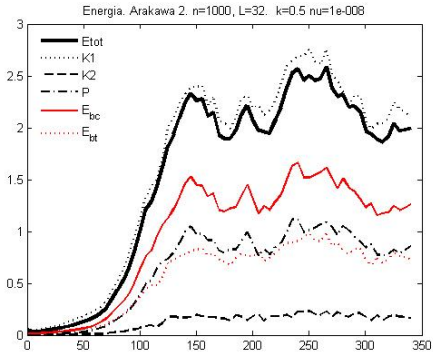

(a) Energy

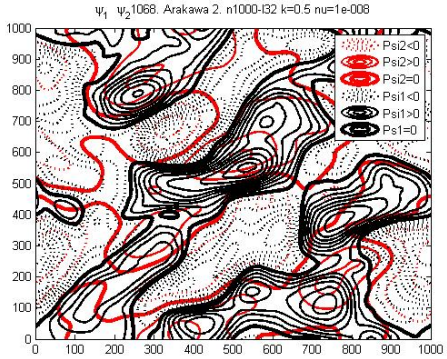

(b) Stream functions ψ_1 and ψ_2

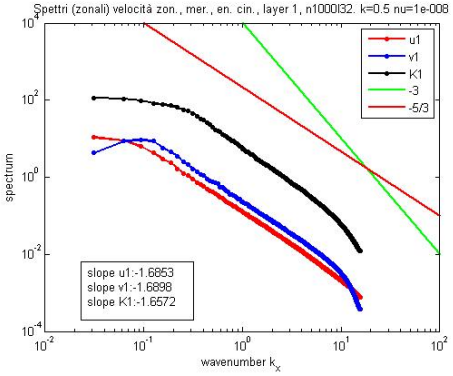

(c) Zonal spectra layer 1

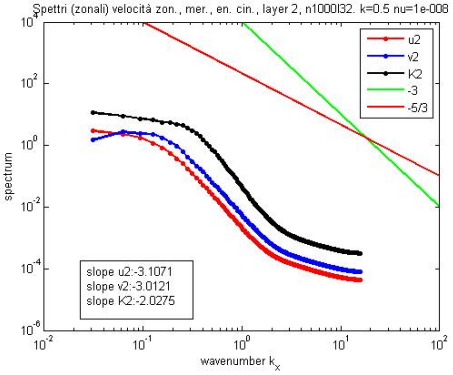

(d) Zonal spectra layer 2

Figure 5.15.: High-resolution simulations

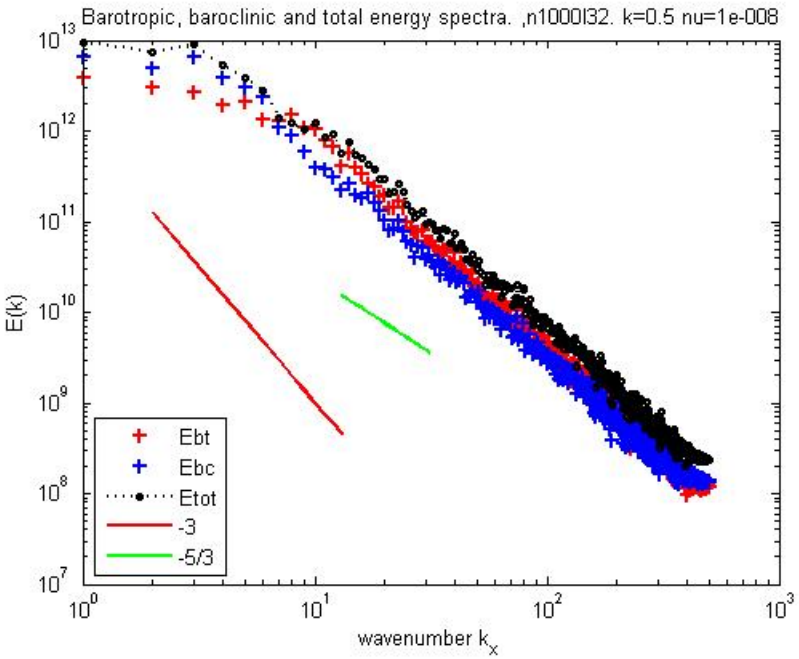

Figure 5.16.: Total energy spectra for high resolution simulation

6. Conclusions

Two different approaches to formulate mimetic schemes for the vorticity equation have been presented and studied; in this context mimetic refers to the skew-symmetric property of the Jacobian and its capability to conserve energy and enstrophy.
The first approach is quite general and consists of a systematic method to construct mimetic finite-difference schemes for non-linear advective problems; with this method it is possible to produce any order non-linear operator on arbitrary stencils and with arbitrary properties. The discrete scheme's coefficients are identified by solving a linear system where the equations are the specific properties required; in this way we can ensure selecting the whole generic family of operators we are looking for, no other operator with such properties can be left out. In this paper I applied the method to select the class of order two discrete Jacobians based on a 9x9 uniform stencil and with skew-symmetric, enstrophy and energy preserving properties and then compared this general solution with the one obtained by Akio Arakawa. I showed there exists a whole set of solutions which satisfies all properties mentioned before and this set depends on one parameter, when the parameter is zero, Arakawa's scheme is recovered. I studied the scheme dependence respect to the parameter in the physical space as well as in the Fourier space. This study has been applied and checked for numerical simulations of analytical models such as the advection equation and the Rankine vortex in different forms. I also showed examples of particular solutions: only skew-symmetric, only energy conserving and only enstrophy conserving schemes in order to compare them with the generic discrete Jacobian found by imposing all these conditions. The numerical example related to these set of solutions underlines the difference between these operators: the general scheme is able to preserve numerical stability as well as the only enstrophy-conserving schemes and a particular skew-symmetric scheme, J^{0*}. This procedure can be applied to various differential problems to obtain higher order schemes and different classes of solutions.
In the second approach, an Arakawa-like scheme for the discretization of the Jacobian was reformulated using a finite difference method based on summation-by-parts (SBP) operators with arbitrary order of accuracy. The proficiency of this technique lies in the power of such discretization to simulate the integration by parts property and maintain the analytical conservation properties in the discrete setting. In this context, the Jacobian approximation found is proved to be skew-symmetric, energy and enstrophy conserving, by using the special structure of the SBP operators and a special way to relate vectors and diagonal matrices. This

work will be extended to explore the non-periodic dynamics and the goal will be to generalize this kind of idea to a three-dimensional model.
These two approaches are different and each one has its own advantages: the first method ensures that the class of solutions found is the biggest one, the second approach is not that general, but it has the property of containing any arbitrary order accuracy in one compact structure, whilst in the first approach we yet can obtain any order scheme, but we should impose it a priori as a specific request.
In the last part of this work, I applied Arakawa's scheme to a geophysical application: the simulation of a two-layer quasi-geostrophic model. The analysis was designed to understand the model behavior depending on physical and numerical parameters: the numerical simulations showed that the first ones (bottom friction and planetary vorticity gradient) affect the large scales, whilst the numerical parameters can affect the stability. High-resolution simulations have also been run in order to study energy spectra and compare them with the experimental ones of Nastrom and Gage. We cannot select the double slopes $-5/3$ and -3 as Tung and Orlando did using a spectral method; this could be explained by the fact that our accuracy (order two) could be not sufficient to study spectral quantities. In this direction, higher-order simulations are being investigated.

A. Poisson's equation

We consider the Poisson's equation

$$\Delta\psi = \zeta \tag{1.1}$$

with periodic boundary conditions. We refer the reader to [93] and [94] for reference about the analytical well-posedness of eq. (1.1) with periodic boundary conditions as well as Dirichlet or Neumann ones.
Numerically, I treated this problem with two different approaches:

- The Gauss-Seidel Method
  The Gauss-Seidel method is an iterative technique for solving a square system of n linear equations with unknown x:

  $$A\mathbf{x} = \mathbf{b}. \tag{1.2}$$

  It is defined by the iteration

  $$L_*\mathbf{x}^{(k+1)} = \mathbf{b} - U\mathbf{x}^{(k)}, \tag{1.3}$$

  where the matrix A is decomposed into a lower triangular component L_*, and a strictly upper triangular component U, such that: $A = L_* + U$.
  The Gauss-Seidel method now solves the left hand side of this expression for x, using previous value for x on the right hand side. Analytically, this may be written as:

  $$\mathbf{x}^{(k+1)} = L_*^{-1}(\mathbf{b} - U\mathbf{x}^{(k)}). \tag{1.4}$$

  However, by taking advantage of the triangular form of L_*, the elements of $x^{(k+1)}$ can be computed sequentially using forward substitution:

  $$x_i^{(k+1)} = \frac{1}{a_{ii}}\left(b_i - \sum_{j<i} a_{ij}x_j^{(k+1)} - \sum_{j>i} a_{ij}x_j^{(k)}\right), \quad i,j = 1,2,\ldots,n. \tag{1.5}$$

  The procedure is generally continued until the changes made by an iteration are below some tolerance, computing the residual.
  The Gauss-Seidel formula is extremely similar to that of the Jacobi method. The computation of $x^{(k+1)}$ uses only the elements of $x^{(k+1)}$ that have already been computed, and only the elements of $x^{(k)}$ that have not yet to be advanced to iteration $k+1$. This means that, unlike the Jacobi method, only one storage

vector is required as elements can be overwritten as they are computed, which can be advantageous for very large problems.
In our specific case the matrix A corresponds to the Laplacian operator (see eq. (1.1)). For this reason, if we use the classical 2^{nd} order central finite difference discretization for the Laplacian, we get the explicit formula:

$$\psi_{i,j} = (\psi_{i,j+1} + \psi_{i,j-1} + \psi_{i+1,j} + \psi_{i-1,j} - h^2\zeta_{i,j})/4. \tag{1.6}$$

Remark A.1. *We need the additional constraint*

$$\overline{\psi} = 0 \tag{1.7}$$

in order to have the solution uniquely defined. By the way, without this condition, we could add any constant to the solution ψ and it would still be a solution of eq. (1.1).

- Stationary solution
  Another possible approach is to look for stationary solution of the fictitious time-dependent equation
  $$\frac{\partial \psi}{\partial t} = \Delta\psi - \zeta. \tag{1.8}$$
  This method will be adopted in the SBP context.

Bibliography

[1] Mikhail Shashkov Konstantin Lipnikov, Gianmarco Manzini. Mimetic finite difference method. *Journal of Computational Physics*, 257:1163–1227, 2014.

[2] A.A. Dezin. Method of orthogonal expansion. *Sib. Math. J.*, 9(4):788–797, 1968.

[3] A.A. Samarskii A.N. Tikhonov. Homogeneous difference schemes. *Comput. Math. Math. Phys.*, 1(1):5–67, 1962.

[4] Akio Arakawa. Computational design for long-term numerical integration of the equations of fluid motion: Two-dimensional incompressible flow. part i. *Journal of Computational Physics*, 1:119–143, 1966.

[5] A. Arakawa. Finite-difference methods in climate modeling. *M. E. Schlesinger (ed.), Physically-Based Modelling and Simulation of Climate and Climatic Change - Part 1*, pages 79–168, 1988.

[6] V.R. Lamb A. Arakawa. A potential enstrophy and energy conserving scheme for the shallow water equations. *Mon. Weather Rev.*, 109:18–36, 1981.

[7] Andrew T. T. McRae and Colin J. Cotter. Energy- and enstrophy-conserving schemes for the shallow-water equations, based on mimetic finite elements. *Quarterly Journal of the Royal Meteorological Society*, ISSN:0035-9009, 2014.

[8] Rick Salmon. A general method for conserving energy and potential enstrophy in shallow-water models. *J. Atmos. Sci.*, 64:515–531, 2007.

[9] Rick Salmon and Lynne D Talley. Generalizations of arakawa's jacobian. *Journal of computational physics*, 83(2):247–259, 1989.

[10] Dennis C. Jespersen. Arakawa's method is a finite-element method. *Journal of computational physics*, 16:383–390, 1974.

[11] George J. Fix. Finite element models for ocean circulation problems. *SIAM J. Appl. Math.*, 29(3):371–387, 1975.

[12] Robert I. McLachlan. Spatial discretization of partial differential equations with integrals. *Journal of numerical Analysis*, 23(4):645–664, 2003.

[13] Miao Hu and Scott R. Fulton. Higher order adaptive multigrid solution of a fluid flow problem. *Technical Report No. 2000-03, Department of Mathematics and Computer Science, Clarkson University, Potsdam, New York*, 2000.

[14] T. Ringler L. Bonaventura. Analysis of discrete shallow-water models on geodesi cdelaunay grids with c-type staggering. *Mon. Weather Rev.*, 133:2351–2373, 2005.

[15] J. B. Perot. Conservation properties of unstructured staggered mesh schemes. *J. Comp. Phys.*, 159:58–89, 2000.

[16] L. Bonaventura A. Abba. A mimetic finite difference discretization for the incompressible navier-stokes equations. *Int. J. Numer. Methods Fluids*, 56(8):1101–1106, 2008.

[17] Rafail V. Abramov and Andrew J. Majda. Discrete approximations with additional conserved quantities: deterministic and statistical behavior. *Methods and applications of analysis*, 10 (2):151–190, 2003.

[18] Arthur E.P. Veldman Bas van't Hof. Mass, momentum and energy conserving (mamec) discretizations on general grids for the compressible euler and shallow water equations. *Journal of Computational Physics*, 231:4723–4744, 2012.

[19] P. Olsson. Summation by parts, projections, and stability i. *Math. Comp.*, 64:1035–1065, 1995.

[20] P. Olsson. Summation by parts, projections, and stability ii. *Math. Comp.*, 64:1473–1493, 1995.

[21] J. Nordstrom K. Mattsson. Summation by parts operators for finite difference approximations of second derivatives. *J. Comput. Phys.*,, 199(2):503–540, 2004.

[22] Nordstrom Svard, Mattsson. Steady-state computations using summation-by-parts operators. *J. Sci. Comput.*, 24 (1):79–95, 2005.

[23] M. Shashkov J.M. Hyman. Natural discretizations of the divergence, gradient and curl on logically rectangular grids. *Comput. Appl. Math.*, 33 (4):81–104, 1997.

[24] M. Shashkov J.M. Hyman. Adjoint operators for the natural discretizations of the divergence, gradient and curl on logically rectangular grids. *Appl. Numer. Math.*, 25:413–442, 1997.

[25] A. Cangiani G. Manzini L.D. Marini A. Russo L. Beirao da Veiga, F. Brezzi. Basic principles of virtual element methods. *Math. Model Methods Appl. Sci.*, 23 (1):199–214, 2013.

[26] A. Buffa F. Brezzi. Innovative mimetic discretizations for electromagnetic problems. *J. Comp. Appl. Mech.*, 234:1980–1987, 2010.

[27] M. Shaskov F. Brezzi, K. Lipnikov. Convergence of the mimetic finite difference method for diffusion problems on polyhedral eshes. *SIAM J. Numer. Anal.*, 43 (5):1872–1896, 2005.

[28] Richardson. Weather prediction by numerical process. *London, Cambridge University Press/ reprinted: Dover*, 1965.

[29] Von Neumann Charney, Fjortoft. Numerical integration of the barotropic vorticity equation. *Tellus*, 2:237–154, 1950.

[30] J. Smagorinsky. General circulation experiments with the primitive equations. i: The basic experiment. *Month. Weath. Rev*, 91:99–164, 1963.

[31] J. W. Deardorff. A numerical study of three-dimensional turbulent channel flow at large reynolds numbers. *J. Fluid Mech.*, 41:453–480, 1970.

[32] D. Randall. An introduction to atmospheric modeling. *Department of Atmospheric Science Colorado State University*, 2004.

[33] D. Randall. General circulation model development - past, present, and future. *International Geophysics Series*, 70, 2000.

[34] Norman A. Phillips. An example of non-linear computational instability. *The Atmosphere and the Sea in Motion (Rockefeller Institute Press in association with Oxford University Press, New York)*, pages 501–504, 1959.

[35] A. Arakawa. Adjustment mechanism in atmospheric models. *J. Meteor. Soc. Japan 75*, pages 155–179, 1997.

[36] Arakawa Mesinger. Numerical methods used in atmospheric models. *Global Atmospheric Research Programme (GARP)*, Volume I, 1976.

[37] V.R. Lamb. A. Arakawa. Computational design of the basic dynamical processes of the ucla general circulation model. *Methods in Computational Physics*, 17:173–265, 1977.

[38] S. Scott Collis. An introduction to numerical analysis for computational fluid mechanics. *Computational Mathematics Algorithms Sandia National Laboratories*, 2005.

[39] Jan Nordstrom. Conservative finite difference formulations, variable coefficients, energy estimates and artificial dissipation. *Journal of Scientific Computing*, 29 (3), 2006.

[40] Bernardo Favini Chiara Sorgentone. A systematic method to construct mimetic finite-difference schemes for incompressible flows. *Submitted to Journal of Computational Physics*, 2014.

[41] *Chiara Sorgentone, Irene Milillo, Sandro Calmanti, Bernardo Favini, Generalization of Arakawa's Jacobian, Workshop on Partial Differential Equations on the Sphere (PDEs), NCAR (National Centre for Atmospheric Reasearch, Boulder (CO), USA), 7th April 2014.*

[42] Jan Nordstrom Chiara Sorgentone, Cristina La Cognata. A new high order energy and enstrophy conserving arakawa-like jacobian differential operator. *In preparation*, 2014.

[43] *Chiara Sorgentone, Numerical Simulation of quasi-geostrophic turbulence, Seminar at Department of Mathematics, "La Sapienza" University of Rome, 28th May 2013.*

[44] Joseph Pedlosky. Geophysical fluid dynamics. *Springer-Verlag*, 1979.

[45] James R. Holton. An introduction to dynamic meteorology. *Fourth edition. Academic Press*, 2004.

[46] Sanjiva K. Lele. Compact finite difference schemes with spectral-like resolution. *Journal of Computational Physics*, 103(1):16–42, 1992.

[47] Jay C. Webb Christopher K.W. Tam. Dispersion-relation-preserving finite difference schemes for computational acoustics. *Journal of Computational Physics*, 107(2):262–281, 1993.

[48] J. Strikwerda. Finite difference schemes and partial differential equations. *Society for Industrial Mathematics, PA, USA*, 2004.

[49] Omer San and Anne E. Staples. High-order methods for decaying two-dimensional homogeneous isotropic turbulence. *Computers Fluids*, 53:105–127, 2012.

[50] Abderrahim Kacimi and Boualem Khouider. A numerical investigation of the barotropic instability on the equatorial β-plane. *Theorical and Computational Fluid Dynamic*, 2012.

[51] Svetlana Dubinkina and Jason Frank. Statistical mechanics of arakawa,Äôs discretizations. *Annals of Physics*, 227(2):1286–1305, 2007.

[52] Douglas Lilly. On the computational stability of numerical solutions of time-dependent non-linear geophysical fluid dynamics problems. *Geophysical Fluid Dynamics Laboratory, U.S. Weather Bureau, Washington, D.C.*, 93(1):11–26, 1965.

[53] John B. Bowles Robert Vichnevetsky. Fourier analysis of numerical approximations of hyperbolic equations. *SIAM books, 3600 University City Science, Center, Philadelphia*, 1987.

[54] Jan Nordstrom Mark H. Carpenter and David Gottliebz. A stable and conservative interface treatment of arbitrary spatial accuracy. *Journal of Computational Physics*, 148:341–365, 1999.

[55] Heinz-Otto Kreiss and Godela Scherer. On the existence of energy estimates for difference approximations for hyperbolic systems. *Technical report, Uppsala University, Division of Scientific Computing*, 1977.

[56] Jan Nordstrom Magnus Svard. Review of summation-by-parts schemes for initial-boundary-value problems. *Journal of Computational Physics*, 268:17–38, 2014.

[57] Heinz-Otto Kreiss and Godela Scherer. Finite element and finite difference methods for hyperbolic partial differential equations. *Mathematical Aspects of Finite Elements in Partial Differential Equations, Academic Press, New York*, 1974.

[58] Bo Strand. Summation by parts for finite difference approximations for d/dx. *Journal of Computational Physics*, 110(1):47–67, 1994.

[59] Edwin van der Weide Magnus Svard Jan Nordstrom, Jing Gong. A stable and conservative high order multi-block method for the compressible navier-stokes equations. *J. Comput. Phys.,*, 228(24):9020–9035, 2009.

[60] Jan Nordstrom Nail K. Yamaleev Charles Swanson Travis C. Fisher, Mark H. Carpenter. Discretely conservative finite-difference formulations for nonlinear conservation laws in split form: Theory and boundary conditions. *Journal of Computational Physics*, 234:353–375, 2013.

[61] Abarbanel Saul. Carpenter Mark H, Gottlieb David. Time-stable boundary conditions for finite-difference schemes solving hyperbolic systems: methodology and application to high-order compact schemes. *J. Comput. Phys.,*, 111 (2):220–236, 1994.

[62] Jan Nordstrom Tomas Lundquist. The sbp-sat technique for initial value problems. *J. Comput. Phys.,*, 270:86–104, 2014.

[63] Jan Nordstrom Jens Berg. Stable robin solid wall boundary conditions for the navier-stokes equations. *J. Comput. Phys.*, 230:7519–7532, 2011.

[64] Jens Berg Jan Nordstrom. Conjugate heat transfer for the unsteady compressible navier-stokes equations using a multi-block coupling. *Computers Fluids*, 72:20–29, 2013.

[65] Shoeybi Mohammad Weide Edwin van der Svard Magnus Mattsson Ken et al. Nordstrom Jan, Ham Frank. A hybrid method for unsteady inviscid fluid flow. *J. Comput. Phys.*, 38:875–882, 2009.

[66] Law Craig Gong Jing Nordstrom Jan, Eriksson Sofia. Shock and vortex calculations using a very high order accurate euler and navier-stokes solver. *J Mech MEMS*, 1:19–26, 2009.

[67] Carpenter Mark Nordstrom Jan Mattsson Ken, Svard Magnus. High-order accurate computations for unsteady aerodynamics. *Comput Fluids*, 36 (3):636–649, 2007.

[68] Tomas Lundquist Jan Nordstrom. Summation-by-parts in time. *J. Comput. Phys.*, 251:489–499, 2013.

[69] Mark H. Carpenter Jan Nordstrom. High-order finite difference methods, multidimensional linear problems, and curvilinear coordinates. *J. Comput. Phys.,*, 173:149–174, 2001.

[70] Wendell Welch Orlando Ka Kit Tung. On the differences between 2d and qg turbulence. *Discrete and Continuous Dynamical Systems*, 3(2):145–162, 2003.

[71] Eleftherios Gkioulekas. A theoretical study of the cascades of 3d, 2d, and qg turbulence. *University of Washington*, 2006.

[72] Patrick Tabeling. Two-dimensional turbulence: a physicist approach. *Phys. Rep.*, 362, 2002.

[73] R. H. Kraichnan. Inertial ranges in two-dimensional turbulence. *Phys. Fluids*, 10:1417–1423, 1967.

[74] R. H. Kraichnan. Inertial-range transfer in two- and three-dimensional turbulence. *J. Fluid Mech*, 47:525–535, 1971.

[75] C. E. Leith. Diffusion approximation for two-dimensional turbulence. *Phys.Fluids*, 11:671,Äì673, 1968.

[76] C. E. Leith. Computation of the energy spectrum in homogeneus two-dimensional turbulence. *Phys.Fluids*, 12(II):233–239, 1969.

[77] E. Lindborg and K. Alvelius. The kinetic energy spectrum of two dimensional enstrophy turbulence cascade. *Phys.Fluids*, 12:945–947, 2000.

[78] T. Ishihira and Y. Kaneda. Energy spectrum in the enstrophy transfer range of two-dimensional forced turbulence. *Phys.Fluids*, 13:544–547, 2001.

[79] C. Pasquero and G. Falkovich. Stationary spectrum of vorticity cascade in two dimensional turbulence. *Phys. Rev. E*, 65, 2002.

[80] Jule G. Charney. Geostrophic turbulence. *J. Atmos. Sci.*, 28:1087,Äì1095, 1971.

[81] Wendell T. Welch Ka Kit Tung. Remarks on charney's note on geostropic turbulence. *J. Atmos. Sci.*, 58(14), 2001.

[82] Ka Kit Tung Eleftherios Gkioulekas. On the double cascades of energy and enstrophy in two-dimensional turbulence, part ii, approach to the klb limit and interpretation of experimental evidence. *Discrete and Continuous dynamical systems*, B-5:103–124, 2005.

[83] Ka Kit Tung. Reply to comments by k. shafer smith. *J. Atmos. Sci.*, 61:943–948, 2004.

[84] Eleftherios Gkioulekas. The effect of asymmetric large-scale dissipation on energy and potential enstrophy injection in two-layer quasi-geostrophic turbulence. *Journal of Fluid Mechanics*, 694:493–523, 2012.

[85] Ka Kit Tung Eleftherios Gkioulekas. On the double cascades of energy and enstrophy in two-dimensional turbulence, part i. *Discrete and Continuous dynamical systems*, B-5:79–102, 2005.

[86] G.D. Nastrom and K.S. Gage. A climatology of atmospheric wave number spectra of wind and temperature observed by commercial aircraft. *J. Atmos. Sci*, 42:950–960, 1984.

[87] Ragnar Fjortoft. On the changes in the spectral distribution of kinetic energy for two-dimensional, non-divergent flow. *A quarterly journal of Geophysics*, 5(3), 1953.

[88] Ka Kit Tung Wendell T. Welch. Nonlinear baroclinic adjustment and wavenumber selection in a simple case. *J. Atmos. Sci.*, 55(8), 1998.

[89] Wendell Welch Orlando Ka Kit Tung. The k^{-3} and $k^{-\frac{5}{3}}$ energy spectrum of atmospheric turbulence: Quasigeostrophic two-level model simulation. *Journal of the Atmospheric Sciences*, 60:824–835, 2003.

[90] I.M. Held D.B. Haidvogel. Homogeneous quasigeostrophic turbolence driven by a uniform temperature gradient. *Journal of the Atmospheric Sciences*, 37(12):2644–2660, 1980.

[91] F. Saleri A. Quarteroni, R. Sacco. Matematica numerica. *Springer*, 2000.

[92] Steve Schaffer. Higher order multi-grid methods. *Mathematics of Computation*, 43(167):89–115, 1984.

[93] Phillip Colella. Online report. *http://www.eecs.berkeley.edu/˜colella/E266AF2010/E266A_Incompressible.pdf*.

[94] Andrew Majda. Introduction to pdes and waves for the atmosphere and ocean. *AMS*, 2003.